

2D and 3D seismic imaging by partial time migration and demigration

Dissertation
zur Erlangung des Doktorgrades
an der Fakultät für
Mathematik, Informatik und Naturwissenschaften
im Fachbereich Geowissenschaften
der Universität Hamburg

vorgelegt von
Yan Yang

Hamburg, 2016

Tag der Disputation: 24.01.2017

Folgende Gutachter empfehlen die Annahme der Dissertation:

Prof. Dr. Dirk Gajewski

PD Dr. Claudia Vanelle

Zusammenfassung

Um ein erstes Abbild des Untergrundes der Erde von seismischen Daten zu erhalten stellt das Stapeln ein wichtiges Werkzeug dar. Die Migration kann dieses erste Abbild verbessern, da es Diffraktionen optimal fokussiert und Reflektoren an ihren richtigen laterale Positionen abbildet. Das Ziel der Migration ist Effekte der Wellenausbreitung zu korrigieren und Bilder zu erzeugen, die die Orientierung und Position von geologischen Strukturen beschreiben. Prestack Zeitmigration ist immer noch ein häufig benutztes Werkzeug um Den Untergrund abzubilden, da sie schnell, robust und wenig sensitiv gegenüber Fehler im Geschwindigkeitsmodell ist. Der übliche Zeitmigrationsoperator (Kirchhoff Zeitmigration) wird durch eine Gleichung mit zwei quadratischen Wurzeln beschrieben. Ein existierender Ansatz um partiell zeitmigrierte Daten zu erhalten ist die mächtige Reparametrisierung der quadratischen Wurzeln mittel Hilfe des Apex der Laufzeit einer Diffraktion. Dieser Ansatz erhält den moveout, wodurch der Datensatz in der prestack Domäne bleibt. Die neu generierten Daten können für konventionelle Prozessierung, wie zum Beispiel die Mehrparameter (MP) Stapelung, genutzt werden.

Der Umgang mit qualitativ schlechten Daten ist eine Herausforderung in der Prozessierung. Auf Grund verschiedener vorherrschender Probleme, werden die seismischen Daten möglicherweise mit einer unregelmäßigen oder dünn besetzten Auslage aufgenommen. Weiterhin führen komplexe Untergründe, Verwerfungssysteme und starke horizontale Änderungen der Geschwindigkeit, wie zum Beispiel bei Salzkörpern, zu einem niedrigen Signal-Rausch Verhältnis. I postuliere eine neue kinematische Methode für die Rücktransformation von stückweise zeitmigrierten Daten in die sogenannte common midpoint (CMP) Domäne, genannt partielle Zeitdemigration. Es ist der Umkehrprozess der partiellen Zeitmigration. Der Operator ist eine einfache quadratische Wurzel.

I schlage einen kaskadierte Anwendung der partiellen Zeitmigration und partiellen Zeitdemigration vor. I demonstriere das Potential der vorgeschlagenen kaskadierten Methode an synthetischen und Felddaten. Durch die zwei Transformationen erhaltene Sektionen sind regularisiert und haben ein besseres Signal-Rausch Verhältnis im Vergleich zu den originalen CMP Sektionen. Statt der originalen Daten kann man diese verbesserten prestack Daten in typischen Prozessierungsschritten benutzen, die zu verbesserten Abbildungen führen. Zusätzlich kann man von

den Unterschieden zwischen originalen Daten und den erhaltenen Daten lernen und zum Vorteil nutzen. Da die zeitmigrierten Daten, die nach der ersten Transformation verfügbar sind, unabhängig von der Neigung sind, eignen sie sich für den Umgang mit sich schneidenden Neigungen. Weiterhin zeigen sie Potential für eine Diffraktionsseparation und die Unterdrückung von Multiplen. Zusätzlich, auf Grund der Fokussierung von Diffraktionen und die Regularisierung von zeitmigrierten Sektionen, ist die Bestimmung von Migrationsgeschwindigkeiten aus den kinematischen Wellenfrontattributen anhand einer Kohärenzanalyse vorzuziehen. Es ist ein rein datengetriebener Ansatz. De-/Migrationsergebnisse können unpräzise werden, wenn geologische Strukturen wie Verwerfungen und Salzkörper abzubilden sind. Das liegt an den Limitierungen von laufzeitbasierten Methoden im allgemeinen.

Abschließend, da die Erde selbst dreidimensional (3D) und Daten von drei dünn besetzten und unregelmäßig dreidimensionalen Akquisitionen aufgenommen werden, habe ich die Technik auf den 3D Fall erweitert und auf einen 3D synthetischen Datensatz angewendet.

Abstract

In order to get a first image of the Earth's subsurface from seismic data, stacking serves as an important tool. However, migration can improve this first image as it ideally focuses diffraction events and moves all reflection events to their correct lateral position. The aim of migration is to reverse the effects of wave propagation and to generate images which can describe the position and orientation of subsurface geological interfaces. Prestack time migration (PreSTM) is still a widely used tool for subsurface imaging because it is fast, robust and rather insensitive to velocity model errors. The conventional time migration operator (Kirchhoff time migration) is described by a double square root (DSR) equation. An existing approach to build 'partly' time migrated data by reparametrising the DSR operator in terms of the diffraction apex traveltimes is powerful. This approach can preserve the moveout, thus make the data still stay in the prestack domain. The newly-generated data can be used in conventional processing, e.g., multi-parameter (MP) stack.

Handling low quality seismic data is a processing challenge. Due to various issues, the seismic data may be acquired in sparse and irregular spatial positions. Also the complexity of the subsurface, the presence of fault structures, and strong velocity contrasts in areas, e.g., with salt bodies, lead to a low S/N ratio of the data. I propose a new kinematic method to back-transform the partially time-migrated data to common midpoint (CMP) domain, namely, the partial time demigration. It is the inverse process of partial time migration, and the operator is formulated in a single square root (SSR) equation.

I suggest a cascaded application of partial time migration and partial time demigration. I demonstrate the potential of the proposed cascaded method for synthetic as well as real datasets. Gathers obtained after these two transformations are regularised and have better signal-to-noise (S/N) ratio compared to the original CMP gathers. Instead of the original data, these improved prestack data can be used in many conventional processing procedures, providing enhanced images. Furthermore, one can learn and take advantage of the differences between the resulting data and the original data. Since the time-migrated data obtained after the first transformation is dip-independent, it is preferable for conflicting dip handling, and also shows potential for diffraction separation and multiple suppression. In addition, due to the focusing of diffractions and the regularity of the time-migrated

gathers, estimation of migration velocities out of the kinematic wavefront attributes based on the coherence measure is preferable. It is a purely data-driven approach. De-/Migration results can be imprecise when imaging complex geological situations, e.g. faults or salt bodies. This is due to the limitations of time imaging in general.

Finally, since the Earth itself is three dimensional (3D), and the data obtained by 3D acquisition is sparse and irregular, I extend the technique to the 3D case and apply the proposed method to a 3D synthetic data set.

Contents

1. Introduction	3
2. 2D Prestack partial time migration	9
2.1. Conventional prestack time migration	9
2.2. Multi-parameter stacking operators	13
2.3. Prestack partial time migration	17
2.4. Practical aspects	19
2.5. Synthetic data example	25
2.6. Field data example	35
2.7. Summary	41
3. 2D Prestack partial time demigration	43
3.1. Theoretical background	43
3.2. Partial time demigration	44
3.3. Practical remarks	45
3.4. Applications	46
3.5. Summary	59
4. 3D extension and application	61
4.1. 3D seismics	61
4.2. 3D extension of partial time de-/migration technique	64
4.3. Synthetic data examples	70
4.4. Summary	80
5. Conclusions	81
6. Outlook	85
Bibliography	91
List of Figures	95
List of Tables	97
Appendices	99

A. Processing parameters	101
B. Used software	107
C. Eidesstattliche Versicherung	109

Chapter 1.

Introduction

The investigation of the Earth's interior, often referred to as the solid Earth, is usually based on indirect geophysical measurements, because it is almost inaccessible by means of direct approaches. Such indirect measurements include reflection and refraction seismics, gravity, magnetic, electrical, and electromagnetic techniques. Geophysics aims at investigating the Earth subsurface and exploring the structure, composition, and dynamics of the Earth using quantitative physical methods, in order to delineate the geological structures that contain hydrocarbons and mineral deposits. Among the processing methods, seismic reflection is the most commonly used one. The method requires a controlled seismic source of energy, such as dynamite, a specialized air gun or a seismic vibrator. The principle is to send seismic waves into the Earth using such seismic sources, where each layer within the Earth reflects (and/or scatters/diffracts) a portion of the wave's energy back and allows the rest to refract through. These waves are recorded over a predetermined time period (called the record length) by receivers that detect the motion of the ground in which they are placed.

To obtain the desired local distribution of the elastic properties, additional processing and imaging techniques have to be performed. As the name 'seismic reflection' indicates, reflected waves are regarded as the kernel of almost all the conventional processing techniques. To be more specific, we need to transform the acquired (measured) data into the desired information of subsurface structure. The measured seismic data initially include signals caused by body wave and surface wave. However, for most seismic reflection imaging, only a part of these signals corresponding to primary waves, i.e., waves that were reflected only once in the subsurface, are considered. All other wave types, including multiple reflected waves, surface waves, refracted waves, and primary reflections of other wave modes represent unwanted signals. One important aim of seismic data processing is to suppress them as well as other types of coherent and incoherent noise in the data to enhance the primary reflection signals.

Over the past decades, the multi-parameter stacking techniques (see, e.g., Müller, 1999; Gelchinsky et al., 1999; Mann, 2002; Schwarz et al., 2014) have become powerful alternative tools to the conventional Common Midpoint (CMP) stack routine (Mayne, 1962). The main advantage of the multi-parameter stacking operator is that it spatially extends over several CMP gathers and approximates the reflection response of a whole reflector segment. In this way, an increased number of traces contribute to the stack which leads to an improved S/N ratio in the simulated zero offset (ZO) section. At the same time, a whole set of stacking parameters, the so-called kinematic wavefront attributes, are obtained for each simulated ZO sample. In addition, a broad application of these attributes in subsequent processing steps is available. Among which the tomographic velocity model determination by Duveneck (2004) is the most prominent one. Further applications of the CRS attributes include, e.g., automatic approximative time migration without velocity model (Mann, 2002), and minimum-aperture time migration (Spinner, 2007).

The simulation of a zero offset section by a stacking procedure always yields a first image of the subsurface in the time domain. However, the reflection events recorded in time domain appear in a wrong lateral position and diffraction events are not yet focused. Various imaging methods exist which provide more accurate information about the subsurface. A process called time migration can improve this first image as it ideally focuses diffraction events and moves all reflection events to their correct lateral position in the time domain. Time migration velocity model is usually needed for time migration. This can, in principle, be extracted from the seismic prestack data without an explicit knowledge of the true subsurface model. However, for its determination, some assumptions are always made, e.g., horizontally layered media with mild to moderate lateral velocity variations. Nevertheless, despite these hypotheses time migration is still advantageous over depth migration for subsurface imaging because it is fast, robust and rather insensitive to velocity model errors.

Various time migration algorithms have been developed which are in general variations of three different approaches (Sheriff and Geldart, 1982): an integral solution of the wave equation (Kirchhoff migration or diffraction stack) (Hagedoorn, 1954), a solution of the wave equation in the frequency domain (e.g. Stolt (1978) or Gazdag (1978)), or a finite-difference approach in the time domain (Claerbout et al., 1996). Among those, Kirchhoff time migration is one of the oldest techniques but still widely used. Yilmaz (2001) described the conventional prestack time migration operator by a double square root (DSR) equation. This is a classical tool of a Kirchhoff-type migration. Ferber (1994) suggested a migration method to multiple offsets, that is a prestack time-migration technique that presents data sets which mimic high-fold, bin-center adjusted, common-midpoint gathers. Bancroft et al. (1998) expanded the method of migration from multiple offset to the equivalent offset by reformulating the DSR operator into a single square root equation and gave a theoretical explanation for the generated gathers, which he introduced as common

scatterpoint (CSP) gathers. In both methods, the partially migrated common-offset gathers are focused in a procedure similar to normal moveout (NMO), i.e., by performing a stack over the offsets.

Dell et al. (2012) proposed a prestack partial time migration method by parametrising the DSR operator with the apex of the diffraction traveltime for each offset. While Ferber (1994) and Bancroft et al. (1998) apply a single parameter stack over offsets, Dell et al. (2012) suggested to apply a multi-parameter stack over offsets as well as midpoints. By doing so, the moveout is preserved, and the data still stays in the prestack domain. In addition, prestack data enhancement are achieved because the number of contributing traces is much higher than for the single parameter stack over the offsets, thus it can improve the S/N ratio of the prestack data.

Another transformation approach, namely the unified approach, proposed by Hubral et al. (1996), represents the forward and inverse process of seismic migration. They use a weighted Kirchhoff-type isochron-stack integral to transform (demigrate) the migrated seismic image from the depth domain back into the time domain. Although their approach is formulated in the depth domain, the concept can be applied to the time domain. Based on the partial time migration proposed by Dell et al. (2012), I propose a new inverse process, which I call partial time demigration.

The aim of this thesis is to develop a technique to improve the image quality of prestack seismic data. I cascade both operators by first applying the partial time migration method (Dell et al., 2012) to the original data and then a partial time demigration to the time-migrated gathers. By doing such forward and backward transformations, we can regularise the traces and improve the S/N ratio of the data. The data regularisation ability is quite important especially for seismic data by irregular acquisition, and with low common-midpoint fold. Time migration conducted directly on these data can lead to bad or wrong images. The main idea of Kirchhoff migration is to treat each point on a sufficiently dense grid in the considered target area as a potential diffraction point in correspondence to Huygen's principle (Hagedoorn, 1954). The Huygens surface can be calculated independently for any of these points from the kinematic part of the Green's function using the known macro-velocity model. After regularisation of seismograms and filling the gaps in cases of missing data by our proposed method, by using these improved prestack data instead of the original data can one gain fine grids, thus obtain enhanced time migration results. In addition, due to the focusing of diffractions and triplications and the regularity of the time-migrated gathers, estimation of migration velocities out of the kinematic wavefront attributes based on the coherence measure is preferable. Furthermore, we can learn and take advantage of the differences between the resulting data and the original data. Since the migrated data obtained after the first transformation (partial time migration) is dip-independent, it is

preferable for conflicting dip handling, and also shows potential for diffraction separation and multiple suppression.

If diffraction-only data are available, the resulting stacking velocities will no longer depend on the reflector dip and thus do not need updates to remove the effect of the reflector dip. Therefore, in the case of diffraction data, time migration velocity analysis can directly use stacking velocities. [Dell and Gajewski \(2011\)](#) and [Bakhtiari Rad et al. \(2014\)](#) proposed techniques to combine the diffraction weighting function and the partial CRS stack technique to generate diffraction gathers. However, issues like conflicting dips and non-point diffractions need to be resolved in order to exploit the full potential of the method. [Walda and Gajewski \(2015\)](#) adapted the conflicting dip treatment in the CRS method to a global optimization scheme, which reveals great potential for diffraction imaging and migration velocity analysis. Another potential application would be multiple suppression. Multiples are seismic arrival that have more than one reflections or scattering. These are the signals we want to get rid of. The most common techniques for multiple suppression are the Surface Related Multiple Elimination (SRME) method ([Verschuur et al., 1992](#)), the inverse scattering series ([Weglein et al., 1997](#)) and the hyperbolic radon transform (see, e.g., [Ryo, 1982](#)). [Dümmong and Gajewski \(2008\)](#) proposed a technique which directly incorporate multiple suppression into the CRS-workflow, so that a processing chain from time to depth imaging with CRS related technology can be established.

Finally, since the Earth is in fact no two-dimensional object, and only 3D imaging can provide the detailed knowledge of reservoir features, I suggest to extend the cascaded technique to the 3D case.

The thesis is structured as follows:

In this chapter, I give a brief introduction to the basic principles of the reflection seismic method. A short summary of conventional and newly-developed techniques for seismic data processing and imaging is presented.

In Chapter 2, I review the conventional Kirchhoff prestack time migration approach. Then I review the theory of multi-parameter stacking operators, and as an example, the Common-Reflection-Surface (CRS) stacking method is briefly reviewed. Afterwards, the prestack partial time migration method, which is based on a new parametrisation of the double square root (DSR) equation is introduced. Finally, application of both migration techniques to a complex synthetic data set as well as to a field data set is performed.

In Chapter 3, I develop a new inverse process of the partial time migration, namely, partial time demigration. I suggest to utilise a cascaded operator of first partial time migration and then partial time demigration, in order to regularise the traces

as well as to improve the S/N ratio of the data. Examples of a generic synthetic data set and the complex synthetic data as well as a marine field data set show the superiority of the proposed approach.

In Chapter 4, I extend the presented technique to three dimensional case. Then I apply the proposed partial time migration technique as well as the conventional prestack time migration method to a complex synthetic data set, i.e., the SEG Salt Model C3 wide azimuth classic data set. Comparison of the results shows the validity of the algorithm. A time migration velocity model which is azimuth-dependent can be built from the kinematic wavefront attributes during the process. This is data-driven and efficient compared to updating approaches often used for conventional time migration velocity determination.

In Chapter 5, I summarise the results of the presented work in this thesis.

In Chapter 6, I give an outlook and suggest related topics of possible future research.

The main processing parameters for both 2D and 3D data sets can be found in Appendix A, and a list of used software is given in Appendix B.

Chapter 2.

2D Prestack partial time migration

In this chapter, I review the conventional prestack time migration technique and one multi-parameter stacking method, i.e. the Common-Reflection-Surface (CRS) stacking method. Followed by that, I give a description of the prestack partial time migration technique, whose operator is based on a new parametrisation of the conventional prestack time migration in terms of diffraction apex traveltimes. In addition, I present some practical remarks, e.g., choosing velocities and apertures (for both migration and stacking). Finally, I apply both conventional prestack time migration and partial time migration techniques to a complex synthetic data set as well as to a field data set.

2.1. Conventional prestack time migration

Seismic migration is a wave-equation based process that removes the influence of the reflector overburden from the data. In detail, migration alters the location and inclination of reflection events, collapses diffraction patterns that are caused by point scatterers and unfolds triplications. Migration can provide more focused images of the subsurface which may not be displayed that simply from stacked section.

Migration can be implemented both in the time and the depth domain, which are so called time migration and depth migration, respectively (see, e.g., [Robein, 2003](#)). Although depth seems to be the natural domain for an image of the geological structure, time migration is frequently applied because the velocity model building is simplified and errors have less impact on the migration results. Moreover, it allows a direct comparison with the unmigrated section for interpretation ([Spinner, 2007](#)). Appropriate velocity information is essential in both cases. However, time migration requires integral velocity information, whereas depth migration demands the true medium velocities, which needs far more accuracy in the velocity determination. Based on the assumption of a laterally homogeneous velocity distribution, seismic

time migration is less sensitive to velocity model errors. With this prerequisite, integral velocities are assumed to be sufficient to characterise the overburden and the velocity model building is considerably simplified. In practice, the assumption is usually extended to media showing mild to moderate lateral velocity variations.

As mentioned in the previous chapter, various time migration algorithms exist. In this thesis I consider Kirchhoff migration. The main idea of Kirchhoff migration is to treat each point on a sufficiently dense grid in the considered target area as a potential diffraction point in correspondence to Huygens' principle. The reflection response is the superposition of all diffraction responses from these points and the reflection traveltime surface is the envelope of these diffraction traveltime surfaces. According to Hagedoorn's imaging condition (Figure 2.1), the diffraction traveltime surface is tangent to the primary-reflection traveltime surface for an actual reflection point which leads to a non-negligible summation results due to constructive interference. Otherwise, the contribution results in destructive interference and

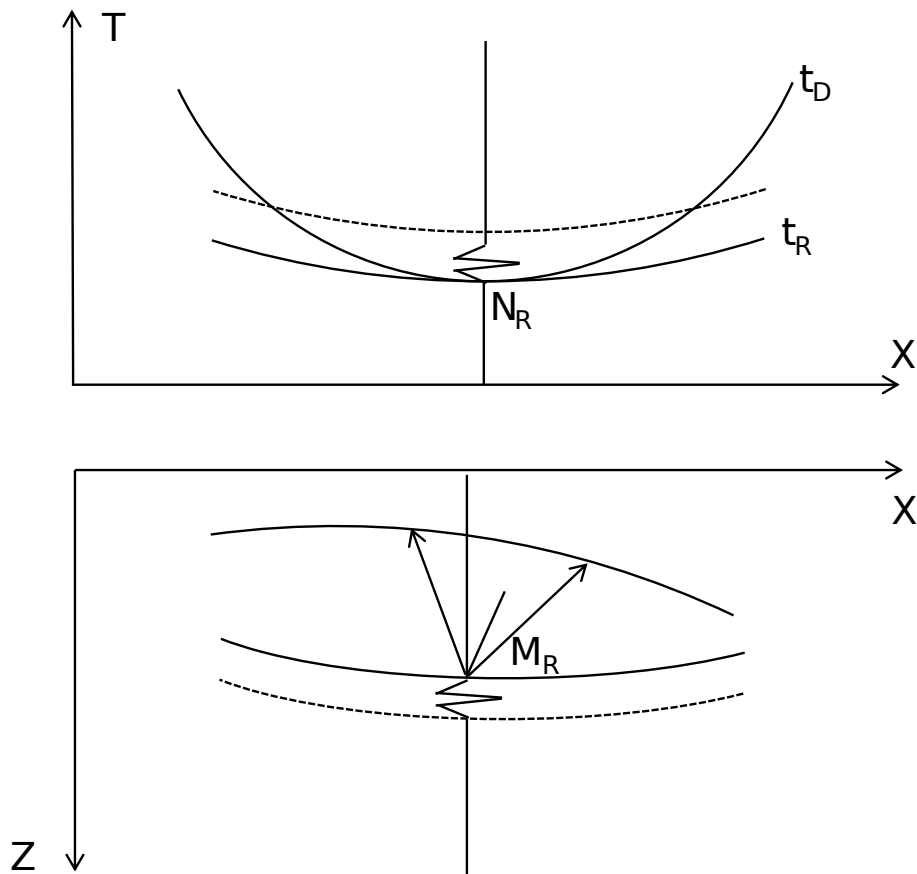


Figure 2.1.: Hagedoorn's imaging condition. The Huygens curve $t_D(M_R)$ of a point on the reflector M_R in the depth domain is tangent to the reflection traveltime curve $t_R(N_R)$ at point N_R in the time domain.

Among Kirchhoff migration techniques, prestack time migration (PreSTM) is a classical tool for subsurface imaging because it is fast, robust and rather insensitive to velocity model errors. The conventional time migration operator is described by a double square root (DSR) equation (see, e.g., [Yilmaz, 2001](#)). The time migration velocity will be discussed in the next section. The classic time migration operator in 2D describes diffraction traveltimes by the DSR equation,

$$t_D(t_0, m, h) = \sqrt{\frac{t_0^2}{4} + \frac{(m-h)^2}{v^2}} + \sqrt{\frac{t_0^2}{4} + \frac{(m+h)^2}{v^2}}, \quad (2.1)$$

where h is the half source-receiver distance, m is the midpoint displacement with respect to the considered CMP position, t_0 is the zero-offset (ZO) two-way traveltime, and v is assumed to be the migration velocity.

Figure 2.2 shows the principle of PreSTM. The reflection response is depicted in light blue, while the diffraction response is shown in dark blue. The time migration is first performed for each (half) offset by summing all traces along the curve t_D for the according midpoint displacement. The summation result is assigned to $(m=0, h, t_0)$ (denoted by the magenta line). In a second step, the contributions for each (h, t_0) are summed into the apex of the operator for the ZO case, i.e., $(m=0, h=0, t_0)$ (denoted by the magenta circle).

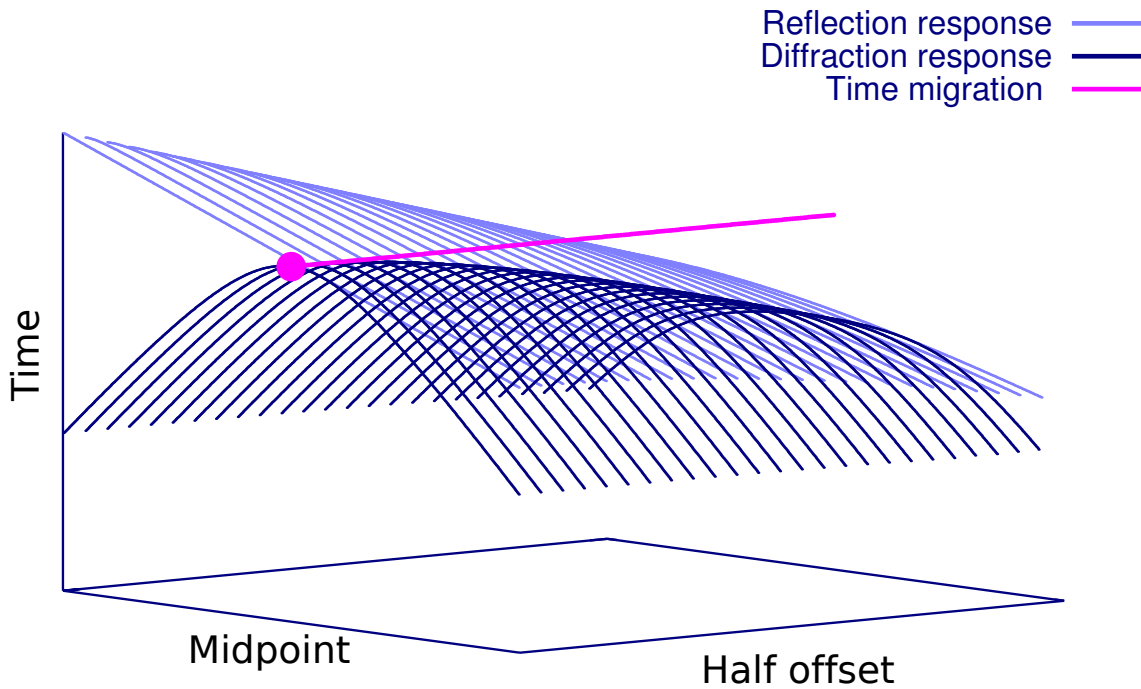


Figure 2.2.: Principle of prestack time migration. The reflection response is depicted in light blue, while the diffraction response is shown in dark blue. The time migration is firstly performed for each (half) offset by summing all traces along the diffraction response for the according midpoint displacement. The summation result is assigned to $(m = 0, h, t_0)$ (denoted by the magenta line). In a second step, the contributions for each (h, t_0) are summed into the apex of the operator for the ZO case, i.e., $(m = 0, h = 0, t_0)$ (denoted by the magenta circle). (after Dell et al. (2012))

2.2. Multi-parameter stacking operators

Stacking plays an important role in seismic data processing. A stacked section can reduce data redundancy and leads to a first and reliable time image with a high signal-to-noise ratio. The Common-midpoint (CMP) stack method introduced by [Mayne \(1962\)](#) is the first widely used data-oriented approach. It is a very robust strategy to simulate a zero-offset (ZO) section from prestack data. This reduces the amount of data and increases the signal-to-noise ratio. For horizontally layered media, the CMP stack collects the energy pertaining to one and the same reflection point at each location in the time domain, thus making use of the redundancy of multi-coverage seismic reflection data. Later on, processes known as normal moveout (NMO) correction and dip moveout (DMO) correction (see, e.g., [Yilmaz and Claerbout, 1980](#); [Deregowski, 1986](#)) were developed to handle the influence of the acquisition geometry due to the overburden of a reflector and to consider the dip of the reflector.

In recent years, the so-called multi-parameter (MP) stacking operator has been established as a powerful alternative to conventional NMO/DMO stacking procedures. Such operators have been introduced with different approaches. [Müller \(1999\)](#) introduced the common reflection surface (CRS) stack method, which takes neighbouring CMP gathers into account. It is based on three surface-related kinematic wavefront attributes, namely α , R_{NIP} and R_N , which are closely related to first- and second-order derivatives of the traveltime near the reference ray. [Gelchinsky et al. \(1999\)](#) and co-workers proposed their homeomorphic imaging methods: multifocusing. It is based on a double-square-root expression for the traveltime, depending on the same set of parameters (the kinematic wavefront attributes) as the CRS method. This operator describes the traveltime of a reflection event in terms of the traveltime of a central ray and corrections applied at source and receiver for a paraxial ray. In addition, [Vanelle et al. \(2010\)](#) and [Schwarz et al. \(2014\)](#) proposed a new multi-parameter stacking operator: the i-CRS (implicit common reflection surface) operator, which better accounts for reflector curvature.

In the following, I will consider the CRS stacking operator (see, e.g., [Müller, 1999](#); [Mann, 2002](#)) as an example and explain briefly the principle. The general idea of CRS technique is to describe a reflection event in the vicinity of a ZO sample by means of a second-order traveltime approximation. The frequently used CRS traveltime equation is a second order Taylor series expansion of the squared traveltime and reads as:

$$t_{CRS}^2(\Delta x_m, h) = \left(t_0 + \frac{2 \sin \alpha}{v_0} \Delta x_m \right)^2 + \frac{2t_0 \cos^2 \alpha}{v_0} \left(\frac{\Delta x_m^2}{R_N} + \frac{h^2}{R_{NIP}} \right) . \quad (2.2)$$

It describes the reflection traveltime in the vicinity of the CMP location under consideration, x_0 , for deviations in midpoint, $\Delta x_m = x_m - x_0$, and half-offset, h , coordinates. In Equation 2.2, t_0 is the zero-offset traveltime and v_0 is the velocity in the acquisition surface at the CMP. The CRS operator is parametrised by three wavefront attributes which are related to two hypothetical one-way experiments as shown in Figure 2.3. The resulting two fictitious waves are described by the angle of the emergence α of the ZO ray and the corresponding radii of curvature, R_N for the normal (N) wave and R_{NIP} for the normal-incidence-point (NIP) wave Hubral (1983). The normal wave is generated by an exploding reflector segment around the normal-incidence-point. The normal-incidence-point wave is triggered by a point source at the normal-incidence-point for a specific reflector. The three wavefront attributes α , R_N and R_{NIP} are determined by means of coherency analysis (e.g. Mann, 2003; Taner and Köhler, 1969).

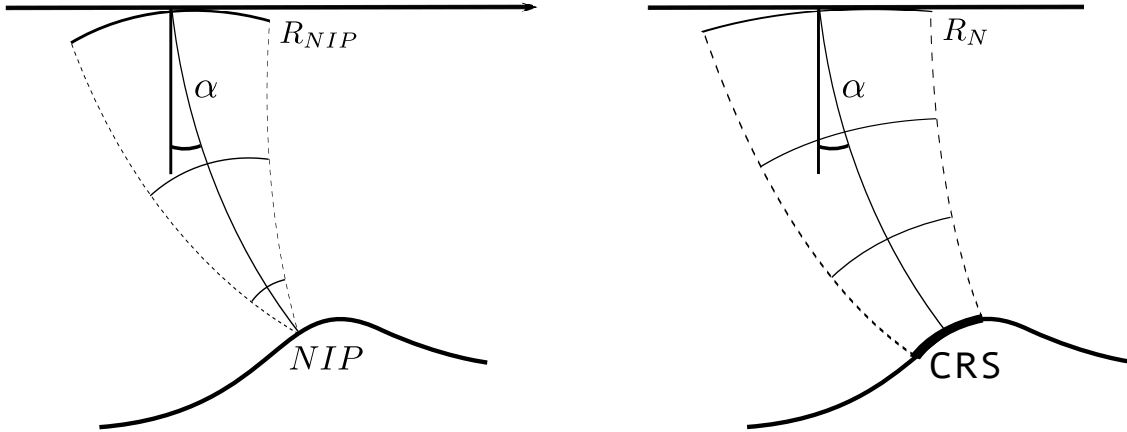


Figure 2.3.: The three CRS wavefront attributes α , R_{NIP} and R_N . The emergence angle of the ZO ray is denoted by α . The resulting two fictitious waves are described by α and the corresponding radii of curvature, R_N for the normal (N) wave and R_{NIP} for the normal-incidence-point (NIP) wave. The normal wave is generated by a fictitious exploding reflector model around the normal-incidence-point. The normal-incidence-point wave is generated by a fictitious point source at the normal-incidence-point for a specific reflector. (after Schwarz et al. (2014))

The main advantage of the CRS operator is that it stacks the seismic traces along neighboring midpoints as well as the offset direction in the time-midpoint-(half-)offset space, that is to use the entire stacking surface while the NMO/DMO approach uses only a trajectory in the time-(half-)offset plane. This means that, in contrast to conventional stacking, the CRS stacking operator spatially extends over several CMP gathers and approximates the reflection response of a whole reflector segment. In this way, an increased number of traces contribute to the stack which leads to a significantly improved S/N ratio in the simulated ZO section. At the same time, a whole set of stacking parameters, the so-called kinematic

wavefront attributes, is obtained for each simulated ZO sample. In this case, no interpolation of these parameters is required as far as stacking itself is concerned. Figure 2.4 shows the common reflection stacking (CRS) surface and CRP trajectory in the time-midpoint-(half-)offset volume. The blue curves in the upper part of the pictures represent reflection traveltime curves for fixed source-receiver offsets for the dome-like reflector in the lower part. The green lines indicate the CRS stacking operator for the ZO sample P_0 which approximates the reflection response of the red reflector segment around the Common-Reflection-Point (here set up by means of neighbouring CRP trajectories). The CRP trajectory (denoted by purple curve) connects all points in the time-midpoint-offset volume which belong to a common reflection point in depth.

In the next section, I will present a new prestack time migration technique and some practical aspects during implementation.

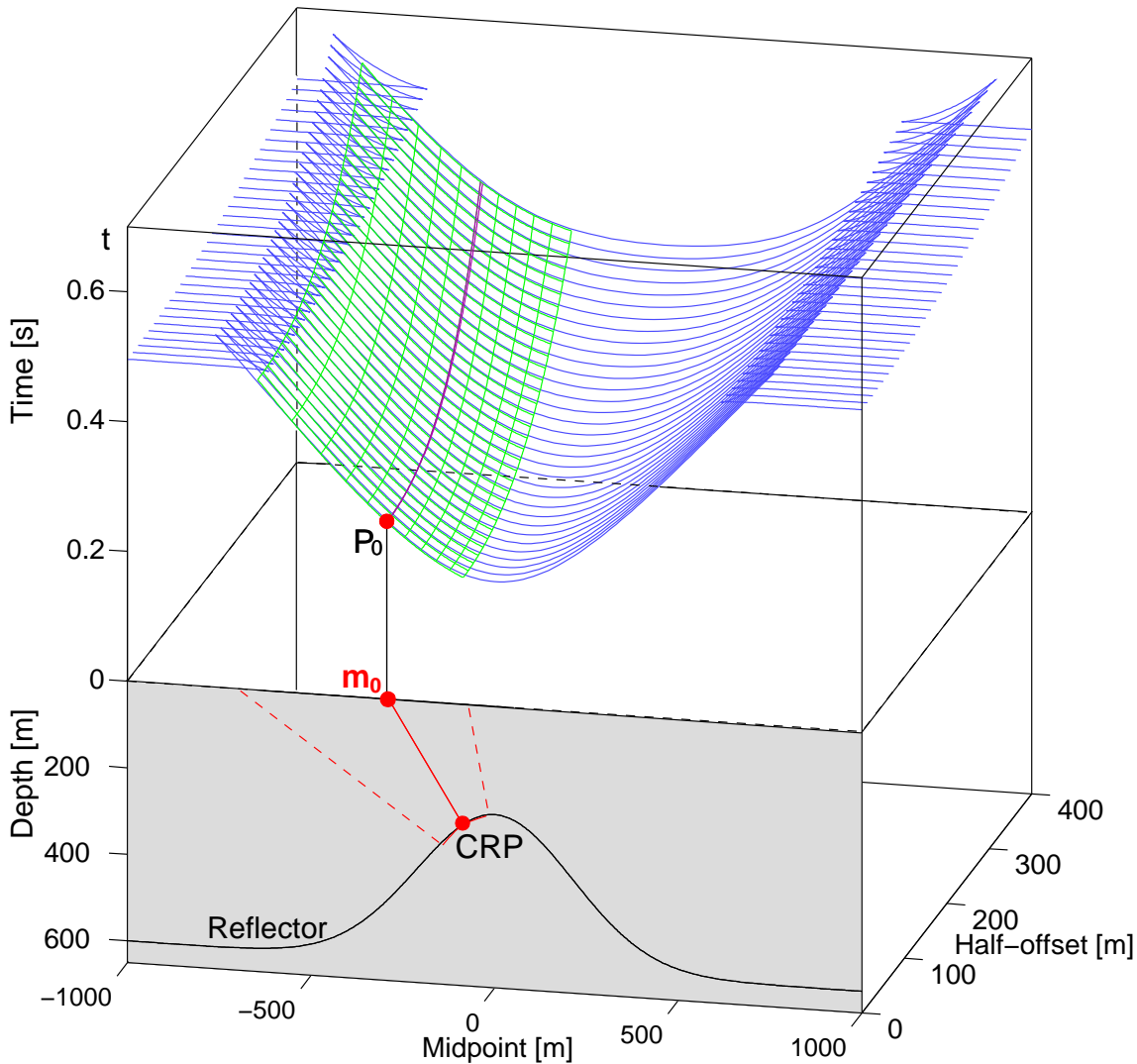


Figure 2.4.: CRS stacking operator in the time-midpoint-(half-)offset volume. The blue curves in the upper part of the pictures represent reflection traveltimes for fixed source-receiver offsets for the dome-like reflector in the lower part. The green lines indicate the CRS stacking operator for the ZO sample P_0 which approximates the reflection response of the red reflector segment around the Common-Reflection-Point (here set up by means of neighbouring CRP trajectories). The CRP trajectory (denoted by purple curve) connects all points in the time-midpoint-offset volume which belong to a common reflection point in depth. (after Müller (1999))

2.3. Prestack partial time migration

As elaborated in section 2.1, for media showing mild to moderate lateral velocity variations, prestack time migration (PreSTM) is a classical tool for subsurface imaging because it is fast, robust and rather insensitive to velocity model errors. The conventional time migration operator is described by a double square root (DSR) equation (see Equation 2.1) (see, e.g., [Yilmaz, 2001](#)). This type of operator implies a straight ray approximation using constant velocities. Assuming that lateral velocity variations are moderate, root mean square (RMS) velocities provide a suitable model. However, these are not generally available. Instead, stacking velocities can be considered as a starting model, and further processing, e.g., normal moveout (NMO) or dip moveout (DMO) (e.g., [Sheriff and Geldart, 1982](#); [Yilmaz, 2001](#)) is applied to refine the velocities. In practice, this means that time migration is carried out for common-offset data (e.g., [Ferber, 1994](#)), corresponding to a 'partial' migration (see Figure 2.5), which is followed by inverse normal moveout analysis ([Robein, 2010](#)). The time migration velocities are further addressed in the next section. [Bancroft et al. \(1998\)](#) expanded the method of migration from multiple offset to the equivalent offset by reformulating the DSR operator into a single square root equation and gave a theoretical explanation for the generated gathers, which he introduced as common scatter point (CSP) gathers. In both methods, the partially migrated common-offset gathers are focused in a procedure similar to NMO, i.e., by performing a stack over the offsets.

In order to preserve the moveout during the partial time migration, [Dell et al. \(2012\)](#) proposed a new prestack time migration method by parametrising the DSR operator with the apex of the diffraction traveltimes for each offset,

$$t_{apex} = \sqrt{t_0^2 + \frac{4h^2}{v^2}} \quad . \quad (2.3)$$

Substituting Equation 2.3 into Equation 2.1, after some simple algebra I obtain the partial time migration operator,

$$t_D(t_{apex}, m, h) = \sqrt{\frac{t_{apex}^2}{4} + \frac{m(m-2h)}{v^2}} + \sqrt{\frac{t_{apex}^2}{4} + \frac{m(m+2h)}{v^2}} \quad . \quad (2.4)$$

Note that both operators 2.1 and 2.4 provide the same diffraction response. The difference lies only in the parametrisation. The advantage of Equation 2.4 against Equation 2.1 is the preservation of the moveout in the data, which is demonstrated in Figure 2.5(a). Like in Figure 2.2, the light blue and the dark blue surfaces illustrate

the reflection and diffraction traveltimes, respectively. In contrast to the magenta line in Figure 2.2, which points out t_0 , I recognise in Figure 2.5(a) that the moveout is preserved. It is represented by the orange (red) line, which, in fact, constitutes the new prestack trace for the midpoint under consideration.

In the techniques suggested by Ferber (1994) and Bancroft et al. (1998), these prestack traces are stacked along the (half) offsets by taking the moveout into account.

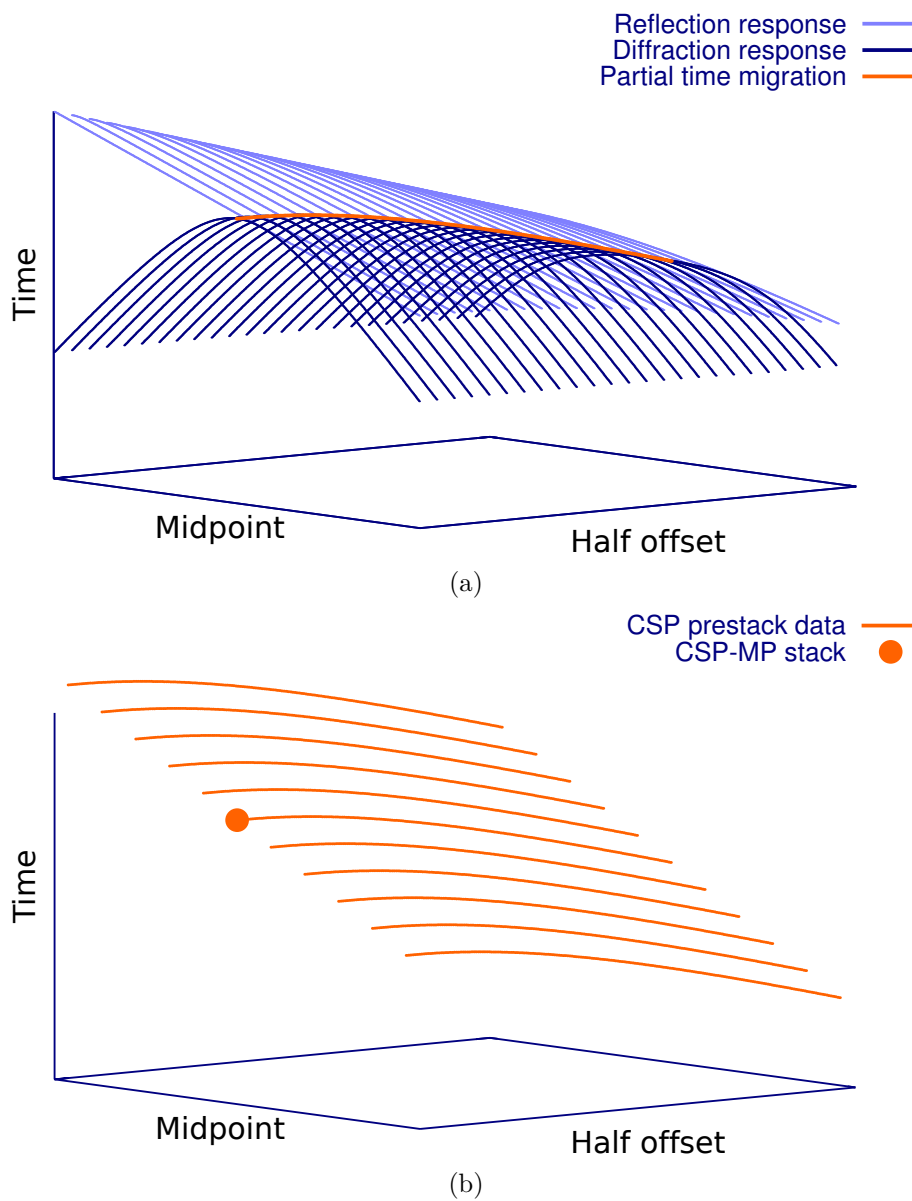


Figure 2.5.: (a) partial time migration, (b) multi-parameter (MP) stacked CSP data. (after Dell et al. (2012))

The proposed method does not follow that approach. Instead, new prestack traces for all midpoints are generated, as pointed out by the orange (red) lines in Figure 2.5(b). These constitute the prestack data in the CSP domain.

While Ferber (1994) and Bancroft et al. (1998) apply a single parameter stack over offsets, Dell et al. (2012) suggest to apply a multi-parameter (MP) stack over offsets as well as midpoints. By doing so, the desired prestack data enhancement is achieved because the number of contributing traces is much higher than for the single parameter stack over h .

The output of the MP stack is then, like for the time migration, assigned to the point (t_0, m, h) , depicted by the orange (red) circle in Figure 2.5(b).

If the same parameters, i.e., velocities and apertures, are applied, both conventional PreSTM and CSP-MP stack are kinematically equivalent. However, due to the data enhancement ability of the latter method, it results in a higher signal-to-noise level and thus better image quality.

2.4. Practical aspects

In this section, some practical remarks regarding e.g., choosing apertures and velocities are given. One should consider these remarks deliberately before performing migration (and/or stack).

2.4.1. Migration apertures

The reliability of migration image quality in Kirchhoff migration strongly depends on the selection of the migration aperture (Schleicher et al., 1997). From a theoretical point of view, the aperture should be limitless for noise-free data to avoid artifacts caused by the abrupt truncation of the migration operator. In practical implementations, the aperture is always limited by the finite acquisition area and recording time. Usually, a taper is applied to reduce aperture-related boundary effects. In general, a user-defined aperture is employed which linearly increases with depth or time of the image location.

For proper prestack migration of seismic data, appropriate migration apertures need to be estimated that can take care of structural dips and fault definitions. Both a strong underestimation and overestimation of the optimal aperture size lead to deteriorated and even meaningless migration results, so it is crucial to choose

the correct migration aperture. Small apertures can produce a poor image due to the destruction of steeply dipping events and can organise random noise signals as horizontal events, while large apertures unnecessarily increase the computational time and produce artefacts and migration noise. The optimum migration aperture can be estimated from data (Schleicher et al., 1997). Optimal apertures mean a balance between the computational cost and the quality of migration results.

For prestack migration, one has to consider both midpoint and offset apertures, while poststack migration requires only midpoint apertures. The size of the offset apertures is often determined by the offset-to-target ratio. This is a good approximation because for a stratified medium the assumption of a hyperbolic travel time curve is valid in that range. The target-to-depth can be estimated with a starting velocity model and the ZO traveltimes. The midpoint apertures are not as easy to determine as the offset apertures. Many authors (see, e.g., Hertweck et al., 2003; Sun, 1998; Schleicher et al., 1997) suggest the size of the first (projected) Fresnel zone as optimal midpoint aperture. The first Fresnel zone is defined in the following way, for example by Sheriff (1980): it is a portion of a reflection of a reflector from which reflected energy can reach a detector within the first one-half cycle of the reflection. The criterion for the minimum migration aperture is that the difference of the traveltimes of the computed diffraction curve and the reflection curve should be less than half a period $T/2$ of the signal, as the equation below shows:

$$|t_d - t_r| \leq \frac{T}{2} \quad , \quad (2.5)$$

where t_d denotes the diffraction travel time, t_r denotes the reflection travel time and T is the predominant period. It provides a constructive summation of the energy for the first Fresnel zone. The energy is added destructively for the second Fresnel zone and added constructively again for the third Fresnel zone and so on. Schleicher et al. (1997) define the projected Fresnel zone as the region at the surface which pertains to the bundle of reflected rays that reflect within the true first Fresnel zone. The Fresnel zone changes for inclined or curved reflectors and the centre is shifted. For diffraction imaging the size of the Fresnel zone is not a good approximation for the midpoint aperture therefore larger apertures are required. In practice, the proper choice of migration aperture is usually achieved after a series of migration experiments with different values, finally choosing the one that produces the best image.

Several authors (see, e.g., Schleicher et al., 1997; Sun, 2000; Vanelle and Gajewski, 2001; Spinner, 2007) also suggest to restrict the aperture to the smallest possible size yet still covers the part of the migration operator constructively contributing in

the summation. Take the work of [Spinner \(2007\)](#) for example, they determine the minimum migration aperture in two steps:

- determination of the constitution of the stationary point that defines the centre for the migration aperture;
- estimation of the size of the projected Fresnel zone which controls its horizontal extension.

Minimum-aperture migration is advantageous with respect to both the efficiency of the migration process and the quality of the migration result ([Spinner, 2007](#)). Also, once minimum aperture is determined, boundary effects can be recognised ([Vanelle and Gajewski, 2001](#)).

2.4.2. Apertures for CRS stack

The CRS stacking operators are approximations of the kinematic reflection responses of curved interfaces in a paraxial vicinity of the central ray under consideration. Therefore, it is necessary to define an appropriate aperture inside of which the approximation is sufficiently accurate ([Mann, 2003](#)).

Apertures for the CRS parameter search and for the stacking might be different. For obtaining optimum CRS parameters, too large apertures means that the hyperbolic traveltimes approximation may lose its validity, while too small apertures can deteriorate the quality of the CRS parameters searched.

For the stacking procedures, the choice of midpoint and offset apertures depends on the data we are processing, and is often determined after some tests with different values. The size of the offset apertures is often determined by the offset-to-target ratio. The choice of midpoint apertures are not as easy to determine as the offset apertures, and it depends on the purpose of the processing. If we want to delineate small objectives, e.g., diffraction, then large apertures should be chosen. If the media is relatively layered, small apertures can be chosen.

Similarly, a user-defined taper is applied to reduce aperture-related boundary effects.

2.4.3. Velocities

Like all migration methods, Kirchhoff migration requires the knowledge of the velocity distribution. A variety of velocity estimation methods is available. In conventional processing, Kirchhoff time migration is usually parameterised in terms of root-mean-square (RMS) velocities defined at the apex of the migration operator. This is strictly valid only for 1D media (a single horizontal layer with constant velocity), otherwise, the required migration velocity constitutes a “best-fit” parameter. These velocities are usually determined from stacking velocities (Yilmaz, 2001). For 1D case, the traveltimes curve for one CMP gather constitutes a hyperbola if displayed as function of source-receiver offset, and the stacking velocities obtained from stacking velocity analysis in a CMP gather are sufficient to construct a 1D interval velocity model by applying Dix inversion (Dix, 1955).

Nevertheless, in case of gentle dips and moderate lateral velocity variations, a hyperbolic approximation is still applicable if the maximum considered offset is small. For a horizontally stratified medium with constant layer velocities, normal moveout (NMO) velocities or stacking velocities equals the root-mean-square (RMS) velocities (Bancroft, 1998). The so-called dip moveout correction (DMO) (e.g., Sheriff and Geldart, 1982; Yilmaz, 2001), which is an extension to the NMO correction, is applied when dips are present. In principle, the definition of NMO and stacking velocities slightly differs: while NMO velocities are based on a small-spread traveltimes assuming horizontal layers, stacking velocities are defined for the hyperbola that fits best over the entire stacking aperture range. However, this difference is often ignored in practice.

For more laterally inhomogeneous media and reflector geometries, the behaviour of the traveltimes curve gets quite complicated, and migration velocities deviate from the stacking velocities, thus more sophisticated methods need to be applied. In order to correct the difference between time migration velocities and stacking velocities, the velocity model is iteratively refined.

Conventional time migration velocity analysis (MVA) is either carried out as an iterative approach based on residual moveout analysis (RMO) or utilises a scanning routine similar to stacking velocity analysis (see, e.g., Robein, 2003). The RMO routine usually starts with an initial velocity field which is set up using the stacking velocities determined by means of a conventional stacking velocity analysis. Selected image gathers are constructed using prestack time migration which usually show residual moveout. Afterwards, an inverse NMO correction is applied using the initial velocities. The gathers then enter into a classical stacking velocity analysis which yields an updated migration velocity model. As the velocity analysis is usually carried out on a rather coarse grid, the velocities have to be interpolated on the migration grid. The RMO chain may be iterated to refine the velocity field.

In contrast, the scanning approach tests for a set of velocities or velocity functions at the same time. The best result is determined on the basis of common image gather (CIG) (see, e.g., Claerbout et al., 1996) flatness and interpretative criteria. CIGs are gathers containing the offset dependent migration result for a fixed lateral location. The correct velocity produces an image, where the CIG is flat. Either overestimating or underestimating the velocity can result in bad migration results. When one considers diffractions, one can see "smiles" and "frowns" in the migrated section. If the considered velocity is too large one obtains a "smile". If it is too small one obtains a "frown". These "smiles" and "frowns" as well as the residual moveout resulting from the CIG's are used to update the velocity model until the migration image is satisfying. The approach is rather compute-intensive as several full prestack time migrations have to be performed. However, it provides better results compared to the RMO routine if a wide range of different velocities is tested.

Fomel (2003) proposed a time migration velocity analysis technique by taking into account both vertical and lateral movement of the reflection events in seismic images with the changes of migration velocity.

Mann et al. (2000) and Mann (2002) suggested a method to determine time migration velocities for the 2D case based on the fact that the CRS operator allows to estimate an approximate diffraction response, the kinematic wavefront attributes defined at the stationary point for ZO can be mapped into the apex of the corresponding diffraction operator and serve as input for the determination of time migration velocities. Spinner (2007) states that although the migration velocity derived from the wavefield attributes does not exactly provide the required "best-fit" time migration velocities from the true diffractor response with the DSR operator, the CRS-based velocity model building is attractive as the obtained migration velocities are defined at their correct locations and provide a good estimate of the searched-for values. Velocity values are obtained for each (reliable) attribute set which can be extracted by means of the automatic picking procedure. The velocity model building itself is straight-forward and can be applied in a highly automated manner.

Furthermore, authors (see, e.g., Schwarz et al., 2014; Glöckner et al., 2015) obtain time migration velocities by relating and applying the technique by Mann et al. (2000) the kinematic wavefront attributes obtained from the implicit CRS operator, of which the incidence angle α and the radius of curvature of the so-called normal incidence point (NIP) wave, R_{NIP} are pertinent to this work. The equation reads:

$$V = \frac{v_{NMO}}{\sqrt{1 + \frac{v_{NMO}^2}{v_0^2} \sin^2 \alpha}}$$

with $v_{NMO} = \sqrt{\frac{2v_0 R_{NIP}}{t_{apex} \cos^2 \alpha}}$. (2.6)

where V denotes the time migration velocities and t_{apex} is the apex travelttime. Equation 2.6 includes the normal move out (NMO) velocity , v_{NMO} . Besides, by considering the incidence angle, a dip correction is obtained. This means, they receive root-mean-square (RMS) like velocities which make them directly applicable for time migration. In their case the velocities (Equation 2.6) depend on four parameters: α , R_{NIP} , a prescribed near-surface velocity v_0 , and the considered time t_{apex} . The kinematic wavefront attributes here are obtained after the i-CRS stack. In fact, any operator of the multi-parameter stacking family can provide the wavefront attributes.

2.4.4. Amplitudes

While the wave propagates through the medium, its initial energy is "spreading" on the expanding wavefront, causing a decrease in the wave amplitudes. This phenomenon is called geometrical spreading. Although migration is already a very powerful tool to enhance image quality, there is one aspect that also matters: amplitudes. The conventional diffraction stack migration produces "only" an image of reflectors in the subsurface, whereas in a modified diffraction stack, specific weight functions are applied which compensate the effect of geometrical spreading, thus recovers the reflection amplitudes. This processing is named true-amplitude migration or amplitude-preserving migration (see, e.g., [Hubral, 1983](#); [Vanelle and Gajewski, 2002](#); [Spinner, 2007](#)). From an analysis of amplitude variation with offset (AVO) (see, e.g., [Mosher et al., 1996](#)) or reflection angle (AVA), conclusions can be drawn on the elastic properties of the medium and anomalies that might indicate gas or oil accumulation. In this work, I consider only kinematic aspect, thus the amplitudes are beyond the scope of this thesis.

2.4.5. Smoothing of attributes

Time migration needs smooth velocity model. Therefore, the attributes are expected to vary smoothly along the reflection event in lateral direction as long as the paraxial

approximation is valid. As the attributes are independently determined for each ZO sample, this might not always hold and unwanted fluctuations and outliers might occur which deteriorate the attributes. Within the event-aligned window, local statistics can be applied to determine reliable attributes. [Duveneck \(2004\)](#) suggested an event-consistent smoothing algorithm which applies a combined median filtering and averaging filter for each ZO sample and CRS parameter to remove such fluctuation and outliers.

In the following sections, I follow the approach by [Dell et al. \(2012\)](#) and apply the partial time migration as well as a subsequent multi-parameter stack to a complex synthetic Sigsbee 2A data set and a marine field data set to show that the proposed method leads to considerable improvement of the image quality compared to conventional time migration. This has already been published by [Yang et al. \(2014\)](#).

2.5. Synthetic data example

We have applied the partial time migration plus a MP stack method to the synthetic Sigsbee 2A data set. Sigsbee 2A is a constant density acoustic data set released in 2001 by the "SMAART JV" consortium. Sigsbee 2A models the geologic setting of the Sigsbee Escarpment in the deep water Gulf of Mexico. The data is isotropic and without multiples. In the left part of the model, a number of normal and thrust faults separate the sedimentary blocks, and diffractions are caused by scatter points. Furthermore, two lines of point diffractors are embedded in a horizontal layering of sediments at the lower left part. The model contains a large irregularly-shaped salt body in the right part, which causes strong diffractions. The syncline segments of the top of salt focus reflection energy from the bottom of salt and the subsalt reflections and produce non-hyperbolic arrival traveltime curves. The velocity model is displayed in [Figure 2.6](#). Velocities of the sediments vary from 1500 m/s at the seafloor up to 3500 m/s at the bottom of the sediments. The velocity of the salt is 4500 m/s. The most important acquisition parameters are summarised in [table 2.1](#).

In this thesis, I apply the partial time migration method to the data. I add a random noise with a signal-to-noise ratio of eight to the synthetic data set in the following tests. [Figure 2.7](#) shows the CMP stack of the data. I recognise the sedimentary part been separated by a number of faults at the left part and the upper right part as well. I also observe the diffractions at the salt body area. Several weak events below the salt body can be seen.

In a first test, I applied RMS velocities obtained from the velocities shown in [Figure 2.6](#). I perform conventional PreSTM as well as for the generation of the partially

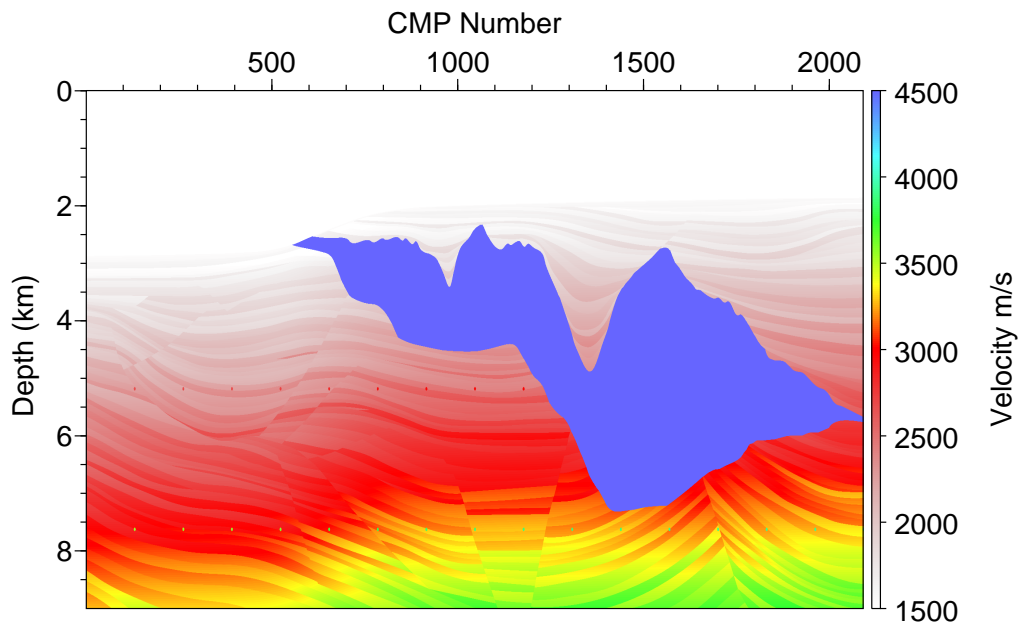


Figure 2.6.: Velocity model for Sigsbee 2A data set, which contains a large irregularly-shaped salt body.

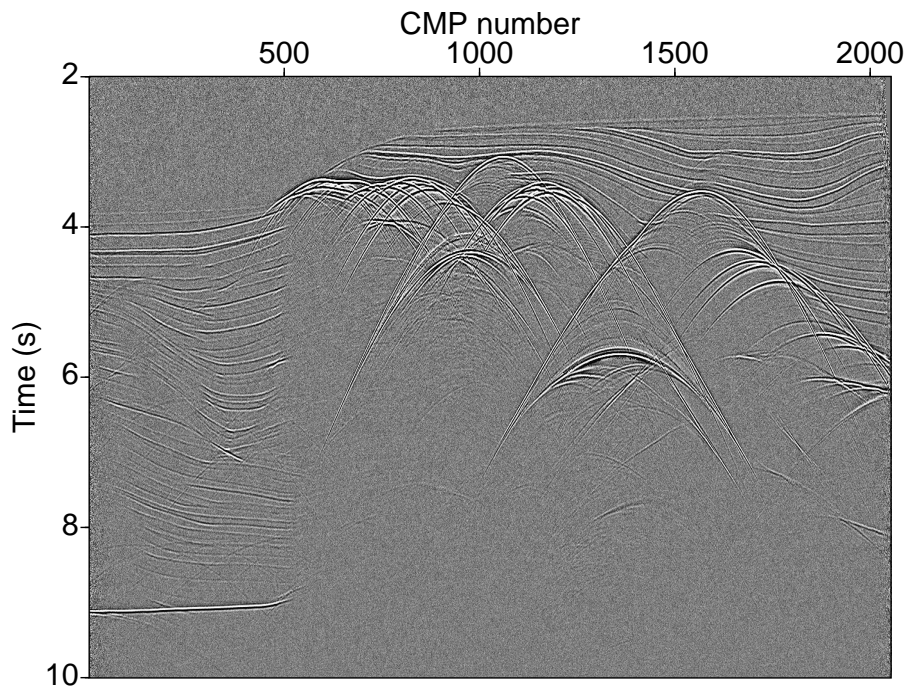


Figure 2.7.: CMP-stacked section of the Sigsbee 2A data set with random noise. Several weak events are present below the salt.

Shot and receiver geometry	
Number of shots	500
Shot interval	45.72 m
Number of receivers	348
Receiver interval	22.86 m
Midpoint and offset geometry	
Number of CMP bins	2053
Maximum CMP fold	87
CMP bin spacing	11.43 m
Minimum offset	0 m
Maximum offset	7932 m
Recording parameters	
Recording time	12 sec
Sample interval	8 ms
Frequency contents	
Dominant frequency	20 Hz
Peak frequency	40 Hz

Table 2.1.: The main acquisition parameters of Sigsbee 2A model.

time-migrated CSP gathers. On the latter, I executed a multi-parameter stack of the CRS type (Mann, 2002) to the new prestack data in order to obtain the final section. Figure 2.8 shows a conventional PreSTM section of the data with RMS velocities and Figure 2.9 shows the result of the MP-stacked partially time-migrated gathers. Note that I have used the same parameters, e.g. velocities and apertures, for both methods (see Appendix A.2 for detailed parameters). I find that the overall image quality of the suggested method is better than that of the conventional PreSTM technique. Diffractions in Figure 2.9 are more focused than in Figure 2.8, e.g., the first line of point diffractors at around 6.2 s at the left sedimentary part.

However, RMS velocities are usually not available in the real world. Hence, I tested our method followed Equation 2.6 by using stacking velocities estimated from a CRS stack of the original data by Equation 2.6, and repeated the previously-described procedure with these velocities instead of the RMS velocities. Again, the same parameter sets were used for both methods. Figures 2.10 and 2.11 show the respective results. Again, I recognise the better image quality of the CSP-MP stack over the PreSTM result. Both migrated images show collapsed diffractions and a well imaged reflection. However, with the CSP-MP method, I obtain an image with higher signal-to-noise ratio comparing with the PreSTM result.

For a more detailed investigation of the properties of the two methods, I have chosen three regions with different structural features from the comparisons of Figure 2.10

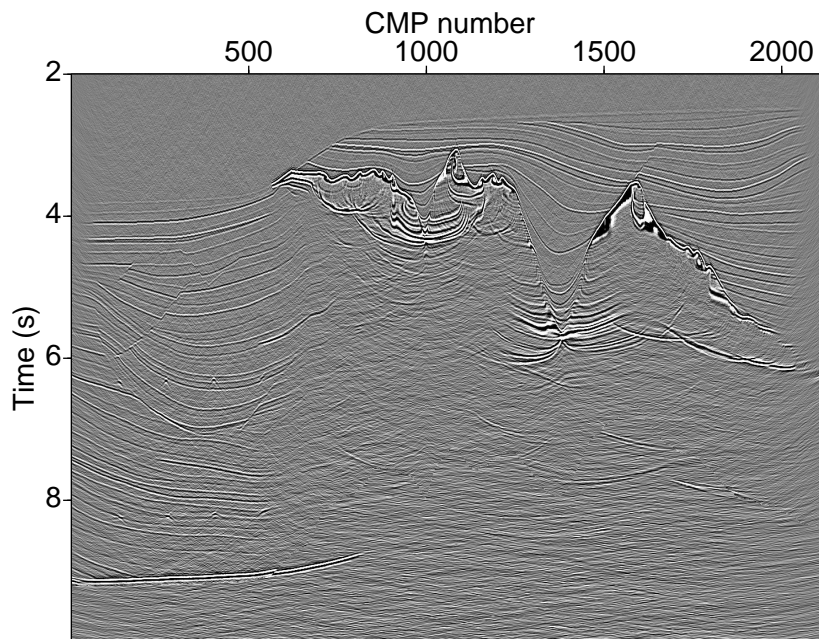


Figure 2.8.: Prestack time-migrated section of the Sigsbee 2A data set with random noise using RMS velocities provided with the data set.

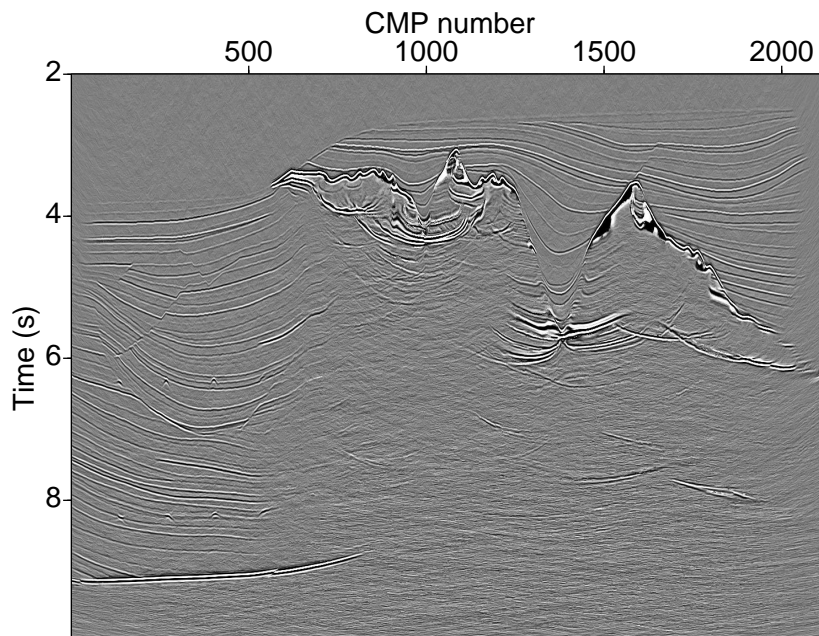


Figure 2.9.: CSP-MP-stacked section of the Sigsbee 2A data set with random noise using RMS velocities provided with the data set.

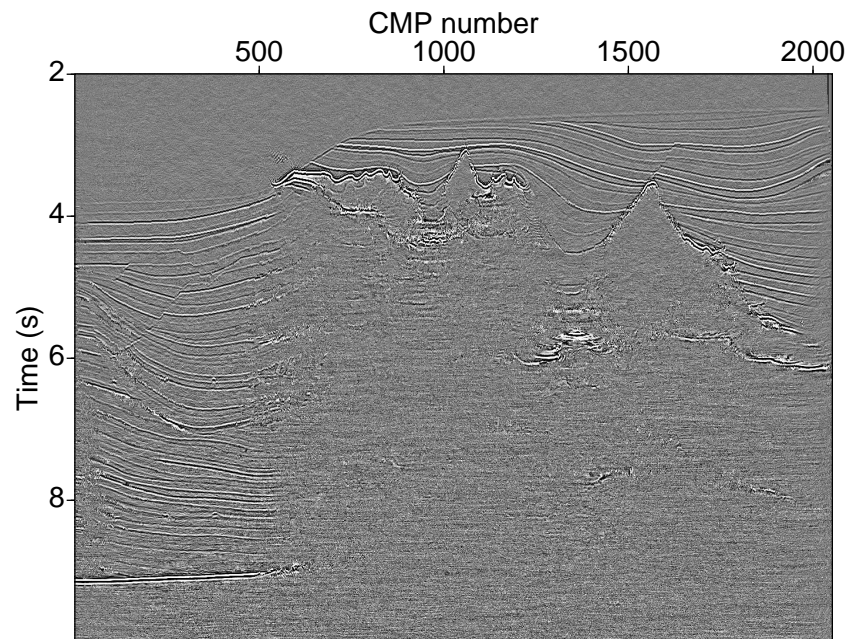


Figure 2.10.: Prestack time-migrated section of the Sigsbee 2A data set with random noise using stacking velocities determined from a CRS stack of the data.

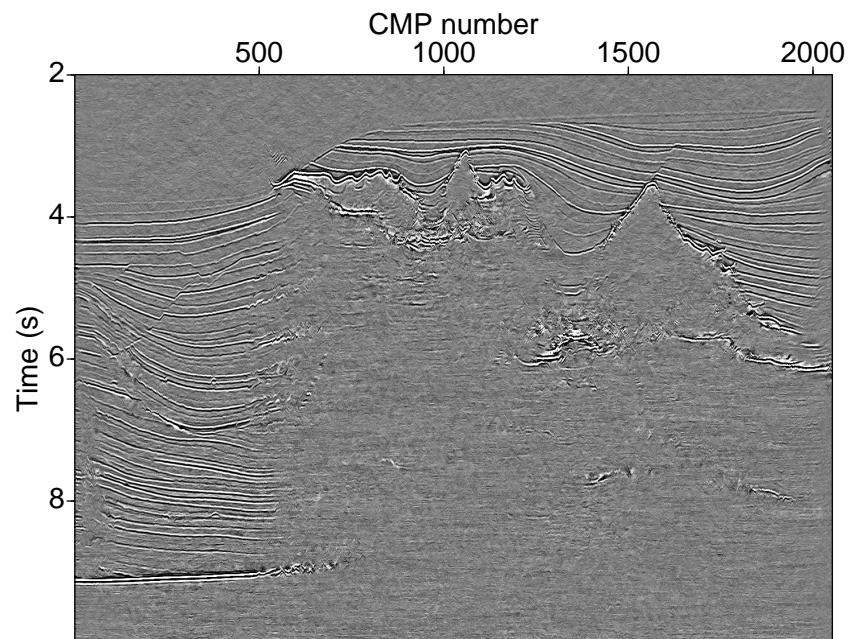


Figure 2.11.: CSP-MP-stacked section of the Sigsbee 2A data set with random noise using stacking velocities determined from a CRS stack of the data.

and Figure 2.11, as indicated by the white boxes in Figure 2.12.

The first close-up in Figure 2.13 reveals that the CSP-MP stack leads to better continuity of reflections and higher resolution of faults and diffractions. There are noise in both images, this is due to the fact that I didn't smooth the velocities in all 2D tests. Even though, we still can see the superiority of the method.

The imaging of salt bodies is always a challenging endeavour in seismic data processing. The data quality below the salt is usually fairly low due to the strong acoustic impedance contrast between the salt and the surrounding sediments as well as due to the irregularity of their surfaces. Figure 2.14 shows the left part of the salt dome, a region with rugged topography. Again, I find higher resolution in the CSP-MP image, not only at the top of salt but also and particularly at the bottom of the salt. In addition, the overall continuity of the CSP-MP result is more pronounced..

Finally, in Figure 2.15, I recognise an enhancement of the events below the salt with higher S/N ratio.

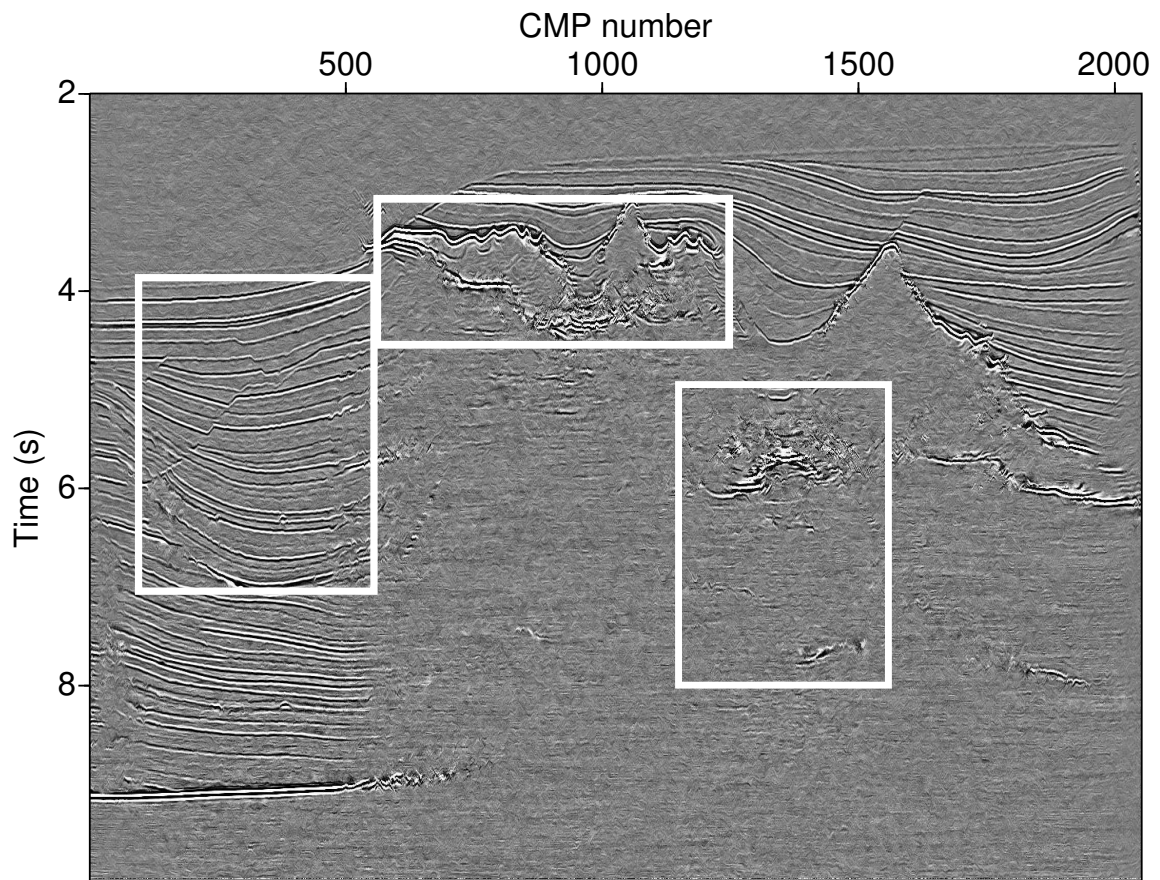


Figure 2.12.: Three selected regions with different structural features for a detailed investigation (see Figures 2.13, 2.14 and 2.15).

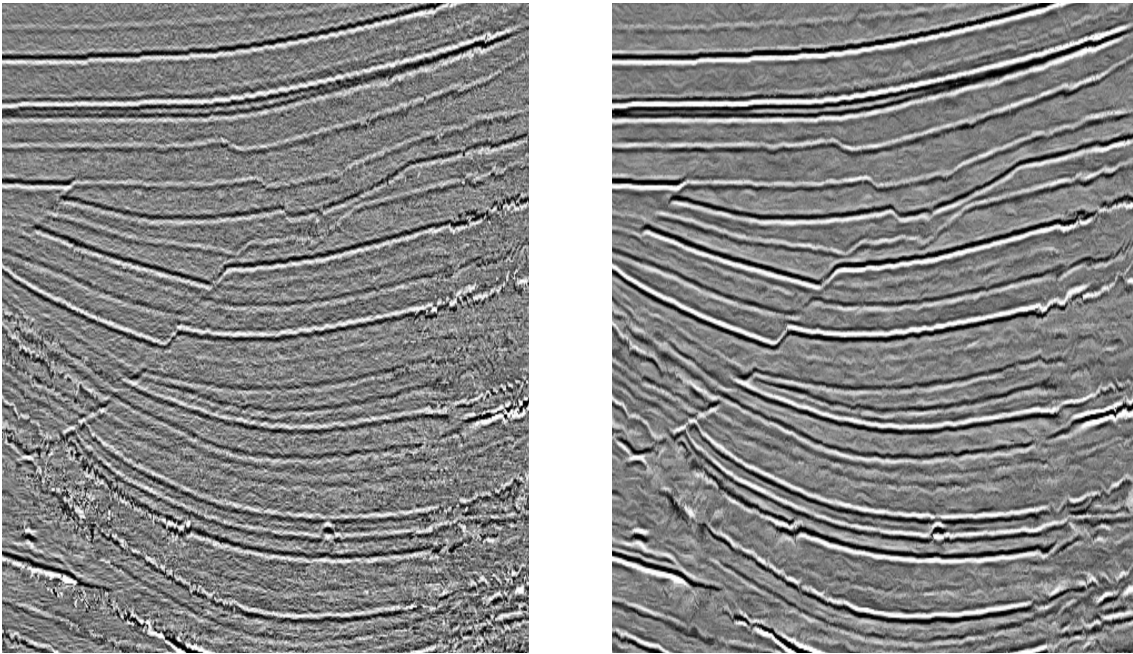


Figure 2.13.: Close-up: layering and fractures. Left: PreSTM result; right: CSP-MP result. I observe higher resolution, more continuous reflections, and more clearly-defined faults in the CSP-MP section.

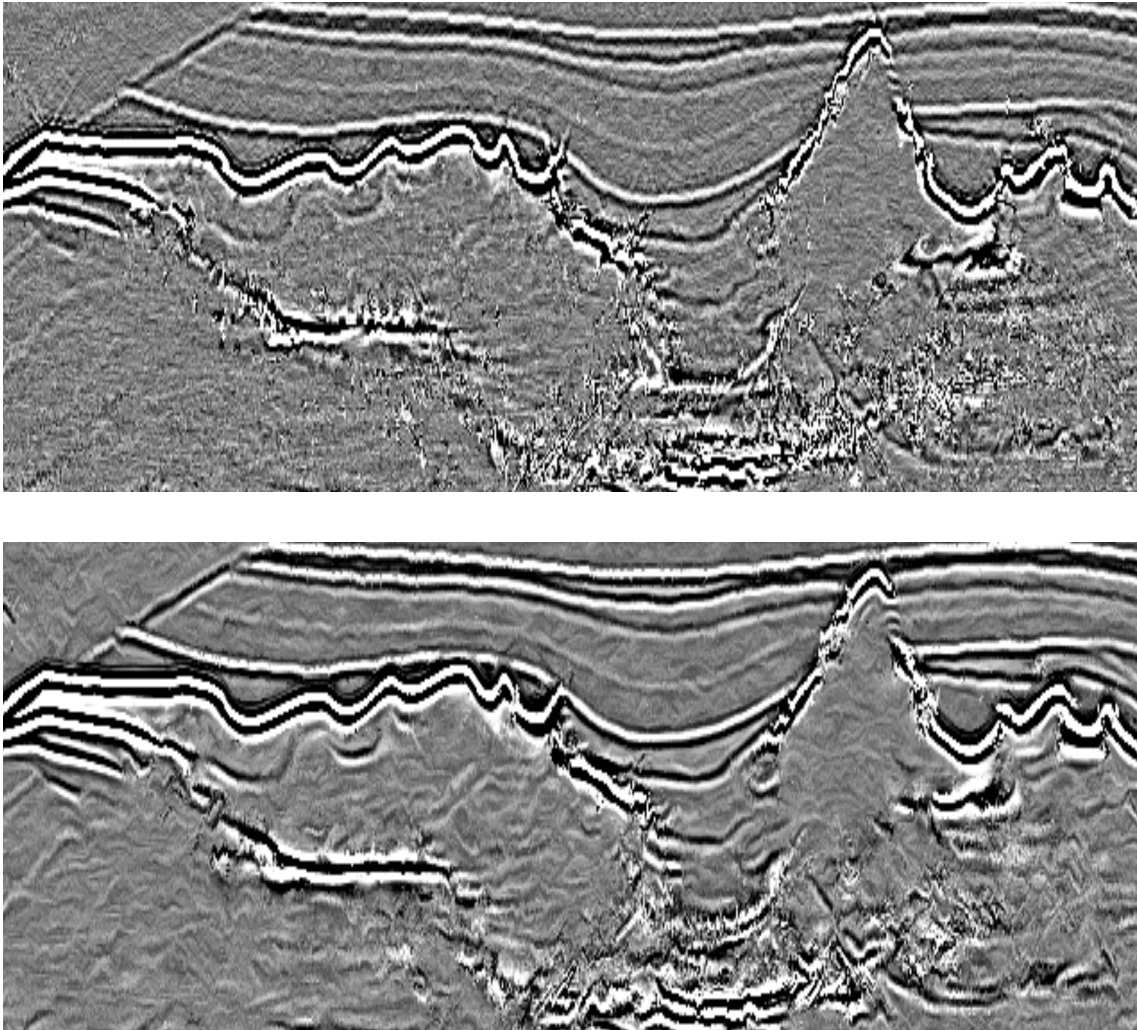


Figure 2.14.: Close-up: top of salt. Top: PreSTM result; bottom: CSP-MP result. I obtain higher resolution and a better definition of the top of the salt as well as the bottom of the salt. The overall continuity of the CSP-MP result is more pronounced.

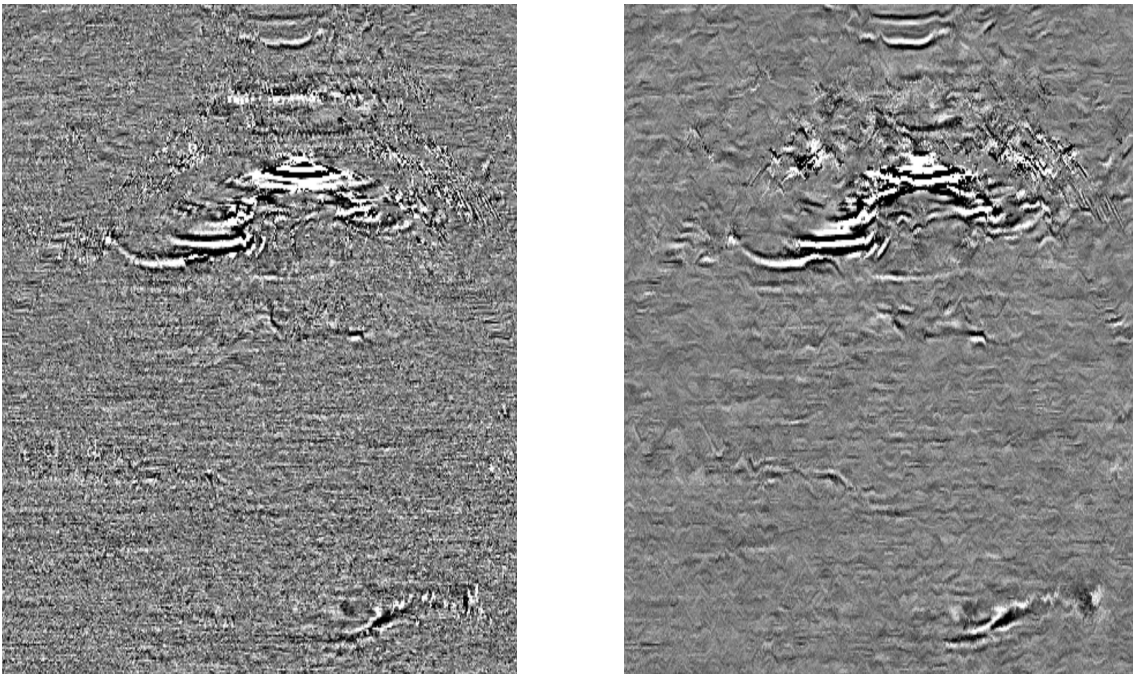


Figure 2.15.: Close-up: sub-salt. Left: PreSTM result; right: CSP-MP result. I obtain an enhancement for the subsalt region in the CSP-MP section compared to the PreSTM section.

2.6. Field data example

In this section, I demonstrate the application of the proposed imaging technique to a marine field data set from south-eastern Mediterranean Sea. The data was kindly provided by TGS company.

2.6.1. Study area

For a second and more realistic investigation, I have applied the method to a marine data set. The seismic data was acquired in the Levantine basin in the south-eastern Mediterranean Sea. I tested a seismic line out of this data. The approximate position is shown in Figure 2.16. The line was acquired from southeast to northwest. The basin is bounded by the Cyprus arc in the north, the Levantine coast in the east and the Egyptian coast in the south.

The Levantine Basin has a complex seismic stratigraphy of the basinal succession. The deformation pattern of the intra-evaporitic sequences include folds and thrust faulting, which gives evidence for extensive salt tectonics and shortening during the depositional phase. Post-depositional gravity gliding caused salt rollers in the extensional marginal domain, compressional folds, and faults within the Levantine basin (Dümmong and Hübscher, 2011). Figure 2.17 provides a structural overview of the seismic line. The seismic line is located in the extensional part of the basin, thus salt rollers emerge. Above the salt (orange) parallel pre-tectonic units (yellow) are identifiable. They are separated from the divergent syntectonic units (ochre) by a slump complex (grey). Note that this line shows the opposite direction of the following seismic sections.

A part of the data consisting of 2000 CMP gathers with a total line length of 15 km was chosen for the processing. A 2D acquisition with a shot spacing of 25 m and a receiver spacing of 12.5 m was performed. The minimum offset is 150 m, and the maximum offset is 7338 m. The record length is 8 s with 4 ms sample rate.

2.6.2. Results

Figure 2.18 shows the CMP stack of the original data up to 5 seconds. The water depth increases from left to right. The sediments under the seafloor are in some part horizontally layered and in some part with flower structures. The top of the salt is at 2.6 s at CMP 2000, the base of the salt at 3.2 s. I recognise many diffraction

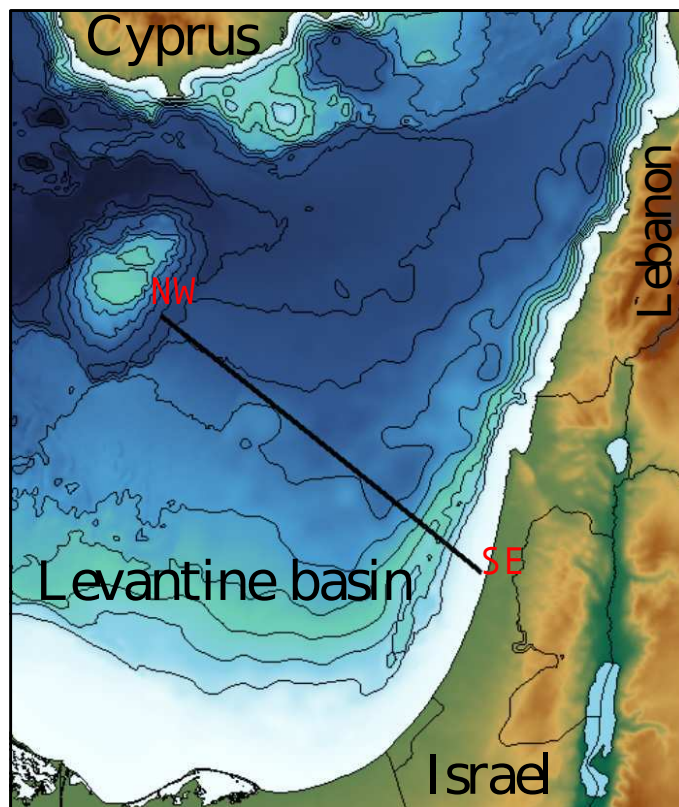


Figure 2.16.: The approximate position of our tested seismic line out of the marine data set acquired in the Levantine basin in the south-eastern Mediterranean Sea. (after [Bakhtiari Rad et al. \(2014\)](#))

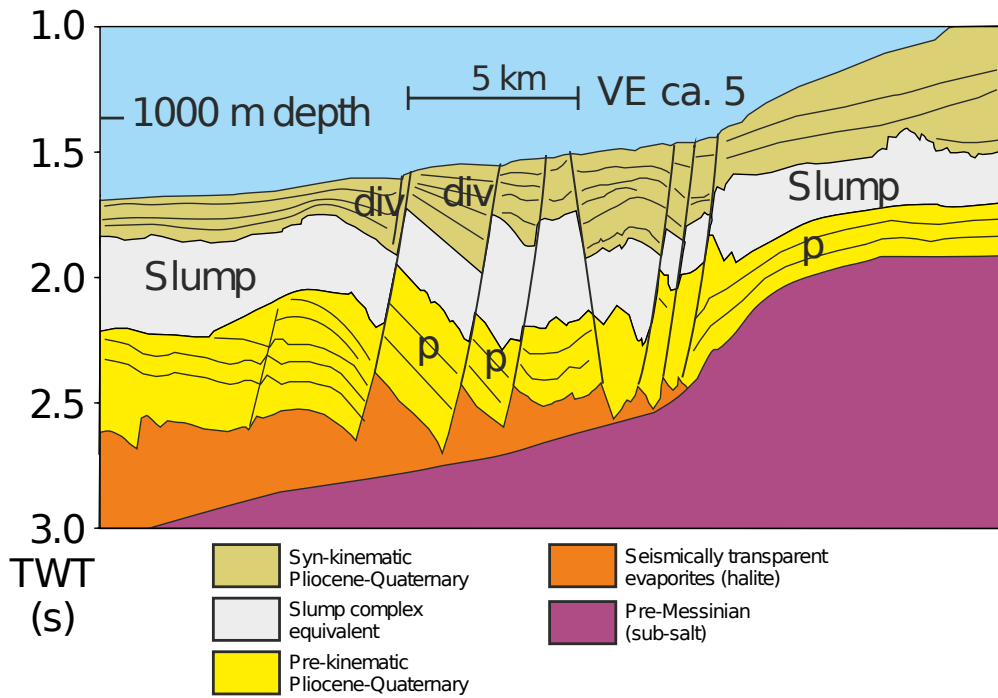


Figure 2.17.: Structural overview of the tested seismic line (Dümmong and Hübscher, 2011). Note that the following seismic sections show the opposite direction of this line.

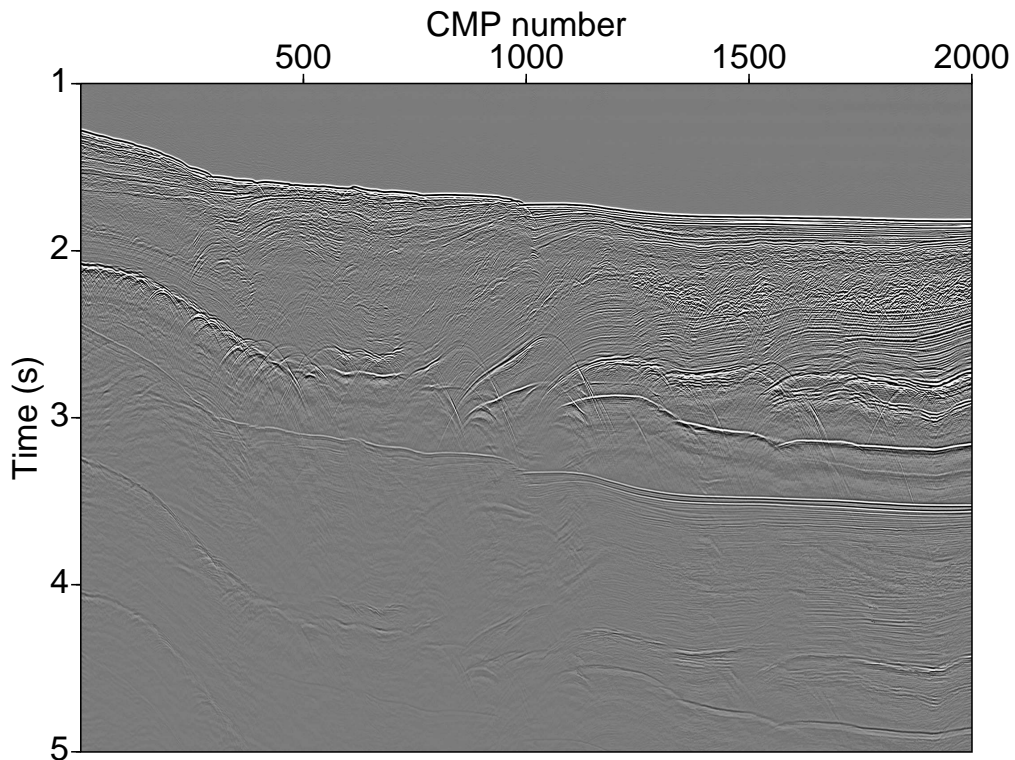


Figure 2.18.: CMP-stacked section of the marine field data set. The top of the salt is at 2.6 s at CMP 2000, the base of the salt at 3.2 s.

hyperbolas caused by the salt rollers in the left part. As usual for field data, one can observe the seafloor multiple and the multiple of the downward dipping reflection.

I used stacking velocities estimated from a CRS stack of the original data (see Equation 2.6), and repeated the previously-described procedure with these velocities to compare the results of the conventional PreSTM and CSP-MP methods. Note that I have used the same parameters, e.g. velocities and apertures, for both methods (for detailed parameters, please see Appendix A.3). Figure 2.19 and 2.20 show the PreSTM and CSP-MP results. Like for the complex Sigsbee 2A data results, I recognise the better image quality of the CSP-MP stack with higher S/N ratio and better continuity of the events comparing to the PreSTM result. Although this is not as significant as for the synthetic data result comparison.

A close-up on the salt rollers (see Figure 2.21 for the excerpted part) in Figure 2.22 provides a more detailed investigation. It reveals that the CSP-MP stack leads to better collapsed diffractions at the left part where the downward dipping reflection merges into the salt rollers. Better resolved salt flanks are achieved where the triangle structures exist in the middle and right parts. Furthermore, the subsalt region exhibits clearer events.

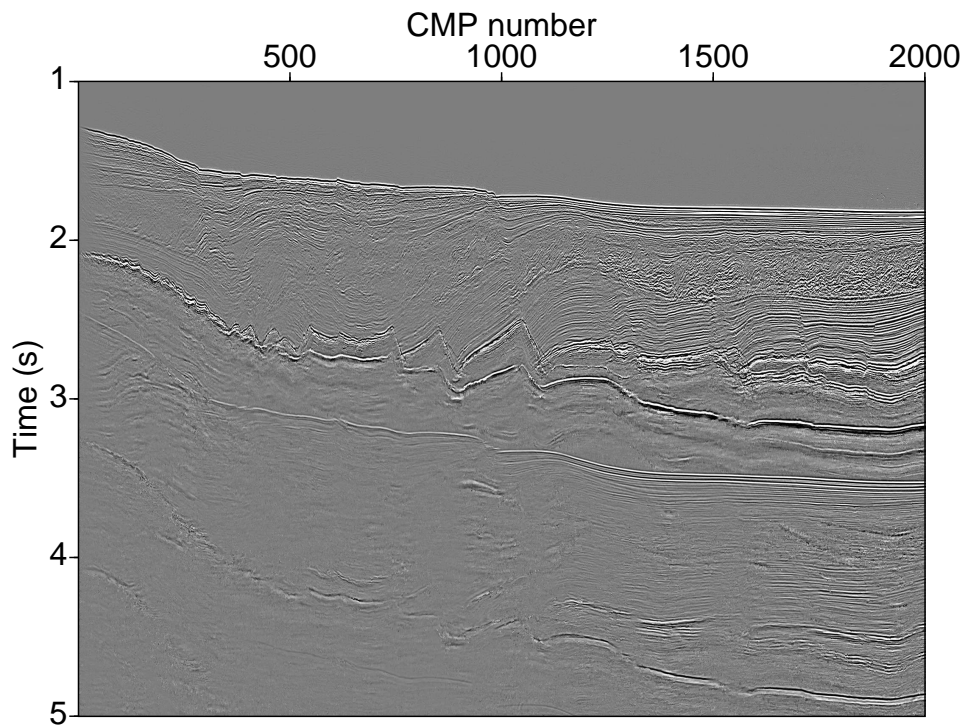


Figure 2.19.: Prestack time-migrated section of the marine field data set using stacking velocities determined from a CRS stack of the data.

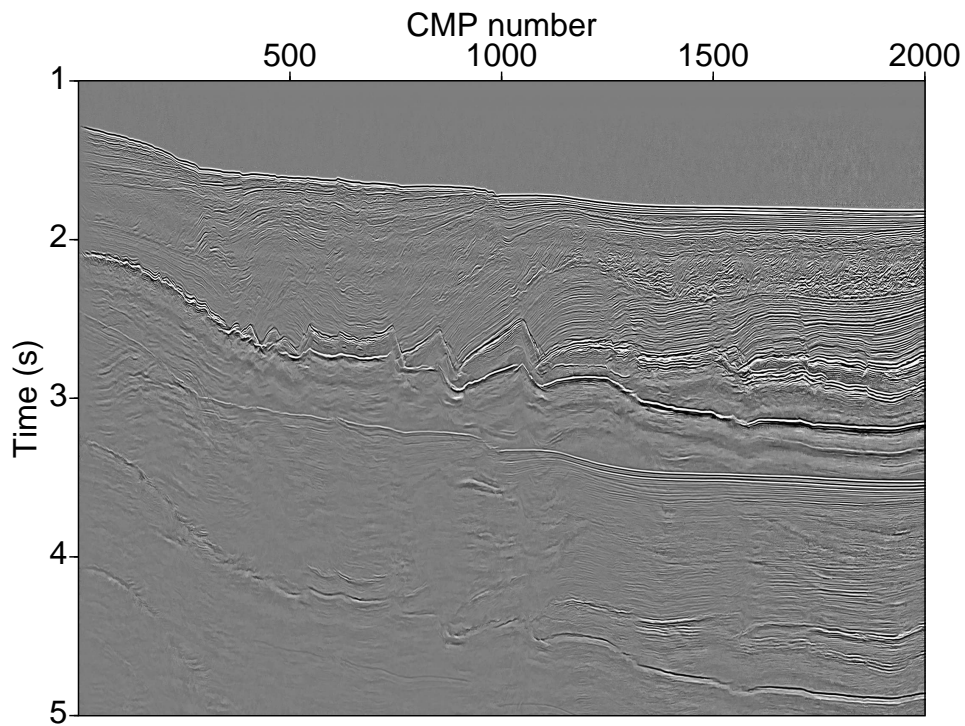


Figure 2.20.: CSP-MP-stacked section of the field marine data set using stacking velocities determined from a CRS stack of the data.

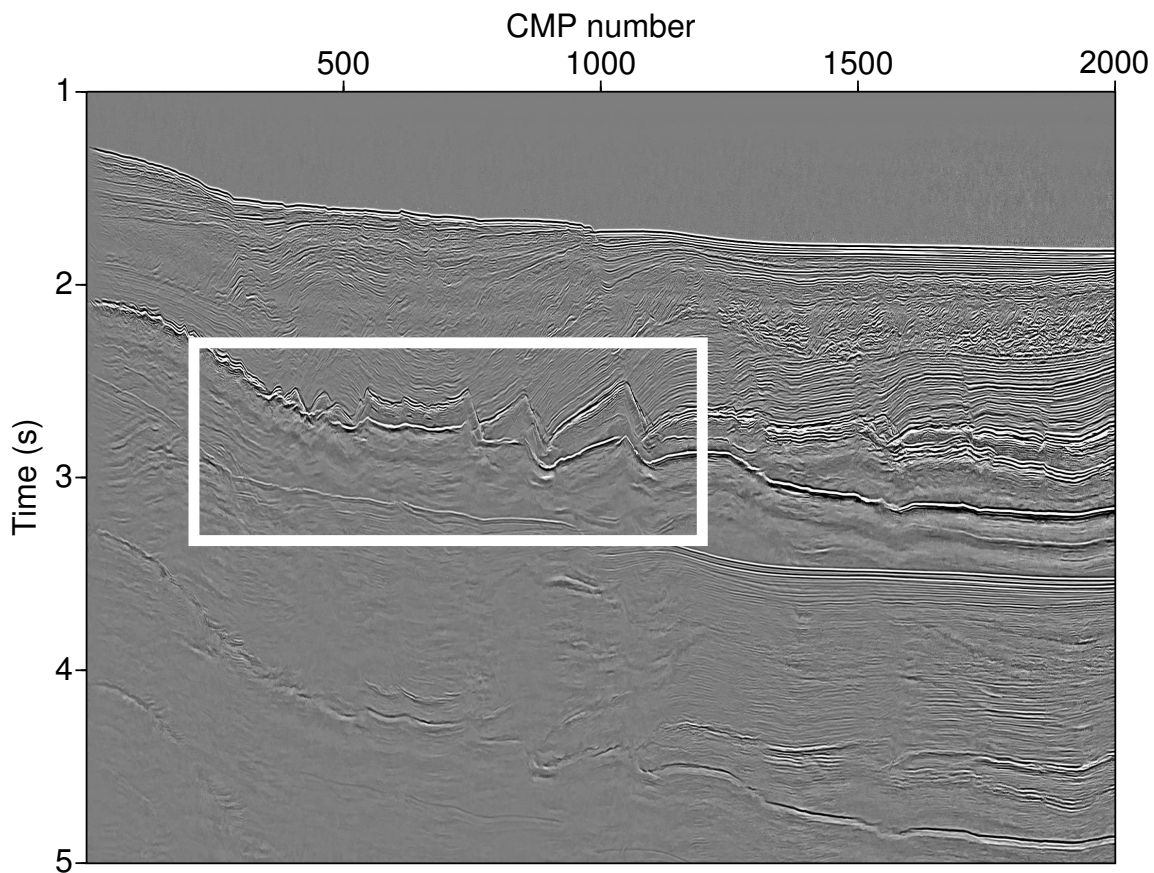


Figure 2.21.: The selected region for a detailed comparison of the PreSTM and CSP-MP stack results (see Figure 2.22).

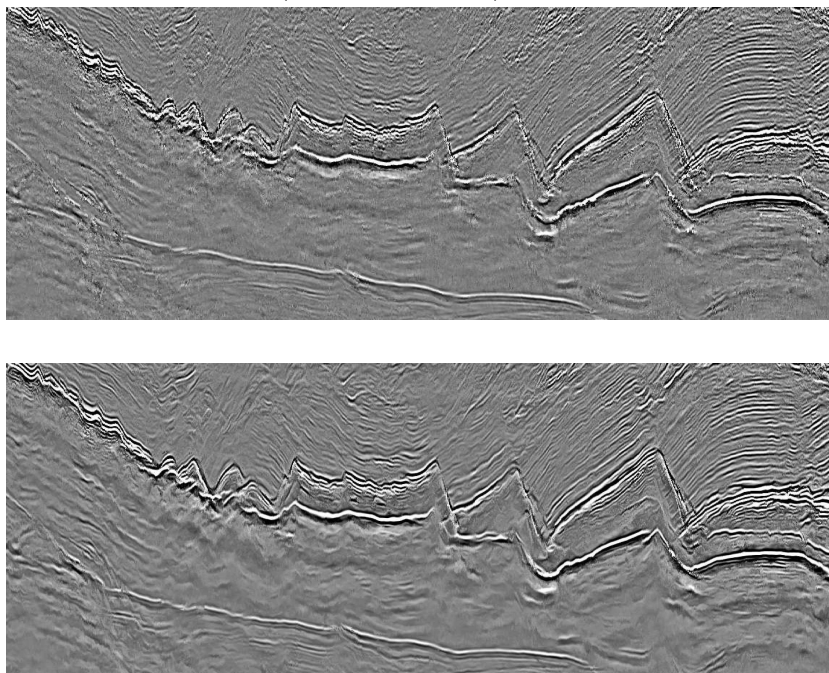


Figure 2.22.: Close-up: salt rollers. Top: PreSTM result; bottom: CSP-MP result. The CSP-MP section exhibits higher resolution, better resolved salt flanks, and more information at the bottom of the salt.

2.7. Summary

I have reviewed a recently developed time migration method proposed by [Dell et al. \(2012\)](#). It is based on the DSR equation parametrised in terms of the diffraction apex time. This operator is applied in a first step to generate new prestack gathers in the Common Scatter Point (CSP) domain. A subsequent multi-parameter (MP) stack is then applied to these data. Results after the above-mentioned two steps are kinematically equivalent to conventional prestack time migration results, but the new technique leads to a considerable enhancement of the data quality because the method combines the robustness of time migration with the data enhancement properties of MP.

I applied this partial time migration method to the complex synthetic Sigsbee 2A data and field data set. Application shows that the CSP-MP results are superior over those obtained by conventional prestack time migration. They show a better S/N ratio and generally clearer definition of faults and better continuity of reflections. Furthermore, they lead to improvement of the image quality not only at the bottom of salt, but also in subsalt regions.

The main advantage of the CSP-MP method, or partial time migration method, is that the moveout is preserved during migration, and the data still stays in the prestack domain. This makes it suitable for many complementary applications, e.g. time migration velocity model building, image-ray tomography ([Dell et al., 2014](#)).

Choosing a correct velocity model is crucial for migration. In principle, root mean square (RMS) velocities can serve as time migration velocities, but they are not available for field data sets. In this work, I have used the calculated velocities from the MP stack as initial migration velocities. Migration results can be imprecise when imaging complex geological situations, e.g. faults or salt bodies. This problem could be solved by standard migration velocity analysis (MVA) (see, e.g., [Robein, 2003](#); [Claerbout et al., 1996](#)).

The main idea of Kirchhoff migration is to treat each point on a sufficiently dense grid in the considered target area as a potential diffraction point in correspondence to Huygen's principle ([Hagedoorn, 1954](#)). Poor quality seismic data cause low quality imaging results, and regularised data is always wanted. In the next chapter, I propose a new technique, namely kinematic time demigration. This method can be used for prestack data regularisation and improve the prestack data quality. Parts of the results have been published by ([Yang et al., 2016](#)).

Chapter 3.

2D Prestack partial time demigration

In the previous chapter I have presented a method to produce partial time-migrated data. In this chapter, I propose a new inverse process of partial time migration, which I call partial time demigration. By a cascaded application of a migration and a demigration, I can regularise the traces and improve the S/N ratio of the data. Furthermore, one can learn and take advantage of the differences between the resulting data and the original data. I will first present the new method, and then apply the cascaded technique to a simple synthetic data set and the complex synthetic Sigsbee 2A data as well as to a marine field data set to demonstrate the proposed method.

3.1. Theoretical background

Handling low quality seismic data is a processing challenge. The quality of reflection seismic data depends on various issues, such as the topography of the earth's surface, the complexity of the subsurface, and the technical equipment used in the acquisition stage. Natural and anthropogenic factors can also affect seismic measurements. Inhomogeneities in the subsurface, the presence of fault structures, and strong velocity contrasts, in, e.g., areas with salt plugs, lead to a decrease of signal-to-noise (S/N) ratio of the data (see, e.g., [Baykulov and Gajewski, 2009](#)). These poor quality seismic data cause low quality imaging results. I suggest a method of cascaded partial time migration and demigration to enhance the prestack data quality.

Demigration is the inverse process of seismic migration. [Hubral et al. \(1996\)](#) proposed a unified approach to 3D seismic reflection depth imaging. The approach is composed of

1. *migration*: a weighted Kirchhoff-type diffraction-stack integral to transform

(migrate) seismic reflection data from the measurement time domain into the model depth domain,

2. *demigration*: a weighted Kirchhoff-type isochron-stack integral to transform (demigrate) the migrated seismic image from the depth domain back into the time domain.

Although their approach is formulated in the depth domain, the concept can be applied to the time domain (Hubral et al., 1996). Iversen et al. (2012) have generalized a migration and demigration process in time domain, considering traveltime, slope and curvature characteristics of seismic reflection events. Papers presenting relationships between seismic modeling and demigration are available (see, e.g., in Hubral et al., 1996; Santos et al., 2000). Another kinematic time demigration method was recently developed by Glöckner et al. (2015). Their technique is based on the implicit CRS (i-CRS) operator and the operator is formulated in terms of midpoint displacement, half-offset, and migration velocity, whereas in this work, my algorithm is based on the CSP operator (Dell et al., 2012).

3.2. Partial time demigration

Since processing in the time domain is fast, robust, and less sensitive to velocity model errors, which makes it still attractive in spite of its known limitations, e.g. the output is in time instead of depth, complex structured data may not be focused and positioned correctly. It cannot handle lateral velocity variations (see, e.g., in Bancroft, 1998; Yilmaz, 2001). In this work, we propose a new operator for partial time demigration, which is the inverse process of partial time migration. The new partial time demigration operator is based on a single square root equation in terms of midpoint displacement, half-offset, and migration velocity. By applying the partial time migration which is based on a double square root equation in terms of the same parameters mentioned above, we obtain data in the CSP domain (Dell et al., 2012). Potential applications for data processing in this domain are, e.g., diffraction separation (Dell and Gajewski, 2011) and multiple suppression (Dümmong and Gajewski, 2008). In a subsequent step, the new partial time demigration is applied to generate new prestack data in the original CMP domain. However, with an improved signal-to-noise ratio compared to the original data. Furthermore, the proposed method of migration followed by demigration can be used to generate regularised prestack data (Baykulov and Gajewski, 2009). Note that geometric spreading, obliquity, filtering, etc. are not addressed in this work.

Whereas the seismic migration is carried out by stacking the energy along the diffraction operator and assigning the summation result to the corresponding

diffraction location. Demigration, the inverse process, redistributes the collapsed energy back to each potential diffraction event in the original time domain.

I achieve this by solving Equation 2.4 for t_{apex} . After applying some algebra, I obtain our partial time demigration operator in terms of t_D , which is now the isochron time:

$$t_{apex}(m, h, t_D) = \sqrt{t_D^2 - \frac{4m^2}{v^2} + \frac{(4mh)^2}{v^4 t_D^2}} . \quad (3.1)$$

As can be seen, the partial time demigration operator is a single square root equation, where h is the half source-receiver distance, m is the midpoint displacement with respect to the considered CMP position, t_D is the diffraction traveltime, and v is the migration velocity.

If the same parameters, i.e., velocities and apertures, are applied in both steps, partial time migration and partial time demigration, the resulting data are theoretically equivalent to the original data (Hubral et al., 1996). Note that here we use the same migration velocities to conduct the demigration, which is to follow Equation 2.6. Under a demigration, the data is transformed from migrated time domain back to the original time domain. However, due to the data enhancement capability of our method, we obtain a higher signal-to-noise level and thus better image quality. Poststack time-demigrated gathers can be generated by stacking (either by CMP stacking or MP stacking) the prestack time-demigrated data.

3.3. Practical remarks

To obtain a reliable de-/migration image, certain apertures and velocities have to be chosen. In this work, since I propose a cascaded operator of first partial time migration and then demigration, I apply the same apertures and velocities (see Section 2.4 in Chapter 2) for both transformations. In addition, I am mainly dealing with kinematic operators, so geometric spreading, obliquity, filtering, etc. are beyond the scope of this work.

In order to investigate the performance of my proposed demigration technique, I apply the above-mentioned migration velocities as well as the root mean square (RMS) velocities that are available to two synthetic data sets and a marine field data set.

3.4. Applications

3.4.1. Generic data example

To verify my method, I applied it to a simple synthetic data set that consists of three diffractors and a horizontal reflector in a homogeneous background (see Figure 3.1). The data were generated with the Seismic Unix routine *susynlv*, which is for generating synthetic seismograms for linear velocity function. The offset range is 0 to 2 km and the midpoint range is 0 to 2 km with a CMP interval of 12.5 m. A constant velocity of 2 km/s was chosen. The peak frequency of the wavelet used for the modelling is 30 Hz. Furthermore, I added random noise with a signal-to-noise ratio of five. Figure 3.2(a) shows the corresponding CMP-stacked section. Note that conflicting dips are present where diffractors and reflections intersect.

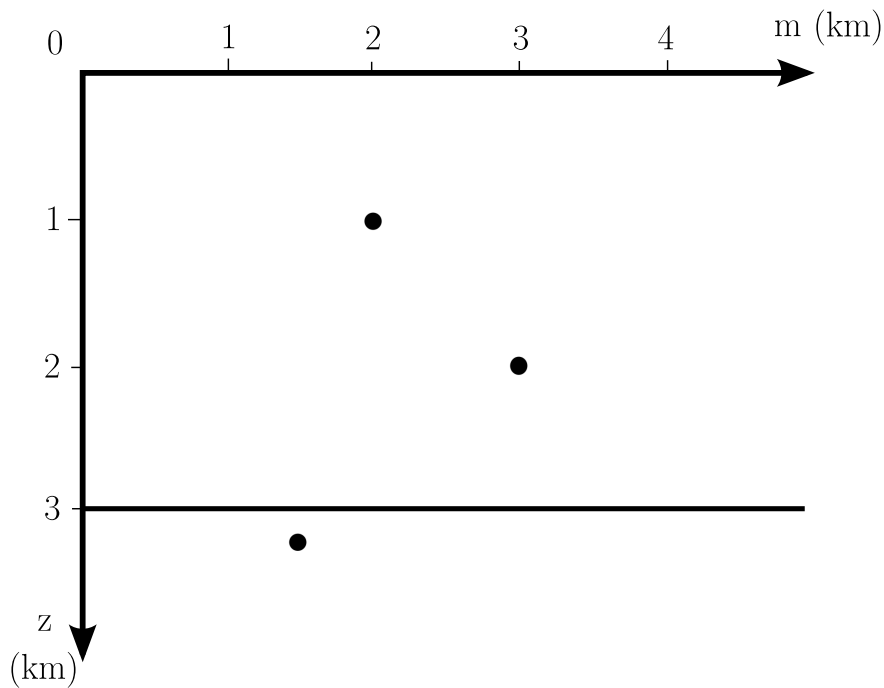


Figure 3.1.: Simple generic synthetic model with three diffractors and one horizontal reflector.

In the following tests, I used migration velocities calculated from Equation 2.6 as shown in Figure 3.2(b). As expected, the velocity was determined to be 2 km/s in areas where events exist, and undetermined otherwise. For comparison, I also applied my method using the known constant velocity of 2 km/s.

Figures 3.3(a) and 3.3(b) show the partially time-migrated and MP-stacked section using the numerical and analytical velocities, respectively. I observe that the

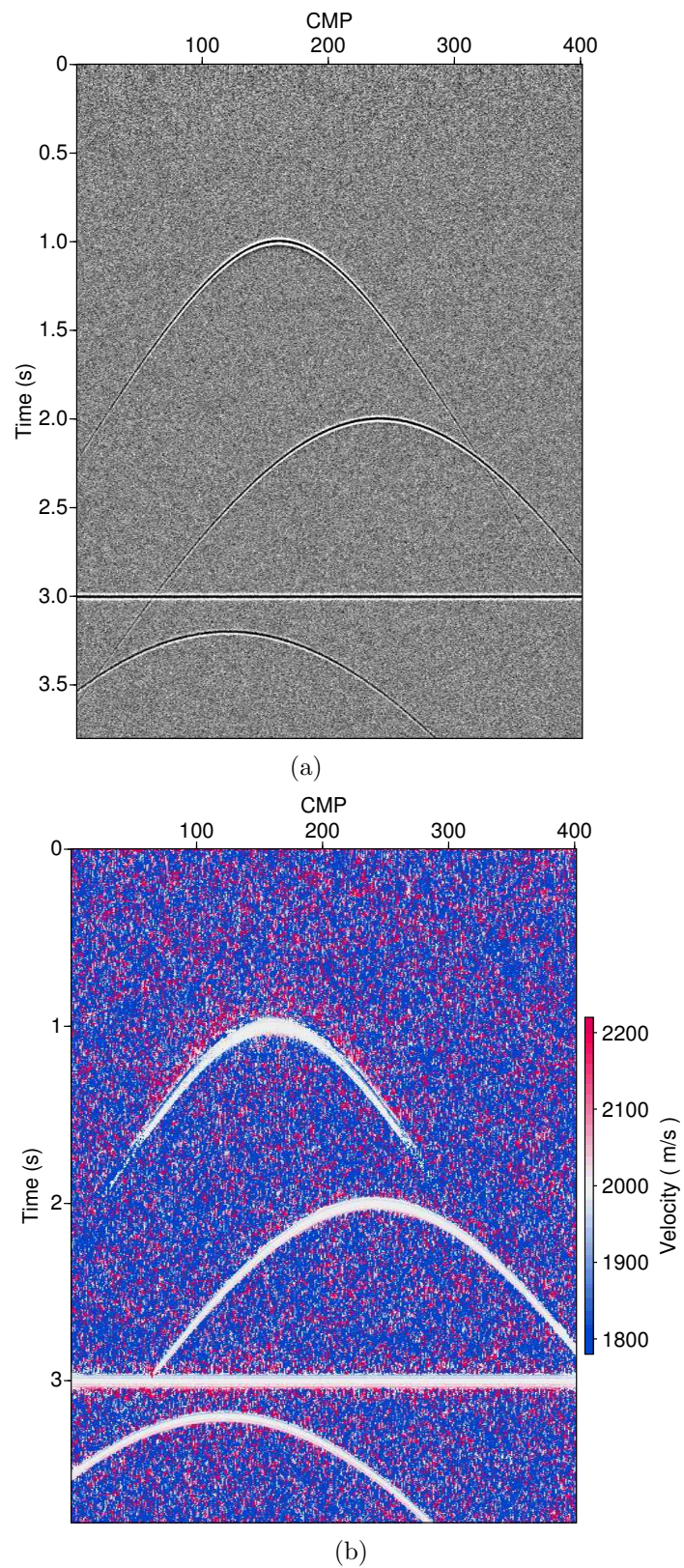


Figure 3.2.: Generic data example: (a) CMP-stack of the original data, (b) velocities determined following Equation 2.6.

diffractors are collapsed and the reflector is mapped to the correct position for both velocity models. Cross-like structures are visible around the apex point, which is due to the fact that the range of validity of the first Fresnel zone (see Equation 2.5) simplifies for diffractions ($t_r = t_d$). All traces are included and an infinite aperture is required, whereas in reality the aperture is restricted to finite value. I notice that the first diffractor on the top in Figures 3.3(a) is not well focused as the other two below. This might be because the calculated velocities (see Figures 3.2(b)) are noisy around the first diffractor. The constant velocities in Figures 3.3(b) leads to better focused diffractors, and the image with higher S/N ratio, comparing to the ones in Figures 3.3(a).

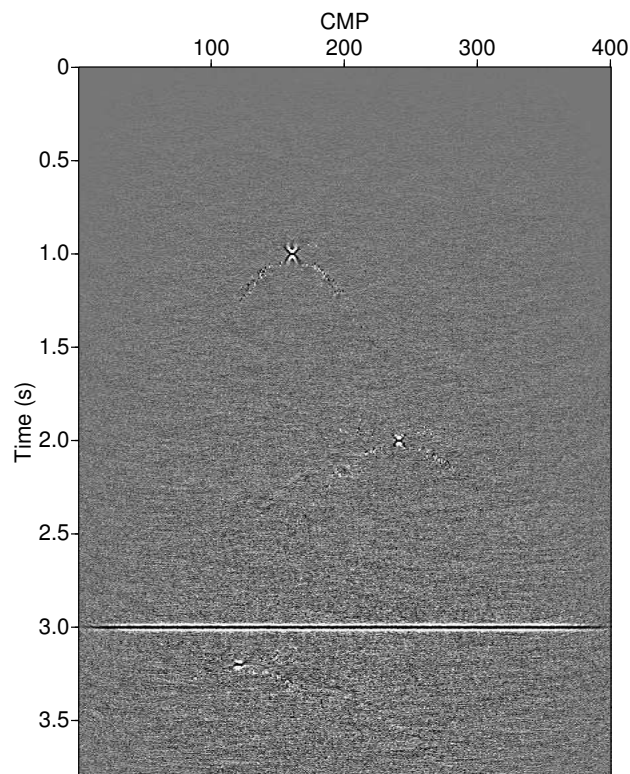
The (unstacked) partially time-migrated data were then used as input for the partial time demigration. In Figures 3.4(a)–(c), I compare the new prestack data resulting from my cascaded migration and demigration for both velocity models with the original data for CMP 145, located at 1.45 km in Figure 3.1. Both newly-generated gathers after the cascaded migration-demigration method (see Figures 3.4(a) and 3.4(b)) show a higher S/N ratio than the original data. The event at 2.3 s is reconstructed with a lower amplitude because the selected CMP position is far off the corresponding diffraction apex and a weighting factor is needed to compensate the amplitude loss. This event is also better reconstructed for the constant velocity case (see Figure 3.4(b)). In the Figures 3.4(a), because of the noisy background of the calculated velocities, some artifacts present.

Finally, Figures 3.5(a) and 3.5(b) show the resulting poststack sections of the newly-generated prestack data. Compared with the stacked original data (see Figure 3.2(a)), I also observe higher S/N. The shorter diffraction tails in the poststack demigration are due to the limited extent of the aperture. Accordingly, choosing larger apertures will result in longer diffraction tails.

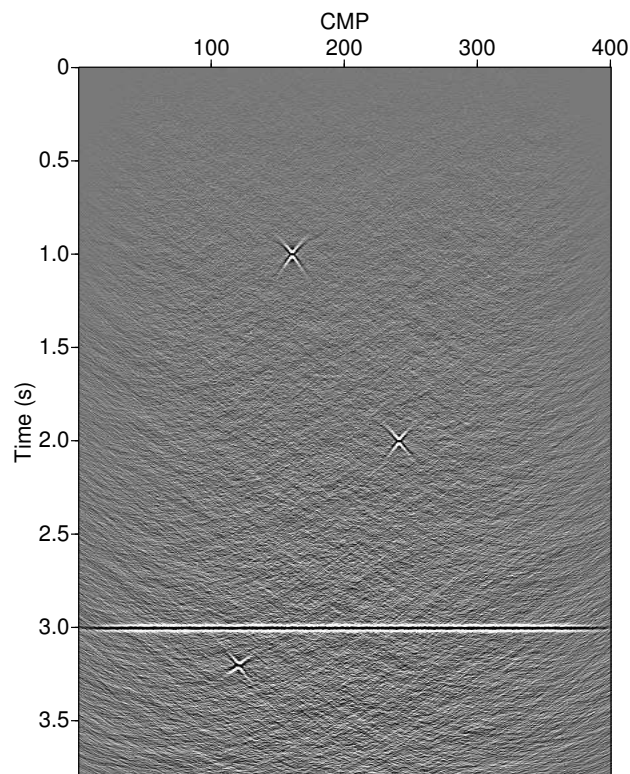
3.4.2. Sigsbee 2A data example

To evaluate the performance of my method in a complex setting, I have applied it to the synthetic acoustic Sigsbee 2A data set (see Figure 2.6). It contains a large irregularly-shaped salt body with a rugged top and two lines of point diffractors embedded in the horizontal layering of sediments. See acquisition details regarding this data set in Section 2.5.

I applied the new method with migration velocities calculated by Equation 2.6 and root mean square (RMS) velocities calculated from the interval velocities of the model provided by the SMAART JV consortium. Due to the large volume of this data set, I show only the results for a common offset of 1 km.



(a)



(b)

Figure 3.3.: Generic data example: partially time-migrated and stacked result using (a) velocities determined following Equation 2.6, (b) constant velocity.

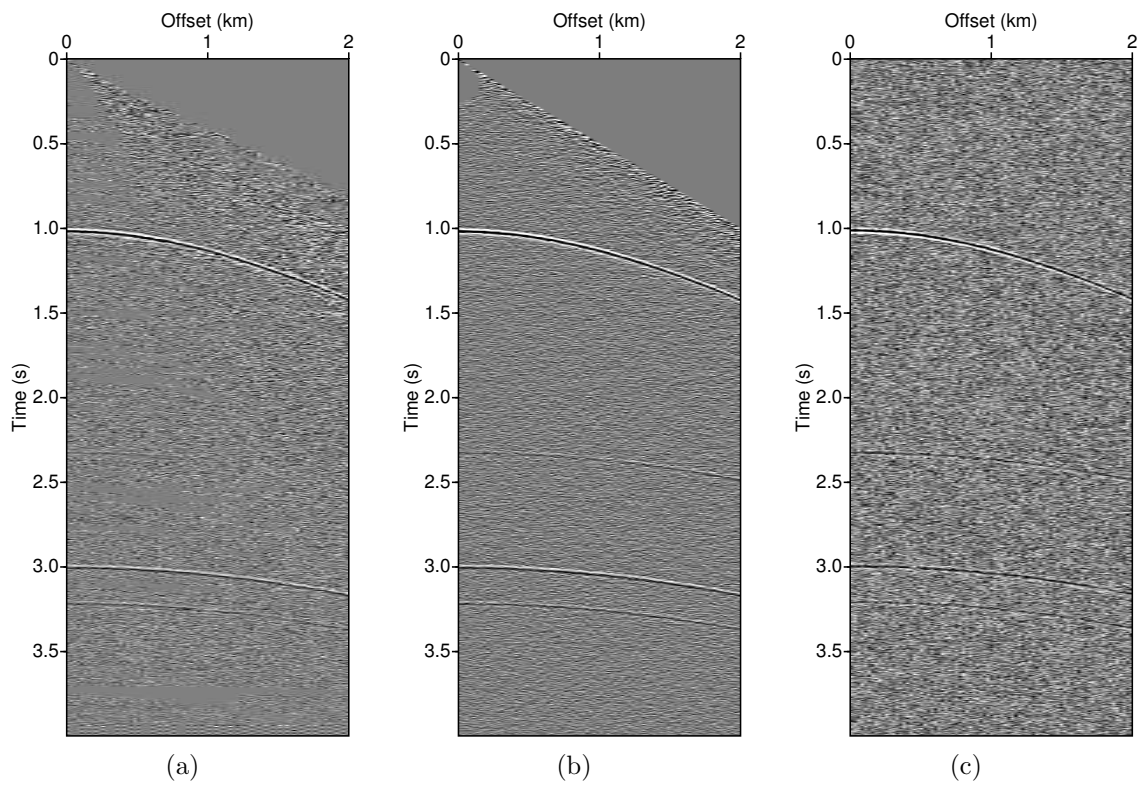
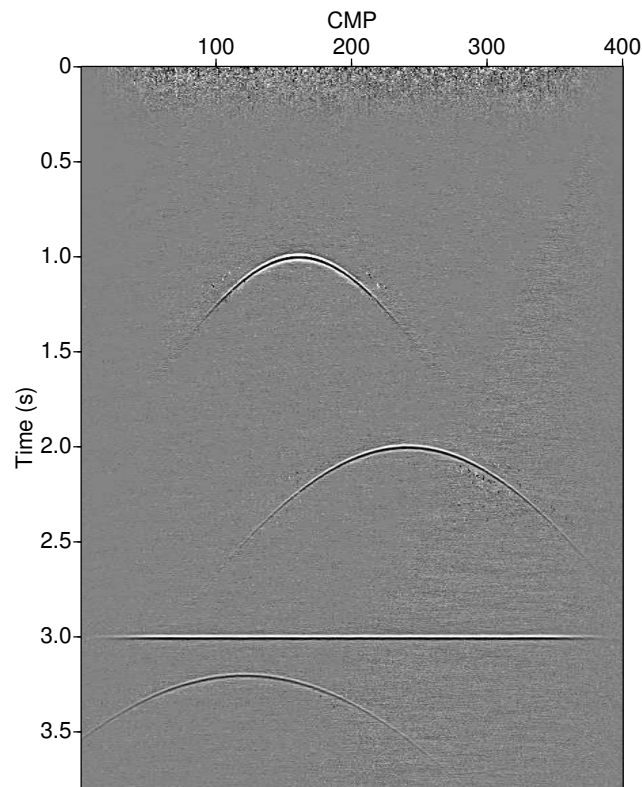
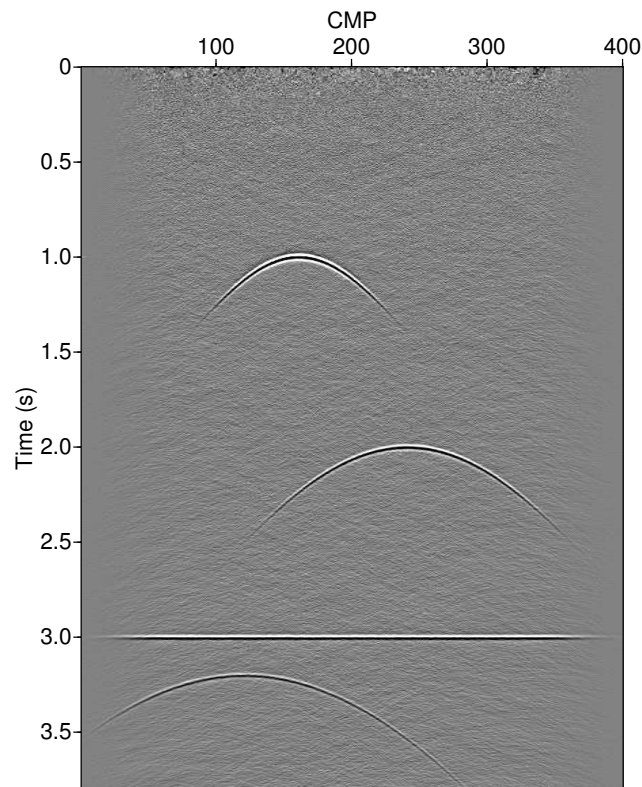


Figure 3.4.: Generic data example: prestack data for CMP 145 obtained from cascaded migration-demigration (a) using velocities determined after Equation 2.6, (b) using constant velocity. (c) shows the original data for comparison.



(a)



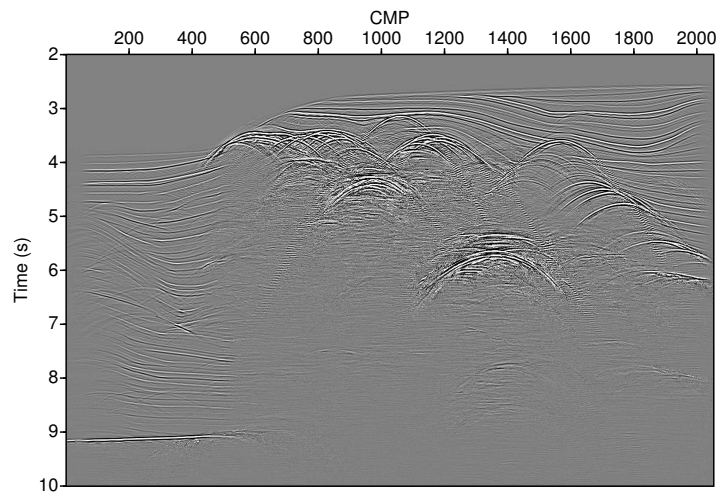
(b)

Figure 3.5.: Generic data example: poststack sections of the newly-generated prestack data using (a) velocities determined following Equation 2.6, (b) constant velocity.

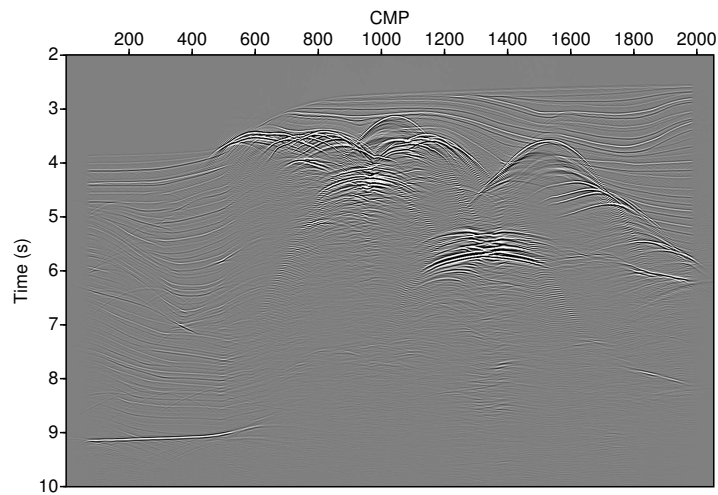
Figures 3.6(a)–(c) display the 1 km common offset sections resulting from the proposed method as well as the original data for comparison. I observe that the events were mostly reconstructed. Especially at the left part where mostly horizontal layering sediments present (from CMP 0 to 500), I obtain better images (Figure 3.6(a) and 3.6(b)) with much higher S/N ratio, more continuous reflections and clearer-defined faults than the original data (Figure 3.6(c)). For the complex salt body part in the middle, where strong velocity contrasts and triplications exist, which make this region highly horizontally inhomogeneous, we are amazed already that most of the structures are reconstructed, despite the limitation of time imaging in general, i.e. mild to moderate lateral velocity variations.

In Figures 3.7(a)–(c), I show the new prestack data resulting from the cascaded migration-demigration as well as the original data for CMP 1026. Again, I observe an overall good reconstruction of the data, in particular with RMS velocities. In detail, I notice that in the original data (see Figure 3.7(c)), there is aliasing problems. But by applying the proposed method, the problem has been eased. Also the conflicting dip problems are handled quite well by the proposed method in an automatic manner because after the first transformation (time migration) there are almost no conflicting dips. This provides an efficient way comparing to the current approaches for conflicting dip problems (Walda and Gajewski, 2014).

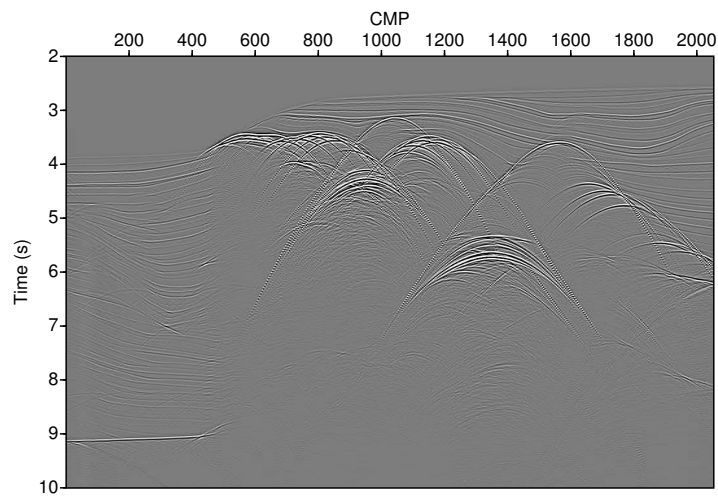
Furthermore, I show the poststack results in Figures 3.8(a)–(c). I have applied a CMP stack. Like in the offset sections in Figures 3.6 we can observe diffractions and conflicting dips. The conclusions regarding data quality and model dependence are the same as for the reconstructed prestack data. Because the data has been stacked twice, poststack results are with higher S/N ratio than the prestack results.



(a)



(b)



(c)

Figure 3.6.: Sigsbee 2A data example: 1 km common offset section for the newly-generated prestack data using (a) velocities calculated by Equation 2.6, (b) RMS velocities. (c) shows the corresponding original section.

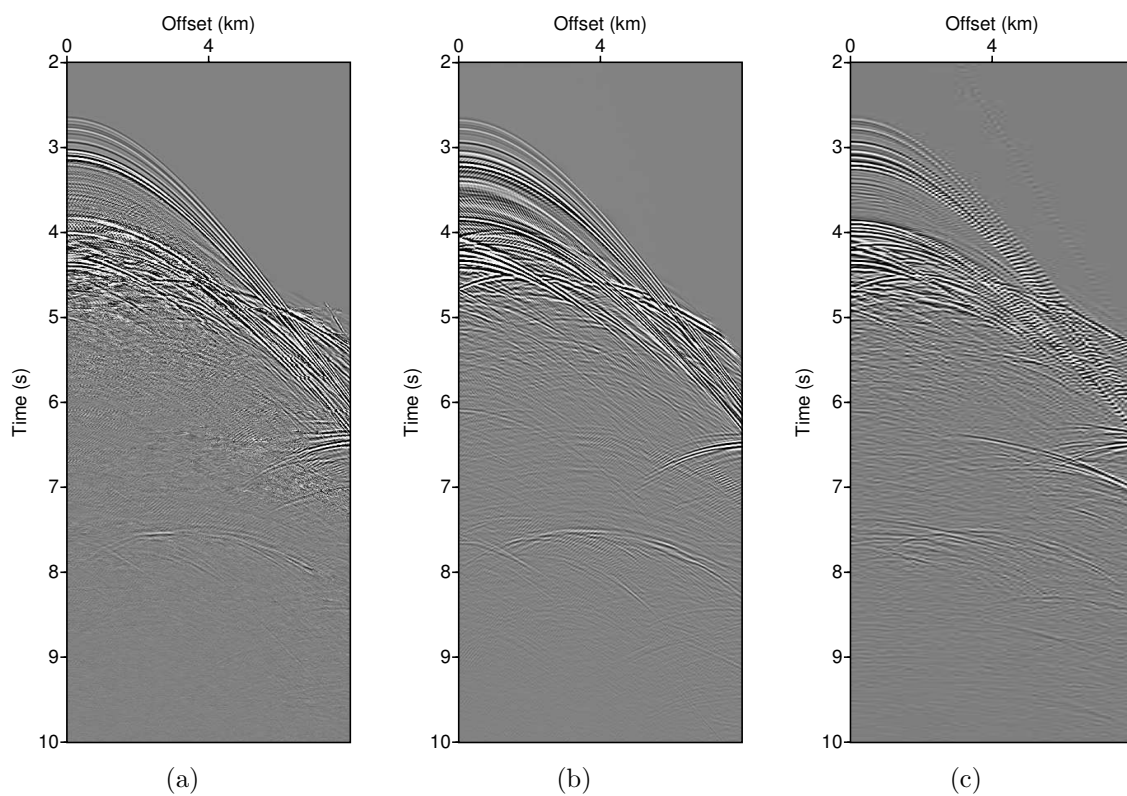
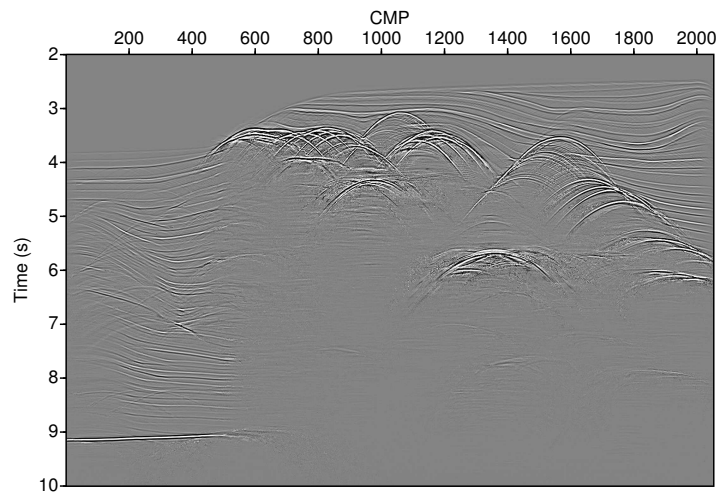
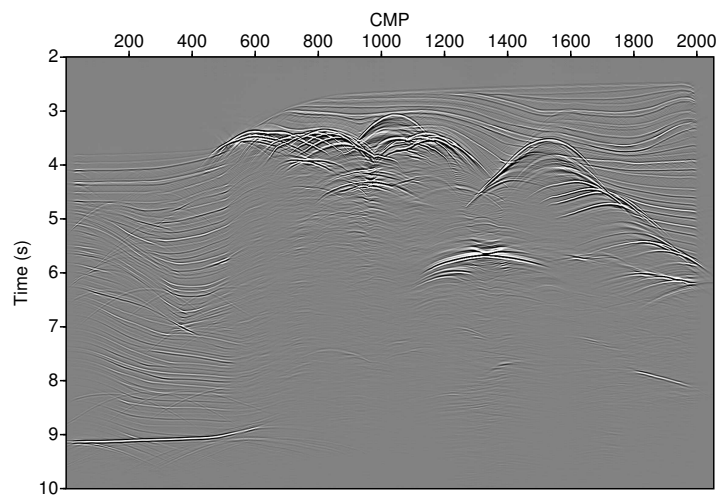


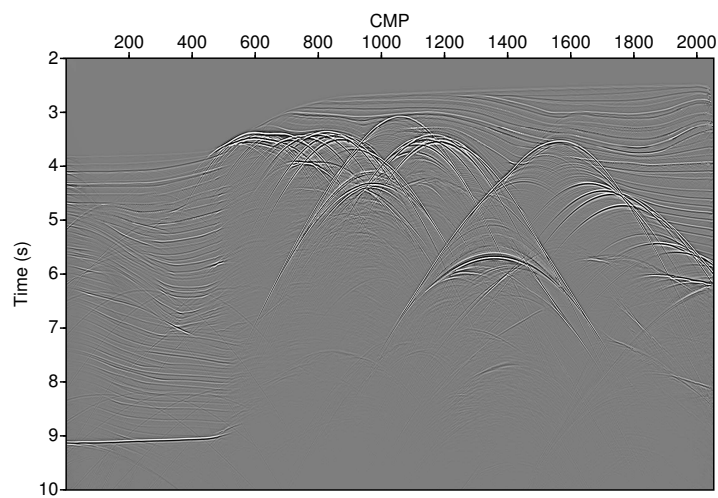
Figure 3.7.: Sigsbee 2A data example: CMP gather 1026 for the newly-generated prestack data using (a) velocities calculated by Equation 2.6, (b) RMS velocities. (c) shows the corresponding original section.



(a)



(b)

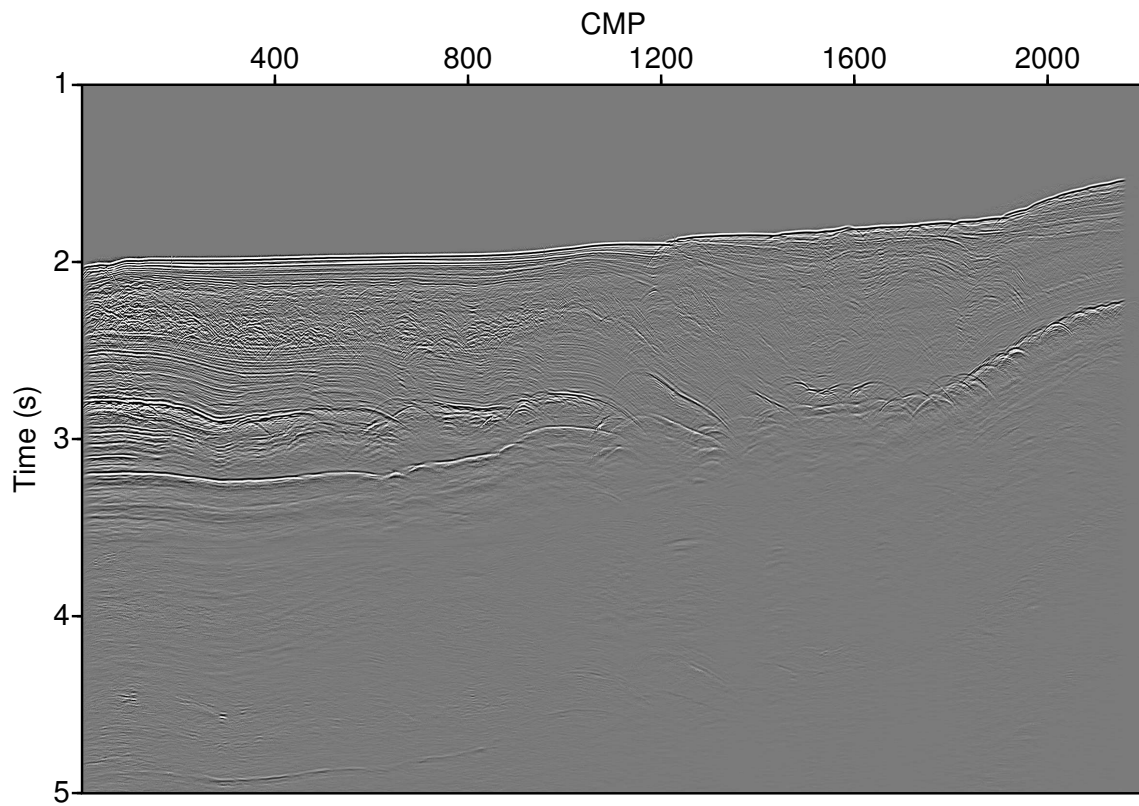


(c)

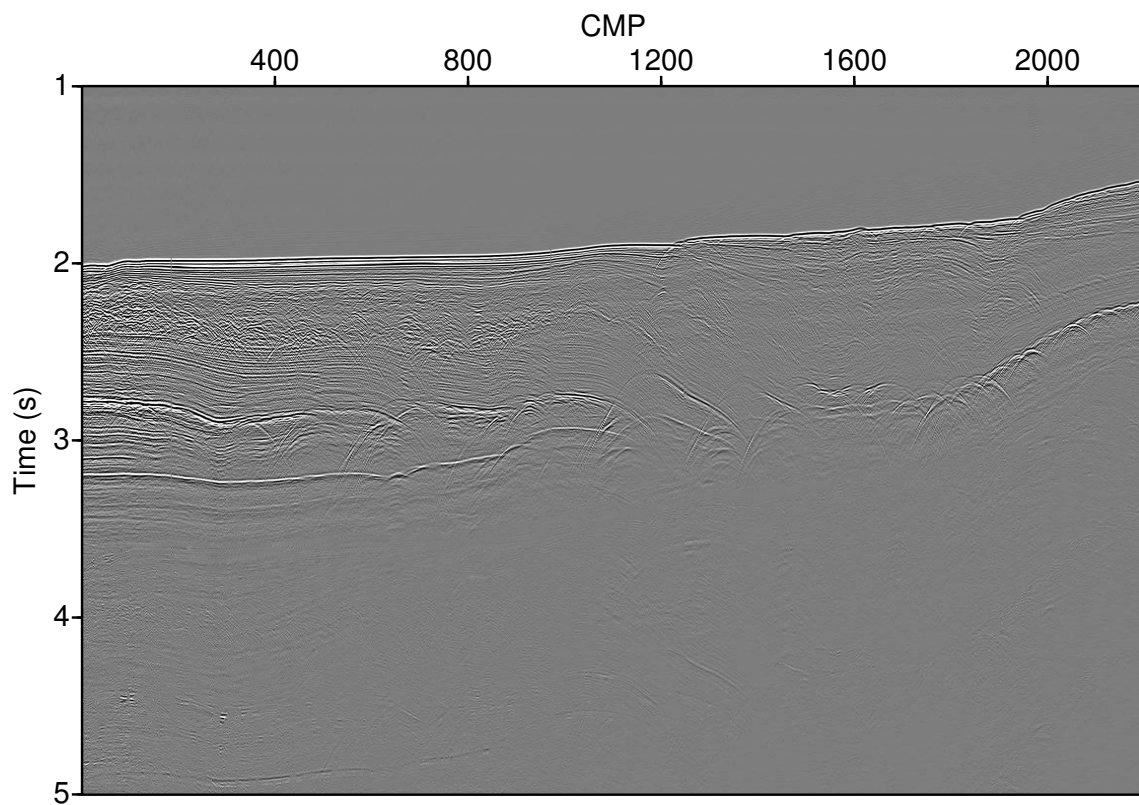
Figure 3.8.: Sigsbee 2A data example: poststack sections of the newly-generated prestack data using (a) velocities determined following Equation 2.6, (b) RMS velocities. (c) shows the corresponding original section.

3.4.3. Marine field data example

Finally, I have applied the method to a marine field data set. The data were acquired in the Levantine Basin in the south-eastern Mediterranean Sea. The acquisition detail regarding this data set can be found in Chapter 2. I applied the proposed method with migration velocities calculated by Equation 2.6. Due to the large volume of this data, I present only results for a common offset of 1150 m. Figure 3.9 shows the offset sections for the newly-generated prestack data and the original data. I observe that the events are reconstructed well in the sedimentary regions as well as in the region with the salt rollers. Figure 3.10 shows the corresponding poststack sections after a CMP stack. They exhibit the same properties as the prestack results.

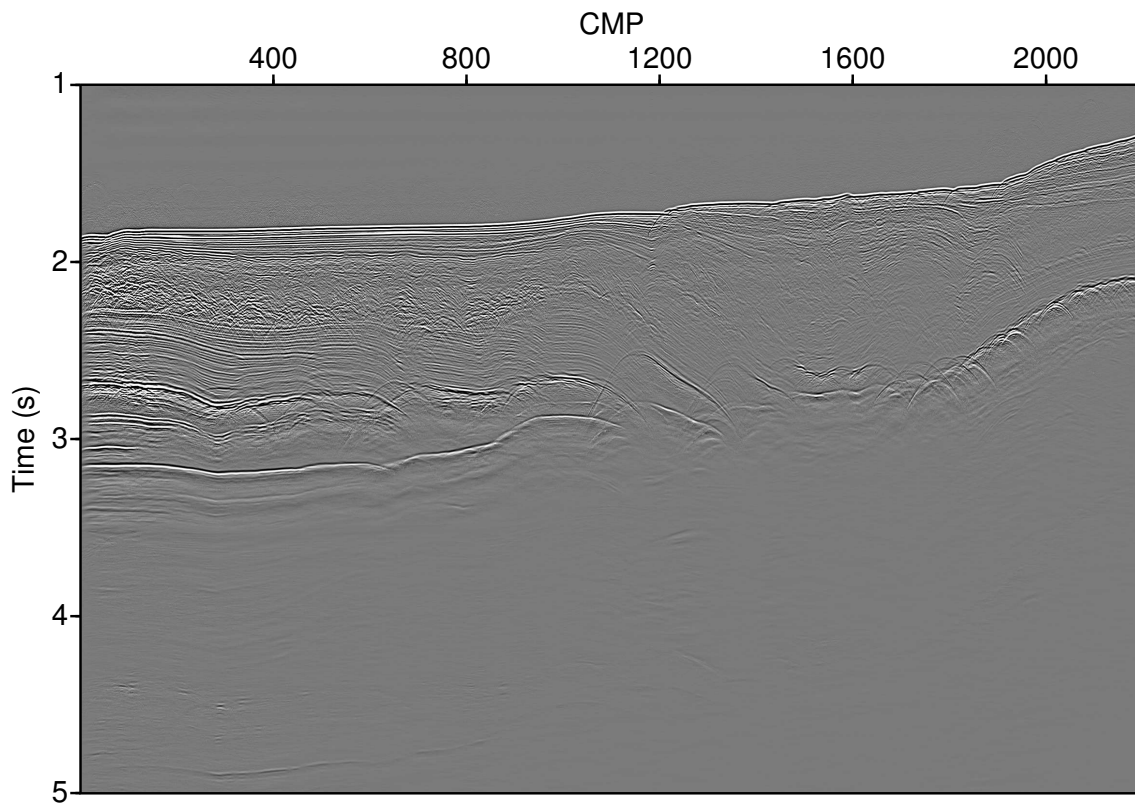


(a)

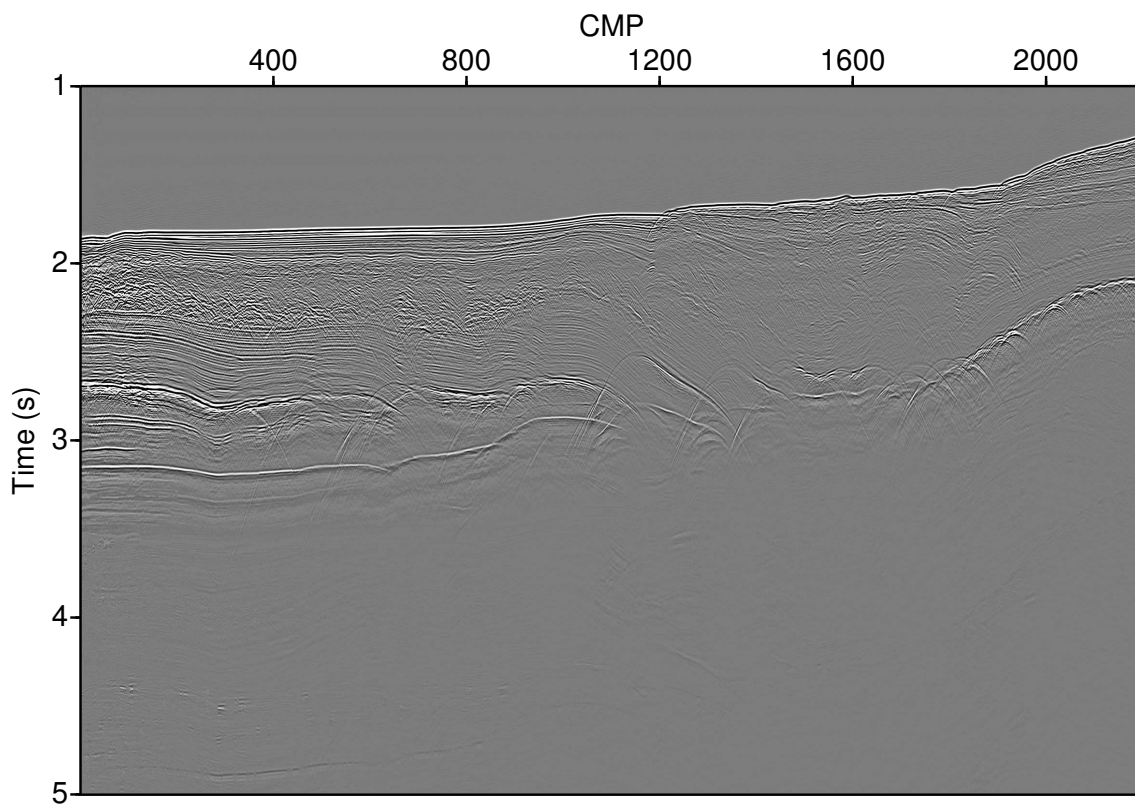


(b)

Figure 3.9.: Marine data example: (a) 1150 m offset section resulting from the new method. (b) shows the corresponding original section.



(a)



(b)

Figure 3.10.: Marine data example: Poststack section of (a) the newly-generated prestack data, (b) the original data.

3.5. Summary

I have proposed a new partial time demigration operator. It is expressed by a single square root equation in terms of midpoint displacement, half-offset and migration velocity. Application of a cascaded operator of partial time migration and the demigration can enhance the quality of the resulting prestack data compared to the original data. Instead of the original data, these newly-generated prestack data can then be used in many conventional processing procedures. Furthermore, my new method can be utilised for regularising prestack data and mitigating aliasing.

Application to a simple generic data set as well as the complex synthetic Sigsbee 2A data and field data set confirms that the suggested method leads to an improvement of data quality in terms of higher S/N ratio.

My examples also show potential regarding conflicting dip problems. By applying my proposed cascaded method, we can handle them in an automatic manner because after the first transformation (time migration) there are almost no conflicting dips. This provides an efficient way comparing with the current approaches for conflicting dip problems ([Walda and Gajewski, 2014](#)).

The velocity model is crucial for the quality of the output, i.e. both migration and demigration. The RMS velocities lead to the best results, however, these are not generally available for field data. In this work, I have used migration velocities calculated from the multi-parameter stacking operator by Equation 2.6. However, these face problems in complex geological situations, e.g. faults or salt bodies. This is due to the intrinsic limitation of the time migration technique, i.e. under the assumption of mild to moderate lateral velocity variations.

Chapter 4.

3D extension and application

In the previous chapters, two methods, or rather a cascaded operator for enhancing prestack data quality was presented. In this chapter, I extend the technique to the three dimensional (3D) case. Then I verify the extension on a 3D synthetic data set: the SEG Salt Model C3 wide azimuth classic dataset. First of all, I will introduce some basics of 3D seismics.

4.1. 3D seismics

For academic research, we study seismology in 2D cases, but the Earth itself is three dimensional (3D), so it is more realistic to investigate the 3D features. The driving force behind this switch from 2D to 3D is the accuracy of images of the subsurface obtained by 3D seismic acquisition compared with the images obtained by 2D seismic. Although recording and processing 3D data is quite challenging and much more expensive, the advantages of 3D seismic are also prominent:

- a more realistic scenario;
- increase in accuracy, e.g. considers out-of-plane energy, corrects mispositioning problems;
- can provide detailed knowledge of small-scale reservoir features, e.g. small faults, thin channels;
- better account for diffractions, anisotropy etc.

Sources and receivers are rarely laid out in dense areal arrays covering the surface above the target in 3D acquisition geometries. The other major challenge of 3D

seismic data processing is that 3D prestack data is sparsely and irregularly sampled along the spatial coordinates.

For 2D prestack data, the data turns out to be a 3D space; but for 3D prestack data, it is defined in a 5D space (t, x_s, y_s, x_g, y_g) , including the recording time (t) , the two components of the receiver position (x_g, y_g) , and the two components of the source position (x_s, y_s) .

3D seismic can provide additional information on the rock parameters, e.g., velocities. This additional information is contained in the data recorded along different source-receiver azimuthal directions. Land data is usually acquired with a fairly wide range of azimuthal directions, whereas marine data has a narrower range. However, even for marine data, the trend goes towards acquiring surveys with a wider range of azimuths for the source-receiver pairs (e.g. the data example SEG Salt Model C3 wide azimuth classic dataset we chose, it is wide azimuth marine data) (Biondi, 2005).

3D acquisition geometries

Although the acquisition design may vary for different situations (e.g., land or marine physical environment, subsurface structural complexity, and the overall goals of the survey), there are a few commonly used schemes.

A typical 3D marine survey is carried out by shooting into closely spaced parallel lines which are called shooting lines. It is done by towing several streamers behind a vessel. In modern acquisition, each vessel tows more than ten streamer cables; each cable contains between 50 to 150 groups of geophones. Each shot is recorded simultaneously on all cables as the boat moves. Land seismic geometry surveys usually have a wider azimuth range than marine ones because receiver locations are not constrained to be attached to a towed streamer.

Figure 4.1 shows a sketch for 3D seismic acquisition. If the source and receiver are preferentially aligned along one direction, we assume that the x -axis is aligned with this preferential direction. In this case we call the x -axis the *in-line* axis and the y -axis the *cross-line* (x -line) axis. The *azimuth* is the angle between the vertical projection of a line of interest into a horizontal surface and the true north or magnetic north measured in a horizontal plane, typically measured clockwise from north.

3D data is often visualized in so called *time slices*. A *time slice* is a horizontal display or map view of 3D seismic data having a certain arrival time value, as opposed to a horizon slice that shows a particular reflection (Schlumberger, 2015). A time-slice view of the data is an improvement over vertical sections for the interpretation of depositional systems because it provides the opportunity to see a portion of

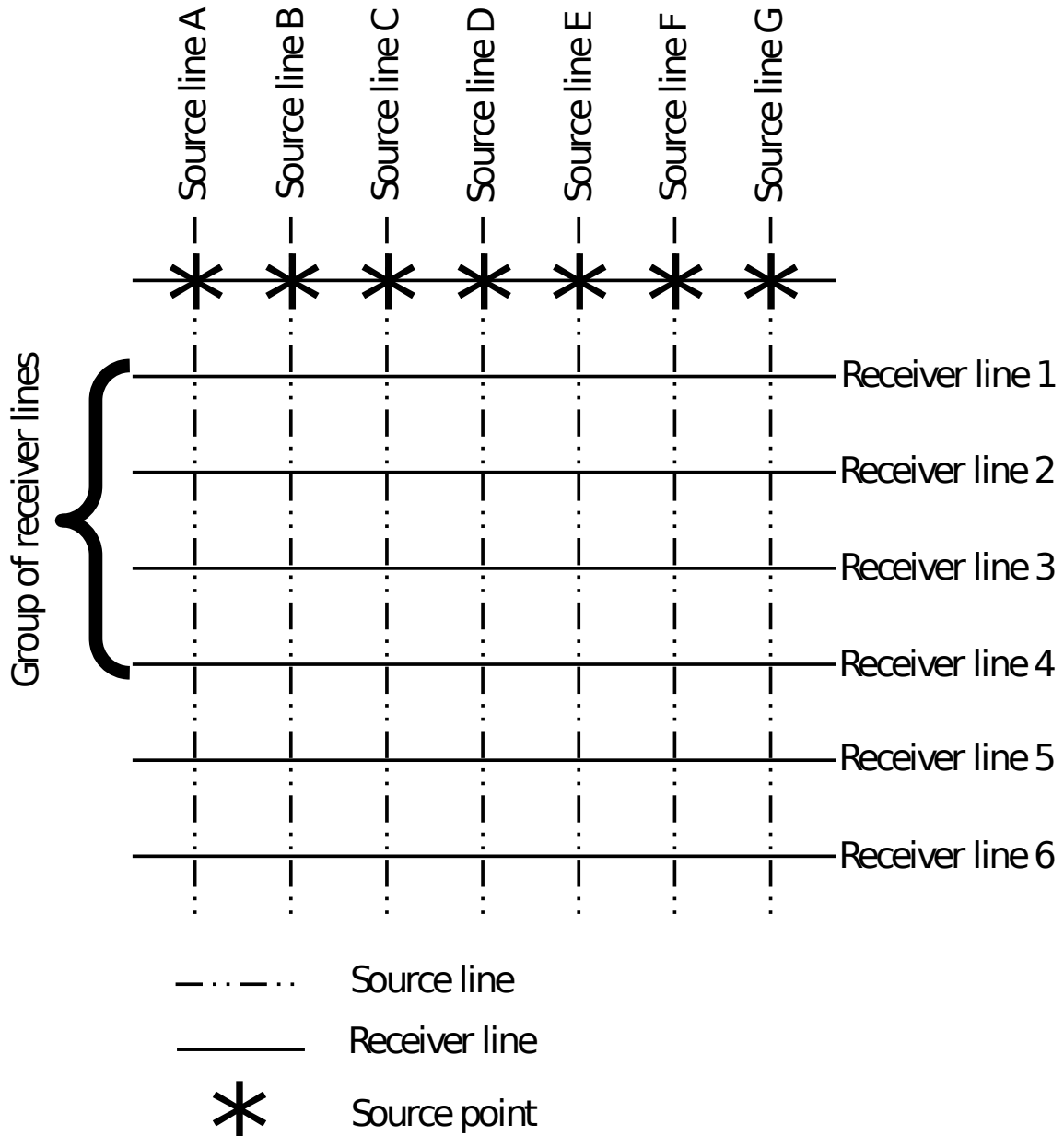


Figure 4.1.: A sketch for 3D seismic acquisition.

depositional systems in map view. This view is key to interpreting these systems because it allows a view of the morphology of the system, which facilitates its recognition (AAPG, 2014).

4.2. 3D extension of partial time de-/migration technique

In chapter 2, I have explained the advantages of the CSP method. It preserves the moveout and the output data is suitable for further applications like a multi-parameter stack or stacking velocity analysis. Another reason which makes this method attractive is that the transformation from prestack domain (the original domain) to a new prestack domain (the CSP domain) does not lead to a significant increase of traces in the output data. This is one of the main driving forces to extend the 2D technique to 3D. A serious drawback of most methods is that they are 2D techniques, whereas the objects to be imaged are essentially 3D objects. Imaging such objects using 2D methods can produce reliable results only in the case when a target object is located directly below the seismic line along which the data is acquired. If this is not the case, either the imaging will fail, or the resulting image will be severely deteriorated, e.g., spatially smeared and appearing at a wrong location (e.g., Dorn, 1998; Dell and Gajewski, 2011).

3D time migration operator

The well-known DSR equation in the 3D case (Hubral, 1977) reads:

$$t_D = \sqrt{\frac{t_0^2}{4} + \frac{(m_x - h_x)^2 + (m_y - h_y)^2}{v^2}} + \sqrt{\frac{t_0^2}{4} + \frac{(m_x + h_x)^2 + (m_y + h_y)^2}{v^2}}, \quad (4.1)$$

where t_0 is the zero-offset travelttime, \mathbf{m} is the midpoint displacement with the coordinates (m_x, m_y) , h is the half-offset, v is a fitting parameter which depends on the wavefront-curvature of the image ray, commonly referred to as the migration velocity (Dell, 2012). Equation 4.1 describes the kinematics of the impulse response of a 3D common offset migration operator applied to 3D prestack data.

In a homogeneous model, the diffraction response of the point diffractor is a hyperboloid, while in a heterogeneous/anisotropic medium, it becomes a

hyperboloid-like complex and multi-valued surface (Dell, 2012).

3D partial time migration operator

Similar to the 2D case, We aim to preserve the moveout during the 3D time migration, that means the minimum of the traveltimes with respect to the offset vector $\mathbf{h}=(h_x, h_y)$ in Equation 4.1 is needed. In order to achieve this, we calculate the first order derivatives of the traveltimes subsurface with respect to offset vector $\mathbf{h}=(h_x, h_y)$ and set it equal to zero. After some algebra, we obtain

$$t_{apex} = \sqrt{t_0^2 + \frac{4(h_x^2 + h_y^2)}{v^2}} \quad , \quad (4.2)$$

which denotes the expression for the minimum (the apex) of the traveltimes surface. Here t_{apex} does not depict a hyperbola but a hyperboloid. Inserting this equation into the formula for 3D migration given by Equation 4.1 leads us to the final 3D partial time migration operator:

$$t_D(t_{apex}, \mathbf{m}, \mathbf{h}) = \sqrt{\frac{t_{apex}^2}{4} + \frac{m_x(m_x - 2h_x) + m_y(m_y - 2h_y)}{v^2}} + \sqrt{\frac{t_{apex}^2}{4} + \frac{m_x(m_x + 2h_x) + m_y(m_y + 2h_y)}{v^2}}. \quad (4.3)$$

Both operators Equation 4.1 and Equation 4.3 provide the same diffraction response (Dell, 2012). The difference lies only in the parametrisation. The advantage Equation 4.3 has over Equation 4.1 is the preservation of the moveout in the data.

Followed by 3D partial time migration, I execute a 3D multi-parameter stack on the generated new prestack data. Like in the 2D case, if the same parameters, i.e., velocities and apertures, are applied, both conventional PreSTM and PartialTM-MP stack are kinematically equivalent. However, due to the data enhancement of the latter method, it supposes to result in better image quality.

In the following part, a multi-parameter stacking method, i.e., 3D CRS, is illustrated.

3D CRS

Over the last decade, the CRS workflow was established as a powerful tool to provide improved images, especially for data with low fold or low S/N ratio.

The 3D CRS stacking operator for the zero-offset (ZO) simulation from seismic multi-coverage data was given by Müller (2003); Bergler (2004) as

$$t^2(\mathbf{x}_m, h) = (t_0 + 2\mathbf{p}_m \cdot \mathbf{x}_m)^2 + 2t_0 (\mathbf{x}_m^T \mathbf{M}_N \mathbf{x}_m + \mathbf{h}^T \mathbf{M}_{NIP} \mathbf{h}) \quad (4.4)$$

where \mathbf{M}_N and \mathbf{M}_{NIP} are symmetric 2×2 matrices that describe the curvatures of the normal and normal-incidence-point (NIP) wavefronts, respectively (Hubral, 1983). These two principle curvatures correspond to two artificial seismic experiments. The NIP wave is emitted from a fictitious point source on the reflector and the normal wave is emitted from an exploding reflector element, the common-reflection-surface (see Figure 4.2). Vector \mathbf{p}_m is the slowness vector that contains the dip angle and azimuth of the central ray (the blue line in Figure 4.2). Furthermore, \mathbf{x}_m is the midpoint displacement vector with respect to the central ray coordinate and \mathbf{h} is the half-offset vector. The 3D CRS stacking method thus has eight independent attributes, which are determined by means of a coherency analysis (e.g., Müller, 2003).

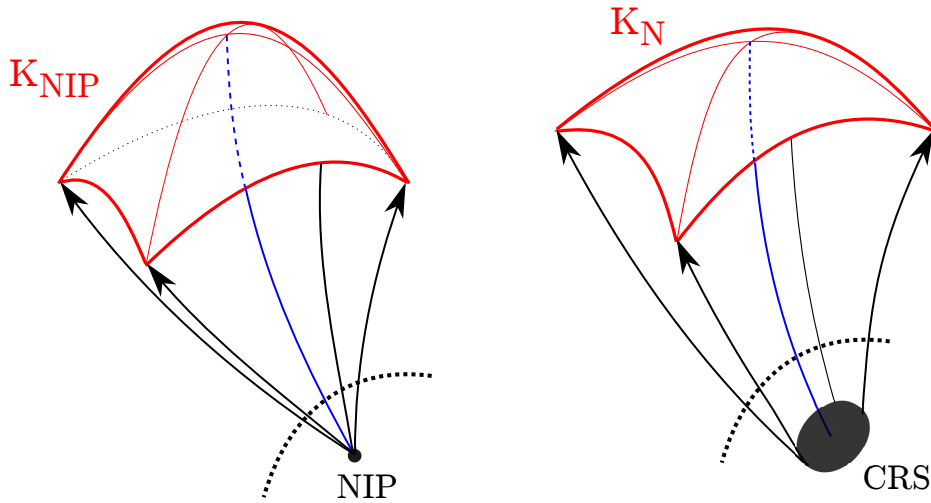


Figure 4.2.: The meaning of the ZO CRS wavefront attributes: (left) curvature of the so-called normal-incidence-point (NIP) wavefront which is emitted from a fictitious point source on the reflector and, (right) curvature of the normal wavefront, which is emitted from an exploding reflector element, the so-called common-reflection-surface. Both curvatures are measured at the surface. (Provided by Bakhtiari Rad, P.)

If a locally constant near-surface velocity v_0 is known, the relation of stacking

parameters and the kinematic wavefront attributes can be expressed as:

$$\mathbf{p}_m = \frac{1}{v_0} (\cos \alpha \sin \beta, \sin \alpha \sin \beta)^T \quad (4.5)$$

$$\mathbf{M}_{NIP} = \frac{1}{v_0} \mathbf{H} \mathbf{K}_{NIP} \mathbf{H}^T \quad (4.6)$$

$$\mathbf{M}_N = \frac{1}{v_0} \mathbf{H} \mathbf{K}_N \mathbf{H}^T \quad (4.7)$$

where α is azimuth, β is dip angle and \mathbf{H} is the 2×2 upper left sub matrix of the 3×3 transformation matrix from the wavefront coordinate system into the registration surface. The slowness vector is denoted by \mathbf{p}_m . During the 3D CRS stack, along with the simulated ZO section, a number of volumes containing the optimum kinematic wavefront attributes and coherence for each ZO sample are obtained.

In the pragmatic 3D CRS stacking approach (Müller, 2003), a coherence volume is provided by evaluating the coherence criterion for the determined attributes. In order to automate the implementation of the CRS stack it is required that the kinematic wavefield attributes are determined without human interaction. For that purpose the CRS operator (4.4) is tested within a range of different attribute values for its fit to the actual reflection response. This so-called coherence analysis provides the fit of the individual test operators by evaluating an underlying coherence criterion. Thus, the determination of the wavefield attributes is formulated as a non-linear eight parameter global optimisation problem in the five-dimensional prestack data. The coherence criterion used in the current implementation of the CRS stack is the widely used semblance criterion (Nelder and Taner, 1971). The refinement of the attributes based on the simulated annealing approach can be performed after parameter search. However, only a few combinations of initial search and refinement are actually useful in terms of accuracy and performance. A simultaneous five parameter refinement is more reasonable than two subsequent refinements due to two reasons: the performance of the refinement is far less sensitive to the number of parameters than the initial grid search and the five parameter refinement provides a higher accuracy as the full CRS operator for the ZO domain is used. Obviously, the eight parameter refinement is a better choice. However, the large number of traces involved in an eight parameter optimisation may severely degrade the computational efficiency (Müller, 2003). There exist alternatives to the presented optimisation strategies. For example, the eight kinematic wavefield attributes can be determined by a series of 2D CRS stacks applied to different azimuthal directions (Höcht, 2002). In this way, the computational cost can be minimised but the stability and accuracy

may be decreased as an appropriate azimuthal distribution of the traces is required.

Recently, [Xie and Gajewski \(2016\)](#) proposed a simultaneous search algorithm to automatically estimate the 3D CRS attributes. They first apply the genetic algorithm ([Holland, 1975](#)) to search an initial set of wavefront attributes and then the Nelder-Mead simplex method ([Nelder and Mead, 1965](#)) is applied to refine these attributes. The attributes obtained by the proposed method are smoother and less noisy, and the computational time is nearly three times faster than the pragmatic approach given the condition that both methods are applied within the same computational environment. Note that conflicting dip problem is so far not considered in their algorithm.

3D partial time demigration operator

As I deduced earlier in this section, the 3D partial time migration operator can be denoted by Equation 4.3. In order to back-transform the resulting data to generate new prestack data in the original domain, I solve Equation 4.3 for t_{apex} . For this purpose, I set

$$A = \frac{m_x(m_x - 2h_x) + m_y(m_y - 2h_y)}{v(\alpha)^2}, \quad B = \frac{m_x(m_x + 2h_x) + m_y(m_y + 2h_y)}{v(\alpha)^2}. \quad (4.8)$$

Note that time migration velocities are azimuth-dependent. After some algebra, I obtain our 3D partial time demigration operator in terms of t_D , which is now the isochronal time:

$$t_{apex}(m, h, t_D) = \sqrt{t_D^2 - 2(A^2 + B^2) + \frac{(A^2 - B^2)^2}{t_D^2}}. \quad (4.9)$$

This equation is a single square root equation, with the same form as in the 2D case formulated by Equation 3.1, but with more parameters. If the same parameters, i.e., velocities and apertures, are applied in both transformations, i.e., partial time migration and partial time demigration, the resulting data are theoretically equivalent to the original data. Poststack time-demigrated gathers can be generated by stacking the prestack time-demigrated data.

Migration velocities

The time migration velocity model is important for time migration. Time migration

velocities can be obtained automatically from the 3D wavefront attributes during our proposed process. For arbitrary 3D media, the time migration velocities (as well as the stacking velocities) associated with the CRS operator are azimuth-dependent (see, e.g., Müller, 1999; Spinner and Mann, 2007). Presuming that the data set under consideration was acquired with an appropriate azimuth coverage to provide three stable independent components of the matrix \mathbf{M}_{NIP} , a time migration velocity matrix can be determined, from which the velocity for each azimuth α can be derived. Here, α denotes the midpoint displacement azimuth as all considerations are restricted to the poststack case (Spinner, 2007).

For the calculation of migration velocities $v(\alpha)$, reliable attributes are extracted from the smoothed 3D attribute volumes (Duvencack, 2004) by means of the CRS-based automatic picking. The migration velocity for a specified azimuth can be obtained according to the equation

$$v(\alpha) = \sqrt{V_{11}(\cos \alpha)^2 + V_{12} \cos \alpha \sin \alpha + V_{22}(\sin \alpha)^2}, \quad (4.10)$$

where $\mathbf{V} = 4\mathbf{M}$ is a 2×2 symmetric matrix

$$\begin{pmatrix} V_{11} & V_{12} \\ V_{21} & V_{22} \end{pmatrix}$$

.

\mathbf{V} is related to the azimuth-dependent time migration velocity $v(\alpha)$ denoted by Equation 4.10, where the element $V_{12} = V_{21}$, and $\mathbf{M} = (4\mathbf{p}_m \mathbf{p}_m^T + t_0 \mathbf{M}_{NIP})^{-1}$ (Spinner, 2007).

In principle, the kinematic wavefront attributes could be directly converted to the desired matrix elements. However, an interpolation of the matrix elements is unphysical as the matrix element V_{12} does not show a smooth distribution. Therefore, the attributes are firstly used to derive azimuth-dependent time migration velocities for the azimuths $\alpha = 0^\circ, 45^\circ, 90^\circ$:

$$v(0^\circ) = (V_{11})^{\frac{1}{2}} \quad (4.11)$$

$$v(45^\circ) = (V_{12} + \frac{1}{2}(V_{11} + V_{22}))^{\frac{1}{2}} \quad (4.12)$$

$$v(90^\circ) = (V_{22})^{\frac{1}{2}}. \quad (4.13)$$

4.3. Synthetic data examples

In order to demonstrate the extended 3D partial time migration technique, I choose the complex synthetic model: SEG Salt Model C3 wide azimuth classic dataset. The data set consists of 26 sail-lines separated by 320 m, 96 shots per line with 80 m shot interval, 8 cables per shot, 68 receivers per cable and a 40 m receiver interval. The model describes a complex salt body in the Gulf of Mexico. The top of the salt is rugged and generates different patterns of diffraction events. I choose a large portion of the data over the salt body for processing with in-line ranges from 0 to 220 and cross-line ranges from 0 to 403. The CDP bin size is $40 \times 20 \text{ m}^2$ in in-line and cross-line (or x-line) directions leading to a maximum fold of 18. The offset ranges from 40 to 2695 m. Figure 4.3 displays the model. The velocity varies from 1000 to 4500 m/s. The rugged top-of-salt generates diffractions. Before the data were released, some pre-processing procedures were performed including, e.g. band pass filter. Note that a top mute was conducted in the original data before further processing. Random noise of a S/N ratio of ten is added to the data for the following application.

Firstly, I applied the 3D simultaneous search algorithm (Xie and Gajewski, 2016) to the data to obtain the wavefront attributes, and a stacked section to get a first impression of the model. See Appendix A.4 for detailed processing parameters for stacking and (partial) time migration. Figure 4.4(a) shows the stacked section of in-line 190 from the center of the salt body. The image exhibits different diffraction patterns, as expected, as well as conflicting dips, where diffractions and reflections intersect. Figures 4.4(b) shows the stacked section of x-line 300 also from the center of the salt body. Figures 4.4(c) shows the time slice through the center of the data set at 2 s. I also chose the same in-line, x-line and time slice sections for the following tests.

Figure 4.5(a) displays the result for in-line 190 by conventional prestack time migration method, and Figure 4.5(b) shows the according result by partial time migration plus a multi-parameter stack. The conventional time migration can be regarded as a benchmark for our proposed partial time migration technique, because the latter is nothing else but a new parametrisation of the former, however the latter preserves the moveout. I used the same migration parameters and velocities in both cases (See Appendix A.4 for detailed parameters). By comparison, I observe that they behave the same, but it is evident that the proposed method leads to slightly better results, and it exhibits higher S/N ratio and shows potential regarding prestack data enhancement compared to the conventional prestack time migration method. Figures 4.6(a) and 4.6(b) show according results for x-line 300. The conclusions regarding data quality and prestack data enhancement ability are the same as for the in-line section. However, we notice that there is stair-stepping

problem in the result of Figure 4.6(b). Figure 4.7(a) shows the result of time slice at 2 s by conventional prestack time migration method, and Figure 4.7(b) shows the according result by partial time migration plus a multi-parameter stack. Somehow the result is not as good as we expected by our proposed method. For example, the diffractor at Inline 90, Cross-line 240, lost its focus in Figure 4.7(b). But the diffractor at Inline 120, Cross-line 300, is more focusing in Figure 4.7(b) than in Figure 4.7(a). We are still working on finding out the reason, so far we assume the calculated velocities are not so accurate at the salt areas, where the lateral velocities vary strongly.

To demonstrate the data enhancement ability, I have chosen a portion of traces from the original data (Figure 4.8 left), and compare them with the chosen traces after partial time migration (Figure 4.8 right). I observe better regularised traces and higher S/N ratio after PartialTM.

For 3D time demigration, I chose a comparison which contains nine CMPs from the original data and the same part from the data after applying the proposed cascaded method. I observe that the signals in the original data shown by Figure 4.9 were masked by noise, while in the newly-generated prestack data shown by Figure 4.10, a significant improvement was achieved in S/N ratio, as well as the regularisation of the data. However, I also notice that some non-physical events were generated, e.g., the events above the sea level (between 0 s to 0.9 s), and also the events between the main strong events. This is because the proposed operator may regard certain noise as reflection energy and thus rebuild events out of these noise. I suggest a way for improvement in Chapter 6.

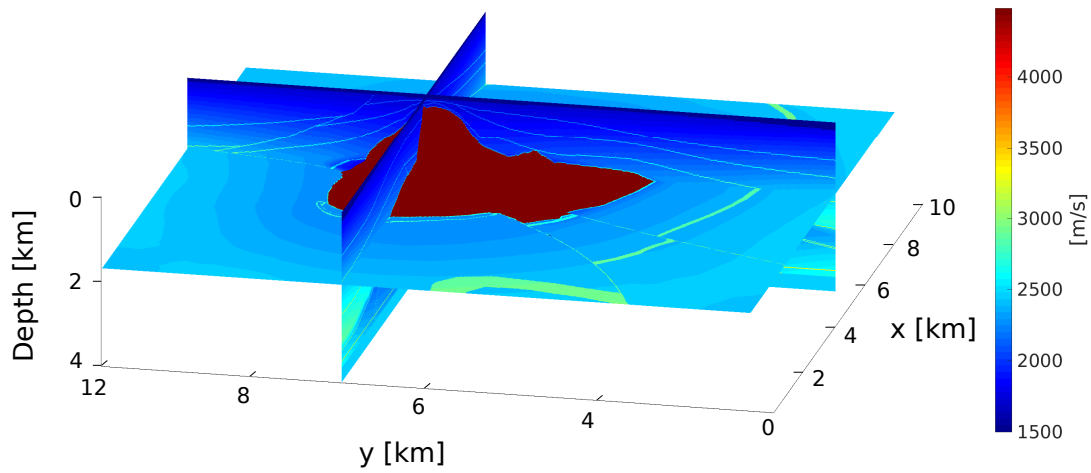


Figure 4.3.: SEG Salt Model C3 wide azimuth classic dataset. The model describes a salt body in the Gulf of Mexico. The velocity varies from 1000 to 4500 m/s. The rugged top-of-salt generates diffractions. (Provided by [Xie and Gajewski \(2016\)](#))

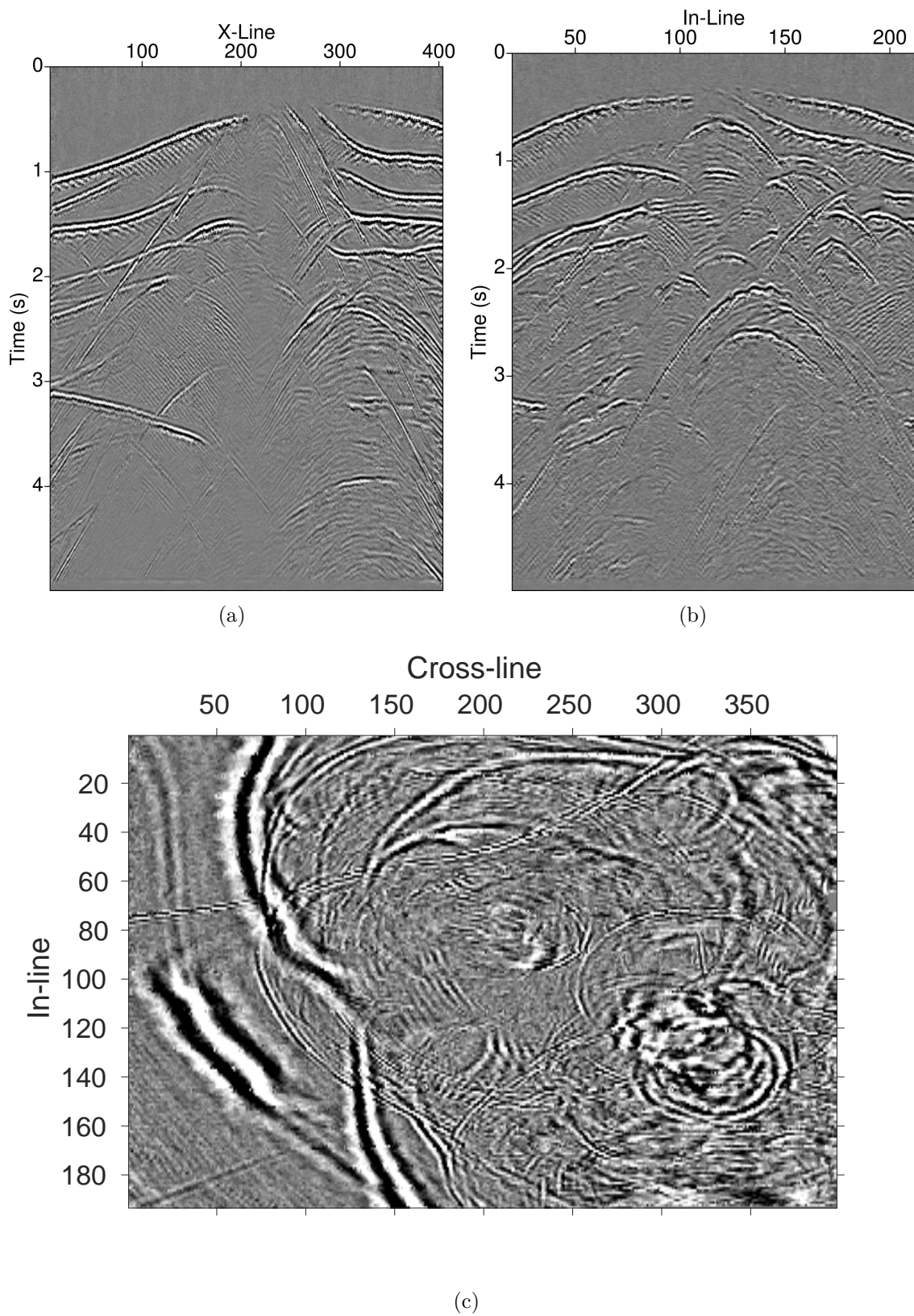


Figure 4.4.: Stacked section of the data to obtain the wavefront attributes, and to get a first impression of the model. (a) in-line 190, (b) cross-line 300. (c) time slice at 2 s.

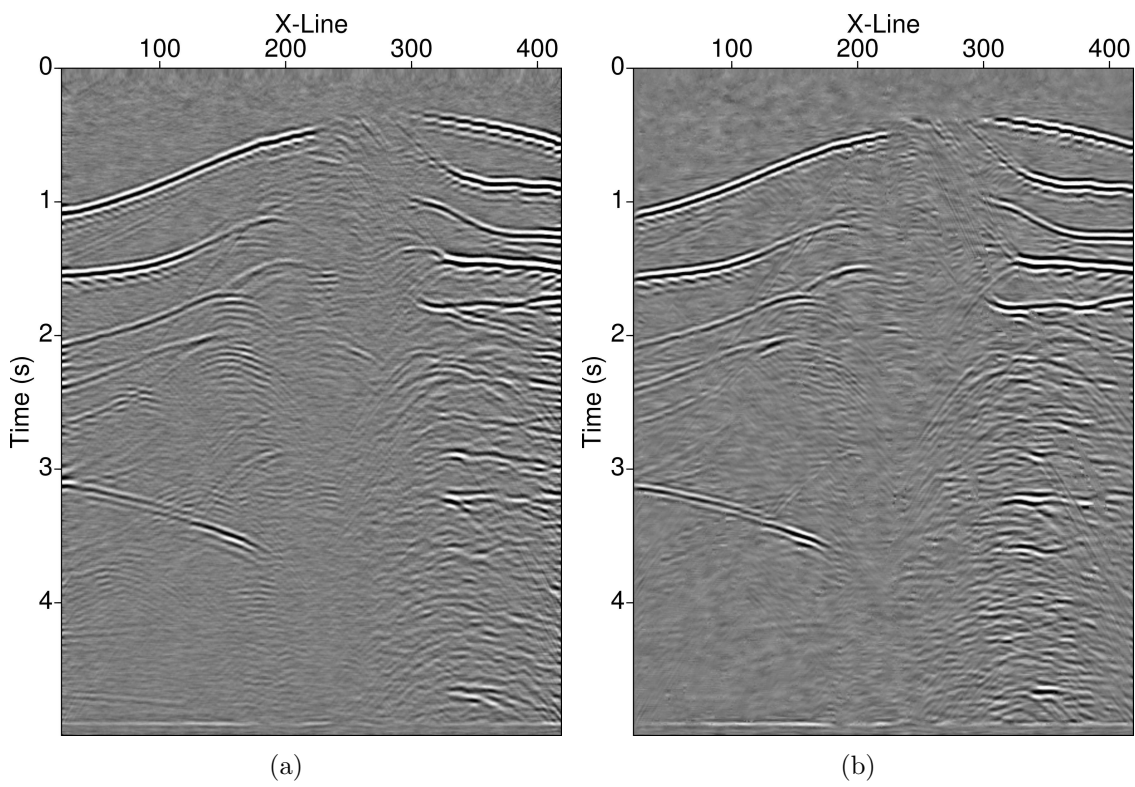


Figure 4.5.: Comparison of in-line 190 from (a) conventional prestack time migration, and (b) partial time migration plus multi-parameter stacked data.

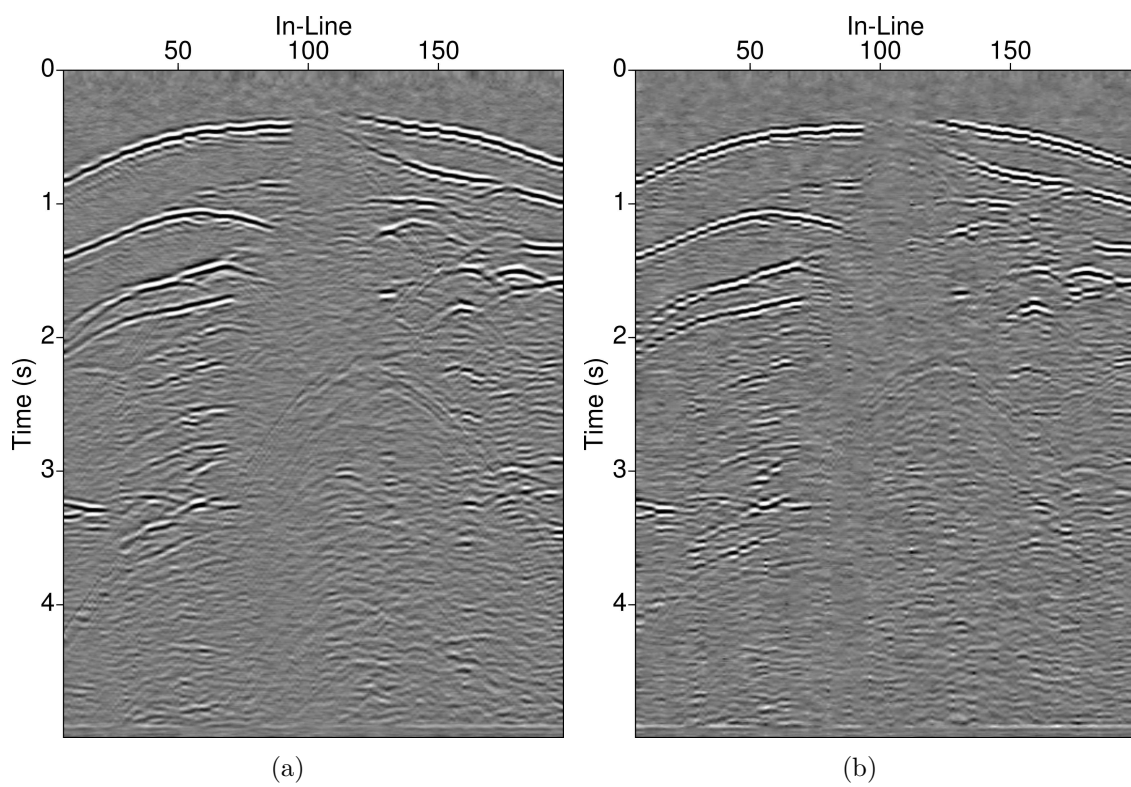
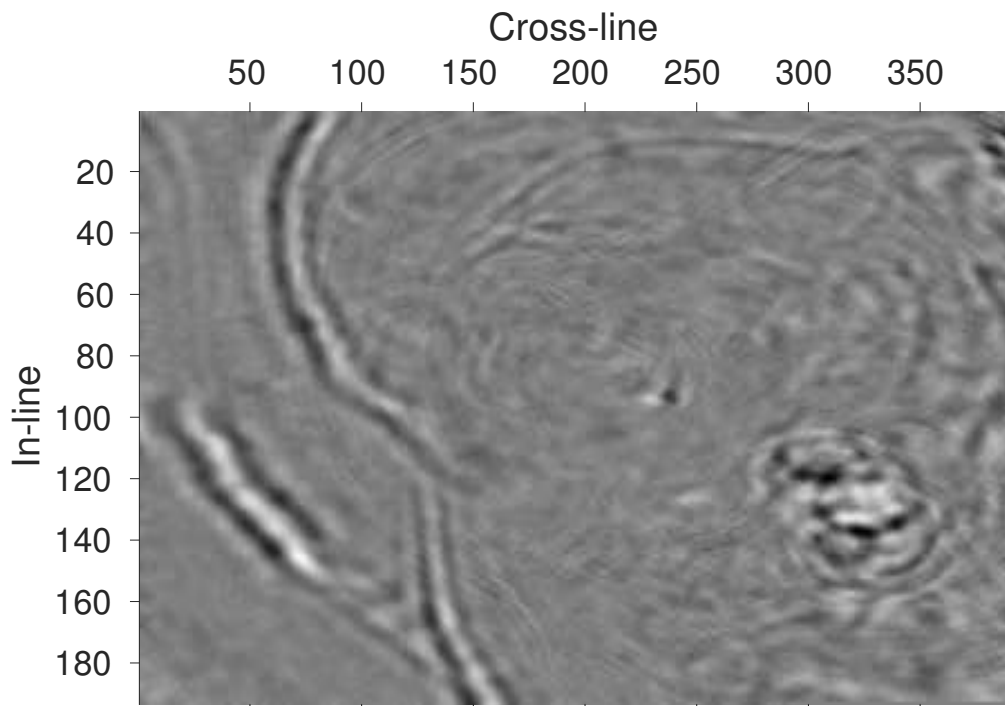
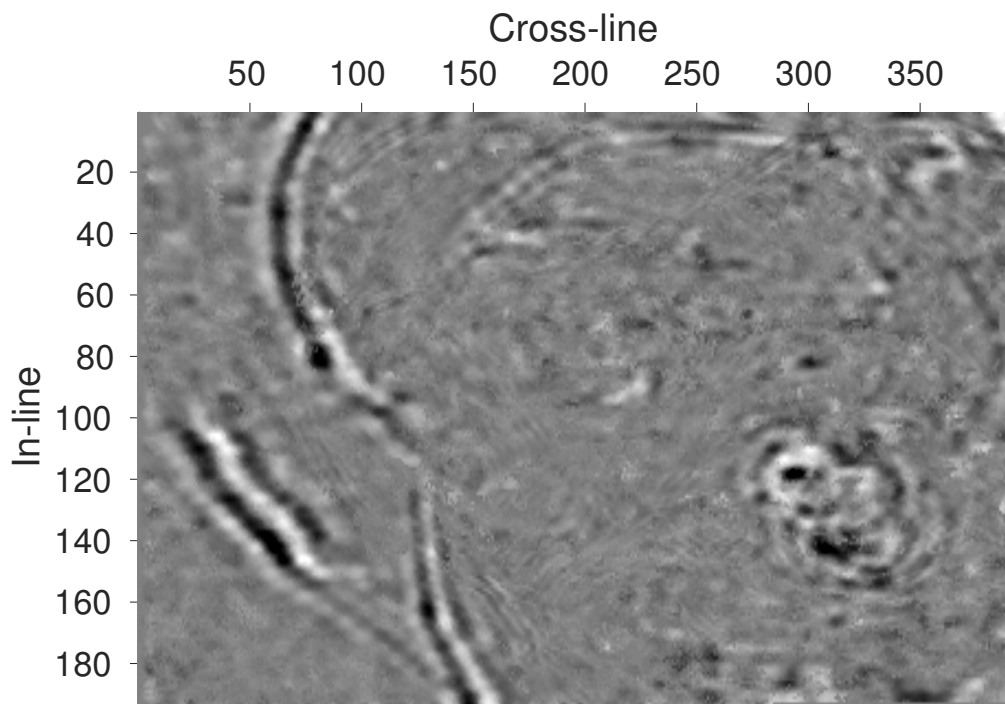


Figure 4.6.: Comparison of cross-line 300 from (a) conventional prestack time migration, and (b) partial time migration plus multi-parameter stacked data.



(a)



(b)

Figure 4.7.: Comparison of time slice at 2 s from (a) conventional prestack time migration, and (b) partial time migration plus MP stacked data.

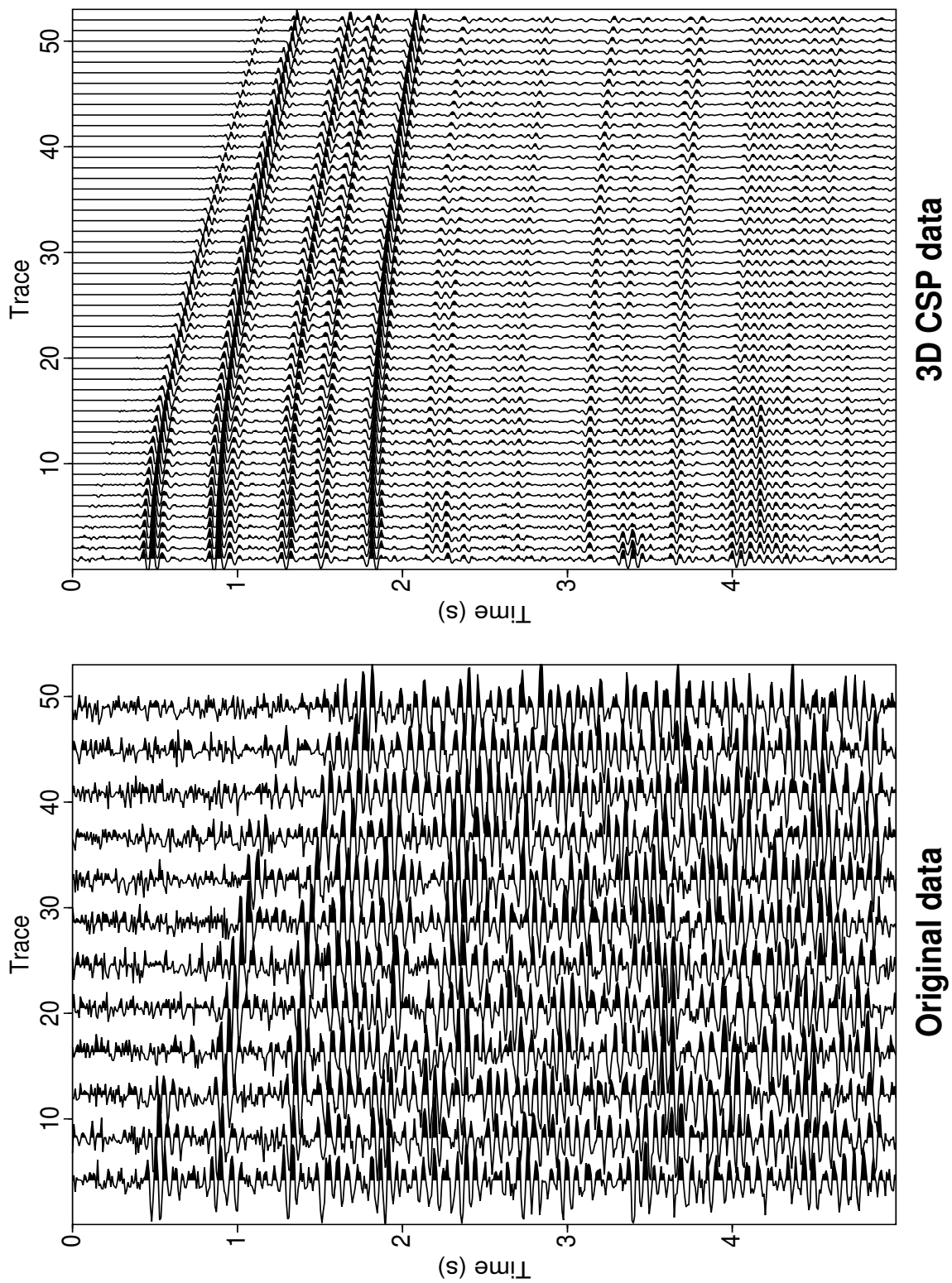


Figure 4.8.: Comparison of chosen traces from (a) the original data with noise of S/N ratio ten, and (b) data after partial time migration. We observe that the traces are regularised and the S/N ratio has been improved after PartialTM.

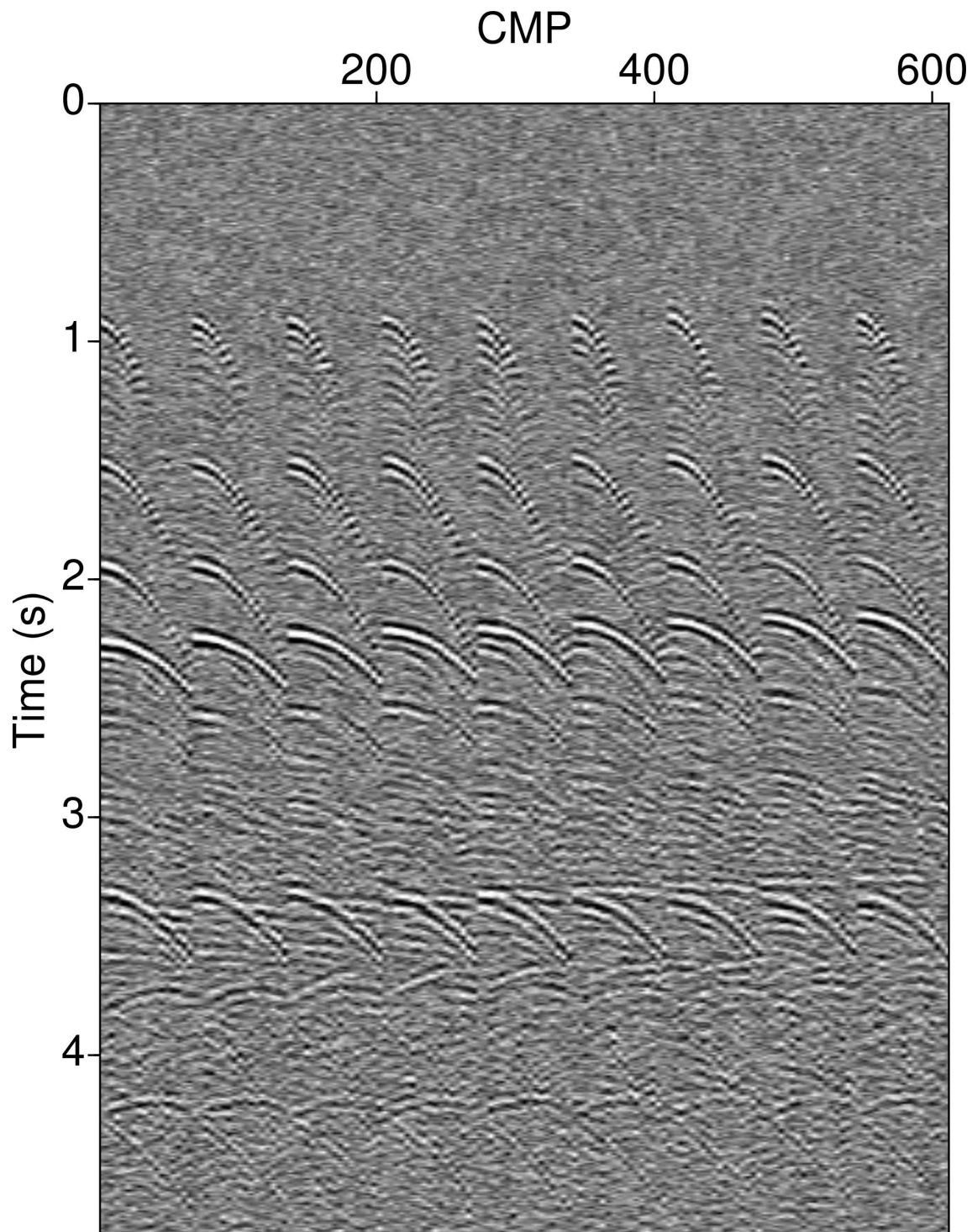


Figure 4.9.: Chosen CMPs from the original data with noise of S/N ratio ten.

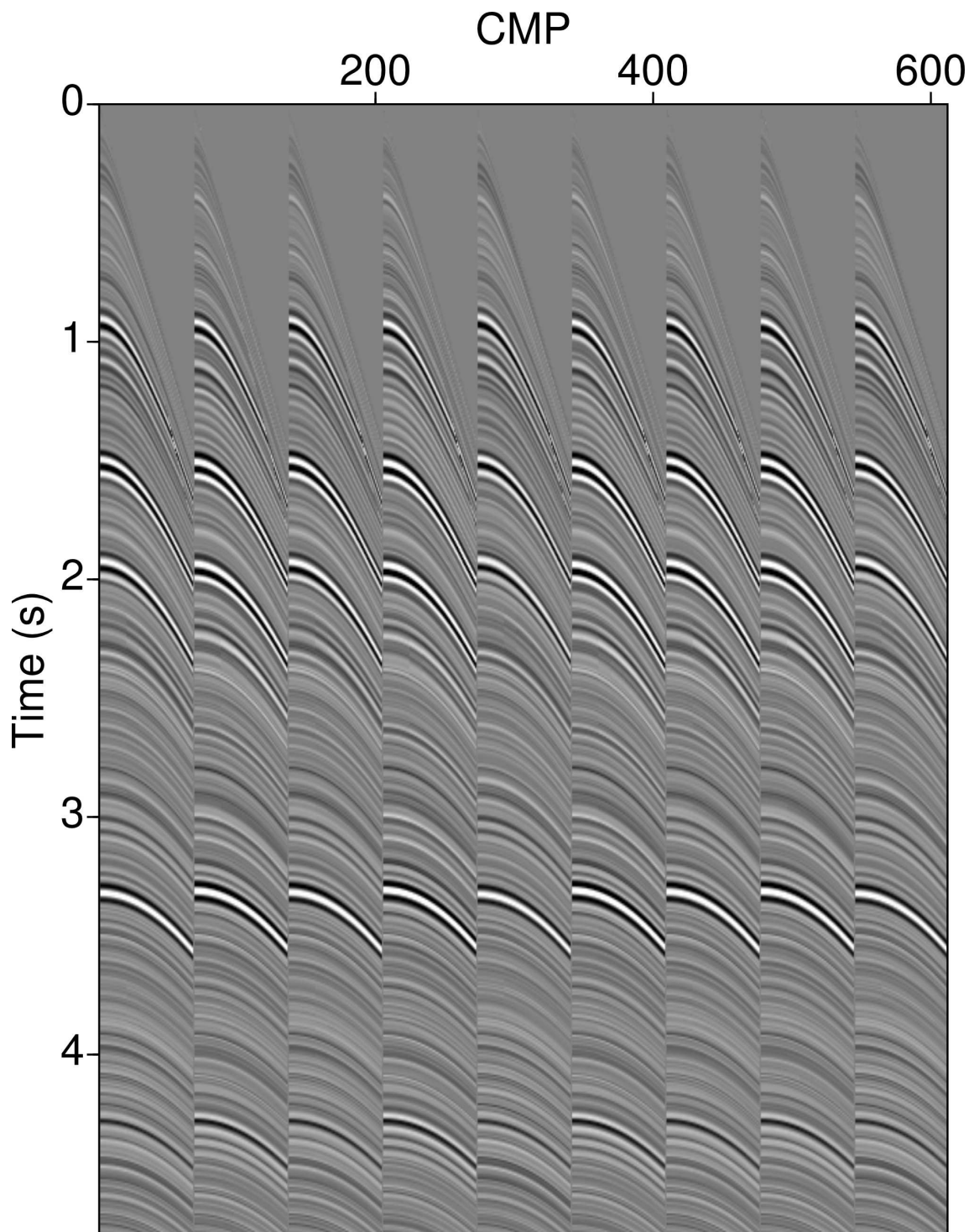


Figure 4.10.: Same chosen part of data after a cascaded operator of partial time migration and partial time demigration. Data regularisation ability of proposed method has been demonstrated.

4.4. Summary

In this chapter, 3D prestack partial time migration and demigration techniques were presented. They are extensions of the 2D counterparts. Prestack partial time migration is carried out by reparametrising the conventional prestack time migration operator, and then followed by a subsequent multi-parameter stack. Prestack partial time demigration is the mathematical inverse to time migration and undoes what the time migration process has done to the original seismic section. I propose a cascaded application of first partial time migration and then demigration, in order to obtain enhanced prestack data. Comparison of the results by the conventional method and the proposed method on a 3D complex data set was executed. The results confirm the ability of regularising the traces and improving the prestack data quality for 3D cascaded partial time de-/migration method. The implementation of the proposed approach is straightforward. Although we faced limitations that time migration is under the assumption of mild to moderate lateral velocity variations. Our first results, however, have already shown that the technique is capable to provide a easy to use imaging tool. An azimuth-dependent time migration velocity model can be built from the kinematic wavefront attributes during the process. This is highly automated (data-driven) and efficient compared to updating approaches often used for conventional time migration velocity determination techniques, which makes the proposed approach attractive.

Chapter 5.

Conclusions

In the scope of this thesis, I have studied the transformations of reflection seismic data from original CMP domain to partially time-migrated domain and from the latter back to the former. Prestack time migration is the major tool in these processes. The main advantage of time migration lies in its speed regarding computation time and low sensitivity to velocity model errors compared to the depth migration process. I reviewed an existing scheme to build ‘partly’ time migrated data by exploitation of Kirchhoff’s diffraction approach. This has been done by reparametrising the DSR operator in terms of the diffraction apex traveltime. This operator is applied in a first step to generate new prestack gathers in the partially time-migrated domain. A subsequent multi-parameter (MP) stack is then applied to these data. Results after the above mentioned two steps are kinematically equivalent to conventional prestack time migration results, but the new technique leads to a considerable enhancement of the data quality because the method combines the robustness of time migration with the data enhancement properties of the MP stack.

The main advantage of the partial time migration method is that the moveout is preserved during migration, and the data still stay in the prestack domain. This makes it suitable for many complementary applications, e.g. time migration velocity model building (Mann, 2002; Spinner, 2007), image-ray tomography (Dell et al., 2014) and multiple suppression (Dümmong and Gajewski, 2008). The multi-parameter stacking operator which depends on the kinematic wavefront attributes sums up data within a proper aperture along both midpoint and offset direction. I have applied this approach as well as a subsequent multi-parameter stack to a complex synthetic data and a marine field data set to demonstrate the potential of the method. In comparison with the results obtained by the conventional prestack time migration approach, the results of the new method shows a higher signal-to-noise level and thus better image quality not only in the sedimentary part, but also in the sub-salt area.

Processing low quality data is a major challenge in seismic data processing. These

poor quality seismic data with low fold and/or low S/N-ratio can cause unreliable imaging results, which may misguide the geological interpretation. In order to address these issues and further investigate the prestack data enhancement, I have proposed a new method to transform the partially time-migrated data back to the original time domain. It is the inverse process of partial time migration mentioned above. Providing that the same parameters, i.e., velocities and apertures, are applied in both steps, by applying a cascade process of first partial time migration and then partial time demigration we can obtain results theoretically equivalent to the original data. However, due to the data enhancement capability of our method, we obtain a higher signal-to-noise level and much more regularised traces. Furthermore, it shows that our method can mitigate aliasing. The prestack results can be further stacked by a MP stack or a CMP stack to generate poststack counterparts. The result demonstrates the superiority over the stacked original data.

Seismic data imaging in three dimension is another challenge since the reflection response is dependent on the azimuth of source and receiver positions. The objects to be imaged are intrinsically 3D objects. Imaging such objects using 2D methods can produce reliable results only in the case when the target object is located below the seismic line in which the data are acquired, otherwise only a part of the reflection and diffraction data is summed up. This will lead to either the imaging failing, or the resulting image being severely deteriorated, e.g., spatially smeared and appearing at a wrong location. Seismic data acquired by 3D geometries is usually more sparsely and irregularly sampled along the spatial coordinates than the data gained by 2D geometries. I extended the technique of the cascaded operator for partial time migration and partial time demigration to the 3D case. I take advantage of the data enhancement ability of the MP stack. For both 2D and 3D time de-/migration cases, I utilised the kernel of the 2D/3D CRS stack method to generate migration velocities. Once the kinematic wavefront attributes are extracted from the automatic picking process during the CRS stack, they can be used as inputs for velocity model building. By means of these attributes, three in 2D case and eight in 3D case, the time migration velocities can be calculated. In order to determine the time-migration velocity values from CRS attributes, the wavefield attributes for one ZO location have to be mapped into the apex of the corresponding time migration operator which is also provided by the CRS approach. This diffraction response approximates the true diffraction response up to second order. However, it only coincides with the DSR operator for either zero offset or a midpoint displacement equal zero. Otherwise, the DSR and the CRS-based diffraction operator deviate from each other. The migration velocity obtained from the CRS attributes does therefore not coincide with the “best-fit” parameter required to build up the DSR operator. Even though, the obtained velocities parametrise the CRS diffraction response rather than the DSR operator, they provide a good approximation of the searched-for velocities, and the whole process is purely data-driven (Spinner, 2007). The CRS-based velocity model building is quite efficient and can be highly automated compared to updating

approaches often used for conventional time migration velocity determination (see, e.g., [Robein, 2003](#)).

The main purpose of this thesis is to study the possible approaches to improve the image quality of seismic data and regularise the traces. Both forward and backward transformations of the seismic data presented in this thesis allow us to take advantage of seismic processing tools, e.g., the time migration and stacking, to provide improved subsurface images to better suit the demand of the geological interpretation. Besides, we can learn the differences between the resulting data and original data from both transformations. Although the data application shows potential of the proposed cascaded technique, we should keep in mind that time imaging has its limitations, this is due to the precondition for media with laterally homogeneous velocity distribution. Time imaging fails for lateral heterogeneities.

Chapter 6.

Outlook

The theoretical derivations and data applications presented in this thesis are mainly focused on two data transformation techniques, namely, prestack partial time migration and partial time demigration. By applying both forward and backward transformations, we can obtain data in new domains. Furthermore, we can learn the differences between these domains and take advantage of newly-generated data in between these domains.

Due to the focusing of diffractions and triplications of the time-migrated gathers, data obtained after the first transformation is almost without conflicting dips and triplications, therefore it is preferable for conflicting dips handling which is the case when two or more seismic events intersect each other. Comparing to the current approaches for conflicting dip problems (Walda and Gajewski, 2014), this method provides an efficient way in an almost automatic manner. Also it shows potential for diffraction separation (Dell and Gajewski, 2011; Bakhtiari Rad et al., 2014) and multiple suppression (Dümmong and Gajewski, 2008).

Instead of the original data, the improved prestack data after the two transformations can be used in many conventional processing procedures, providing enhanced images. In addition, estimation of migration velocities out of the kinematic wavefront attributes is preferable and it is a purely data-driven approach.

We observe in the results of the 3D data set (see Figure 4.10) that some events without physical meanings were generated after the cascaded technique, which means the operator has some limitations that it may regard certain noise as reflection energy and thus rebuild events out of these noise. Inspired by Schwarz (2015), who argued that the partial semblance coefficient serves as an objective criterion for local finite-offset refinement, and the migration coherence not only provides insight into the general fit to diffractions, but also serves as an imaging tool indicating the position of edges, faults and other discontinuities in the partially migrated finite-offset sections. In order to prevent the generating of artificial (non-physical) events,

I suggest to investigate the coherence section of the partial time-migrated result by combining the partial time migration approach with CRS stack, and use the coherence as a mask to detect the real events and the non-physical ones.

Finally, within this thesis, I have focused on kinematic operators. The presented two transformations, i.e., partial time migration and partial time demigration so far are purely data-driven, and are executed kinematically. Geometric spreading, obliquity, filtering, etc. are not addressed in this work. A future suggestion concerning the presented method is to consider amplitudes. The extension to true-amplitude operators can compensate for the geometrical spreading effect during the transformations.

Bibliography

- AAPG (2014). time slice. *AAPG Wiki*.
- Bakhtiari Rad, P., Schwarz, B., Vanelle, C., and Gajewski, D. (2014). Common reflection surface (CRS) based pre-stack diffraction separation. *SEG Technical Program Expanded Abstracts*, pages 4208–4212.
- Bancroft, J. (1997/1998). *A Practical Understanding of Pre- and Poststack Migration, Vol. I and II*. SEG, Tulsa.
- Bancroft, J., Geiger, H., and Margrave, G. F. (1998). The equivalent offset method of prestack time migration. *Geophysics*, 63:2042–2053.
- Baykulov, M. (2008). *Partial CRS stack User's Manual*. Institute of Geophysics, University of Hamburg, version 5.0 edition.
- Baykulov, M. and Gajewski, D. (2009). Prestack seismic data enhancement with partial common-reflection-surface (CRS) stack. *Geophysics*, 74(3):V49–V58.
- Bergler, S. (2004). *On the Determination and Use of Kinematic Wavefield Attributes for 3D Seismic Imaging: Bestimmung und Anwendung Kinematischer Wellenfeldattribute Bei 3D Seismischen Abbildungsverfahren*. PhD thesis, University of Karlsruhe.
- Biondi, B. L. (2005). *3-D Seismic Imaging*. Stanford University.
- Claerbout, J., Green, C., and Green, I. (1996). *Imaging the Earth's Interior*. Free Software Foundation.
- Dell, S. (2012). *Seismic processing and imaging with diffractions*. PhD thesis, University of Hamburg.
- Dell, S. and Gajewski, D. (2011). Common-reflection-surface-based workflow for diffraction imaging. *Geophysics*, 76(5):S187–S195.
- Dell, S., Gajewski, D., and Tygel, M. (2014). Image-ray tomography. *Geophysical Prospecting*, 62:413–426.
- Dell, S., Gajewski, D., and Vanelle, C. (2012). Prestack time migration by common-migrated-reflector-element stacking. *Geophysics*, 77(3):S73–S82.

- Deregowski, S. M. (1986). What is DMO? *First break*, 4:7–24.
- Dix, C. H. (1955). Seismic velocities from surface measurement. *Geophysics*, 20(1):68–86.
- Dorn, G. A. (1998). Modern 3-D seismic interpretation. *The Leading Edge*, 17(9):1262–1272.
- Dümmong, S. and Gajewski, D. (2008). A multiple suppression method via crs attributes. *SEG Technical Program Expanded Abstracts*.
- Dümmong, S. and Hübscher, C. (2011). Levant Basin – Central Basin. In: Atlas of the Messinian seismic markers in the Mediterranean and Black Seas. *Lofi et al., Eds., Atlas of Messinian seismic markers in the Mediterranean and Black seas. Mém. Soc. géol. fr., 179, and World Geological Map Commission*, page 72.
- Duveneck, E. (2004). *Tomographic determination of seismic velocity models with kinematic wavefield attributes*. PhD thesis, University of Karlsruhe.
- Ferber, R. G. (1994). Migration to multiple offset and velocity analysis. *Geophysical Prospecting*, 42:99–112.
- Fomel, S. (2003). Time migration velocity analysis by velocity continuation. *Geophysics*, 68:1662–1672.
- Gazdag, J. (1978). Wave equation migration with the phase-shift method. *Geophysics*, 43:1342–1351.
- Gelchinsky, B., Berkovitch, A., and Keydar, S. (1999). Multifocusing homeomorphic imaging: Part1. basic concepts and formulas. *Journal of Applied Geophysics*, 42(3-4):229–242.
- Glöckner, M., Schwarz, B., Vanelle, C., and Gajewski, D. (2015). *Kinematic time demigration: the i-CRS operator*, pages 74–84. WIT Consortium.
- Hagedoorn, J. (1954). A process of seismic reflection interpretation. *Geophysical Prospecting*, 2:85–127.
- Hertweck, T., Jaeger, C., Goertz, A., and Schleicher, J. (2003). Aperture effects in 2.5D Kirchhoff migration: A geometrical explanation. *Geophysics*, 68:1673–1684.
- Höcht, G. (2002). *Traveltime approximation for 2D and 3D media and kinematic wavefield attributes*. PhD thesis, University of Karlsruhe.
- Holland, J. (1975). *Adaptation in natural and artificial systems*. University of Michigan Press.
- Hubral, P. (1977). Time migration – Some ray theoretical aspects. *Geophysical Prospecting*, 25:738–745, doi: 10.1111/j.1365–2478.1977.tb01200.x.

- Hubral, P. (1983). Computing true amplitude reflections in a laterally inhomogeneous earth. *Geophysics*, 48:1051–1062.
- Hubral, P., Schleicher, J., and Tygel, M. (1996). A unified approach to 3-D seismic reflection imaging, Part I: Basic concepts. *Geophysics*, 61:742–758, doi: 10.1190/1.1444001.
- Iversen, E., Tygel, M., Ursin, B., and de Hoop, M. (2012). Kinematic time migration and demigration of reflections in pre-stack seismic data. *Geophysical Journal International*, 189:1635–1666.
- Mann, J. (2002). *Extensions and Applications of the Common-Reflection-Surface Stack Method*. PhD thesis, Logos Verlag, Berlin.
- Mann, J. (2003). *2-D zero-offset Common-Reflection-Surface Stack User's Manual*. Geophysical Institute, University of Karlsruhe, Version 4.6 edition.
- Mann, J., Hubral, P., Traub, B., Gerst, A., and Meyer, H. (2000). Macro-model independent approximative prestack time migration. *62nd EAGE Conference and Exhibition Expanded Abstracts*.
- Mayne, W. H. (1962). Common reflection point horizontal data stacking techniques. *Geophysics*, 27(6):927–938.
- Mosher, C. C., Kebo, T. H., Weglein, A. B., and Foster, D. J. (1996). The impact of migration on AVO. *Geophysics*, 61(6):1603–1615.
- Müller, A. (2003). The 3D Common-Reflection-Surface stack – theory and application. Master's thesis, University of Karlsruhe.
- Müller, T. (1999). *The Common Reflection Surface Stack Method: Seismic Imaging without explicit knowledge of the velocity model*. PhD thesis, University of Karlsruhe.
- Nelder, J. and Taner, M. (1971). Semblance and other coherency measures for multichannel data. *Geophysics*, 36(482–497).
- Nelder, J. A. and Mead, R. (1965). A simplex method for function minimization. *Computer Journal*, 7:308–313.
- Robein, E. (2003). *Time-imaging and Depth-imaging in Reflection Seismics: Principles and Methods*. EAGE Publications bv.
- Robein, E. (2010). *Seismic Imaging: A Review of the Techniques, their Principles, Merits and Limitations*. EAGE Publications bv.
- Ryo, J. (1982). Ryo, j.decomposition (decom) approach applied to wave-field analysis with seismic reflection records. *Geophysics*, pages 869–883.

- Santos, L., Schleicher, J., Tygel, M., and Hubral, P. (2000). Seismic modeling by demigration. *Geophysics*, 65(4):1281–1289.
- Schleicher, J., Hubral, P., Tygel, M., and Jaya, M. (1997). Minimum apertures and fresnel zones in migration and demigration. *Geophysics*, 62:183–194.
- Schlumberger (2015). time slice. *Oil field glossary*.
- Schwarz, B. (2015). *Moveout and Geometry*. PhD thesis, University of Hamburg.
- Schwarz, B., Vanelle, C., Gajewski, D., and Kashtan, B. (2014). Curvatures and inhomogeneities: An improved common-reflection approach. *Geophysics*, 79(5):S231–S240.
- Sheriff, R. (1980). Nomogram for Fresnel-zone calculation. *Geophysics*, 45:968–972.
- Sheriff, R. and Geldart, L. (1982). *Exploration seismology*. Cambridge University Press.
- Spinner, M. and Mann, J. (2007). CRS-based minimum-aperture time migration - A 2D land-data case study. *SEG Technical Program Expanded Abstracts*, pages 2354–2358.
- Spinner, M. E. T. (2007). *CRS-based minimum-aperture Kirchhoff migration in the time domain*. PhD thesis, University of Karlsruhe.
- Stolt, R. (1978). Migration by Fourier transform. *Geophysics*, 43:23–48.
- Sun, J. (1998). On the limited aperture migration in two dimensions. *Geophysics*, 63:984–994.
- Sun, J. (2000). Limited-aperture migration. *Geophysics*, 65(2):584–595.
- Taner, M. T. and Köhler, F. (1969). Velocity spectra-digital computer derivation applications of velocity functions. *Geophysics*, 34(6):859–881.
- Vanelle, C. and Gajewski, D. (2001). Determining the optimum migration aperture from traveltimes. *Journal of seismic exploration*, 10:205–224.
- Vanelle, C. and Gajewski, D. (2002). True-amplitude migration weights from traveltimes. *Pure Appl. Geophys.*, 159:1583–1599.
- Vanelle, C., Kashtan, B., Dell, S., and Gajewski, D. (2010). A new stacking operator for curved subsurface structures. SEG 80th Annual Meeting, Expanded Abstracts.
- Verschuur, D., Berkhout, A., and Wapenaar, C. (1992). Berkhout, a.adaptive surface-related multiple elimination. *Geophysics*, pages 1166–1177.

-
- Walda, J. and Gajewski, D. (2014). *Handling the conflicting dip problem in the CRS/i-CRS method*, pages 164–172. WIT Report. WIT Consortium.
- Walda, J. and Gajewski, D. (2015). Common-reflection-surface stack improvement by differential evolution and conflicting dip processing. *SEG Technical Program Expanded Abstracts*, pages 3842–3847.
- Weglein, A. B., Gasparotto, F., Carvalho, P., and Stolt, R. (1997). An inverse-scattering series method for attenuating multiple reflections in seismic data. *Geophysics*, pages 1975–1989.
- Xie, Y. and Gajewski, D. (2016). Automatic estimation of the 3D CRS attributes by a metaheuristic-based optimization. *EAGE 78th Conference and Exhibition Expanded Abstracts*.
- Yang, Y., Vanelle, C., and Gajewski, D. (2014). Combining partial time migration and prestack data enhancement: a useful tool for subsalt imaging. *84th SEG Technical Program Expanded Abstracts*, pages 3669–3673.
- Yang, Y., Vanelle, C., and Gajewski, D. (2016). A new kinematic time demigration approach based on the csp method. *EAGE 78th Conference and Exhibition Expanded Abstracts*.
- Yilmaz, O. (2001). *Seismic Data Analysis*, volume 1. Society of Exploration Geophysicists, Tulsa.
- Yilmaz, Ö. and Claerbout, J. F. (1980). Prestack partial migration. *Geophysics*, 45:1753–1779.

List of Figures

2.1.	Hagedoorn's imaging condition.	10
2.2.	Principle of prestack time migration.	12
2.3.	The three CRS wavefront attributes α , R_{NIP} and R_N	14
2.4.	CRS stacking operator in the time-midpoint-(half-)offset volume.	16
2.5.	(a) partial time migration, (b) multi-parameter (MP) stacked CSP data. (after Dell et al. (2012))	18
2.6.	Velocity model for Sigsbee 2A data set.	26
2.7.	CMP-stacked section of the Sigsbee 2A data set with random noise.	26
2.8.	Prestack time-migrated section of the Sigsbee 2A data set with random noise using RMS velocities provided with the data set.	28
2.9.	CSP-MP-stacked section of the Sigsbee 2A data set with random noise using RMS velocities provided with the data set.	28
2.10.	Prestack time-migrated section of the Sigsbee 2A data set with random noise using stacking velocities determined from a CRS stack of the data.	29
2.11.	CSP-MP-stacked section of the Sigsbee 2A data set with random noise using stacking velocities determined from a CRS stack of the data.	29
2.12.	Three selected regions with different structural features for a detailed investigation.	31
2.13.	Close-up: layering and fractures.	32
2.14.	Close-up: top of salt.	33
2.15.	Close-up: sub-salt.	34
2.16.	The approximate position of our tested seismic line out of the marine data set acquired in the Levantine basin in the south-eastern Mediterranean Sea. (after Bakhtiari Rad et al. (2014))	36
2.17.	Structural overview of the tested seismic line.	37
2.18.	CMP-stacked section of the marine field data set.	37
2.19.	Prestack time-migrated section of the marine field data set using stacking velocities determined from a CRS stack of the data.	39
2.20.	CSP-MP-stacked section of the field marine data set using stacking velocities determined from a CRS stack of the data.	39
2.21.	The selected region for a detailed comparison of the PreSTM and CSP-MP stack results	40
2.22.	Close-up: salt rollers. Top: PreSTM result; bottom: CSP-MP result.	40

3.1. Simple generic synthetic model with three diffractors and one horizontal reflector.	46
3.2. Generic data example: (a) CMP-stack of the original data, (b) velocities determined by MP stack.	47
3.3. Generic data example: partially time-migrated and stacked result using (a) velocities determined by MP stack, (b) constant velocity.	49
3.4. Generic data example: prestack data for CMP 145 obtained from cascaded migration-demigration (a) using velocities determined by MP stack, (b) using constant velocity. (c) shows the original data for comparison.	50
3.5. Generic data example: poststack sections of the newly-generated prestack data using (a) velocities determined by MP stack, (b) constant velocity.	51
3.6. Sigsbee 2A data example: 1 km common offset section for the newly-generated prestack data using (a) velocities calculated by MP stack, (b) RMS velocities. (c) shows the corresponding original section.	53
3.7. Sigsbee 2A data example: CMP gather 1026 for the newly-generated prestack data using (a) velocities calculated by MP stack, (b) RMS velocities. (c) shows the corresponding original section.	54
3.8. Sigsbee 2A data example: poststack sections of the newly-generated prestack data using (a) velocities determined by MP stack, (b) RMS velocities. (c) shows the corresponding original section.	55
3.9. Marine data example: (a) 1150 m offset section resulting from the new method. (b) shows the corresponding original section.	57
3.10. Marine data example: Poststack section of (a) the newly-generated prestack data, (b) the original data.	58
4.1. A sketch for 3D seismic acquisition.	63
4.2. The meaning of the ZO CRS wavefront attributes	66
4.3. SEG Salt Model C3 wide azimuth classic dataset.	72
4.4. Stacked section of the data to obtain the wavefront attributes, and to get a first impression of the model. (a) in-line 190, (b) cross-line 300. (c) time slice at 2 s.	73
4.5. Comparison of in-line 190 from (a) conventional prestack time migration, and (b) partial time migration plus multi-parameter stacked data.	74
4.6. Comparison of cross-line 300 from (a) conventional prestack time migration, and (b) partial time migration plus multi-parameter stacked data.	75
4.7. Comparison of time slice at 2 s from (a) conventional prestack time migration, and (b) partial time migration plus multi-parameter stacked data.	76
4.8. Comparison of chosen traces from (a) the original data with noise, and (b) data after partial time migration.	77

4.9. Chosen CMPs from the original data with noise of S/N ratio ten.	78
4.10. Same chosen part of data after a cascaded operator of partial time migration and partial time demigration.	79

List of Tables

2.1. The main acquisition parameters of Sigsbee 2A model.	27
A.1. Main processing parameters: Generic data.	102
A.2. Main processing parameters: Sigsbee 2A data.	103
A.3. Main processing parameters: Marine data.	104
A.4. Main processing parameters: SEG Salt Model C3 wide azimuth classic dataset.	105

Appendices

Appendix A.

Processing parameters

Generic data

General parameters	
Dominant frequency	30 Hz
Coherence measurement	Semblance
Coherence time window	28 ms
Velocity and constraints	
Near surface velocity	2000 m/s
Lower moveout velocity constraints	1400 m/s
Upper moveout velocity constraints	6000 m/s
Prestack de-/migration apertures and taper	
Minimum/Maximum midpoint aperture	none
Minimum offset aperture	80 m
Maximum offset aperture	3000 m
Minimum taper size	56 m
Maximum taper size	2100 m
Stacking of partial time-migrated gathers	
Minimum midpoint aperture	35 m
Maximum midpoint aperture	55 m
Minimum offset aperture	500 m
Maximum offset aperture	2000 m
Poststack de-/migration apertures and taper	
Minimum offset aperture	80 m
Maximum offset aperture	3500 m
Minimum taper size	56 m
Maximum taper size	2450 m

Table A.1.: Main processing parameters for Generic data in Chapter 3. Noise with S/N ratio of five was added in the test. In case of a poststack de-/migration the offset aperture for stacking is zero.

Sigsbee 2A data

General parameters	
Dominant frequency	20 Hz
Coherence measurement	Semblance
Coherence time window	56 ms
Velocity and constraints	
Near surface velocity	2000 m/s
Lower moveout velocity constraints	1400 m/s
Upper moveout velocity constraints	5000 m/s
Prestack de-/migration apertures and taper	
Minimum/Maximum midpoint aperture	none
Minimum offset aperture	1000 m
Maximum offset aperture	3300 m
Minimum taper size	700 m
Maximum taper size	2310 m
Stacking of partial time-migrated gathers	
Minimum midpoint aperture	50 m
Maximum midpoint aperture	75 m
Minimum offset aperture	914 m
Maximum offset aperture	3810 m
Poststack de-/migration apertures and taper	
Minimum offset aperture	800 m
Maximum offset aperture	4000 m
Minimum taper size	560 m
Maximum taper size	2800 m

Table A.2.: Main processing parameters for Sigsbee 2A data in Chapter 2 and 3. In these cases, the only difference is that noise with S/N ratio of eight was added in the test in chapter 2. In case of a poststack de-/migration the offset aperture for stacking is zero.

Marine data

General parameters	
Dominant frequency	40 Hz
Coherence measurement	Semblance
Coherence time window	28 ms
Velocity and constraints	
Near surface velocity	1480 m/s
Lower moveout velocity constraints	1300 m/s
Upper moveout velocity constraints	4500 m/s
Prestack de-/migration apertures and taper	
Minimum/Maximum midpoint aperture	none
Minimum offset aperture	500 m
Maximum offset aperture	1100 m
Minimum taper size	350 m
Maximum taper size	770 m
Stacking of partial time-migrated gathers	
Minimum midpoint aperture	50 m
Maximum midpoint aperture	70 m
Minimum offset aperture	920 m
Maximum offset aperture	3800 m
Poststack de-/migration apertures and taper	
Minimum offset aperture	500 m
Maximum offset aperture	1800 m
Minimum taper size	350 m
Maximum taper size	1260 m

Table A.3.: Main processing parameters for Marine data in Chapter 2 and 3. In case of a poststack de-/migration the offset aperture for stacking is zero.

SEG Salt Model C3 wide azimuth classic dataset

General parameters	
Dominant frequency	20 Hz
Coherence measurement	Semblance
Coherence time window	18 ms
Velocity and constraints	
Near surface velocity	1500 m/s
Lower moveout velocity constraints	1400 m/s
Upper moveout velocity constraints	4500 m/s
Prestack de-/migration apertures and taper	
Minimum midpoint aperture	100 m
Maximum midpoint aperture	100 m
Minimum offset aperture	400 m
Maximum offset aperture	1150 m
Minimum taper size	280 m
Maximum taper size	805 m
Regularisation parameters	
Offset aperture	100 m
Offset interval	20 m
Stacking of partial time-migrated gathers	
Minimum midpoint aperture	40 m
Maximum midpoint aperture	80 m
Minimum offset aperture	350 m
Maximum offset aperture	600 m
Global optimization parameters for attributes search	
Algorithm	Genetic algorithm
Number of individuals	40
Crossover probability	80 %
Number of iterations	50
Crossover probability	20 %

Table A.4.: Main processing parameters for SEG Salt Model C3 wide azimuth classic dataset in Chapter 4.

Appendix B.

Used software

Throughout the thesis I used a PC with the Unix like Debian OS under the GNU General Public License and part of a cluster called thunder, operated by the Central IT Services (CIS), available to the applied geophysics working group in Hamburg.

The thesis is written with the typesetting software L^AT_EX.

The software developed in the framework of the thesis is based on a CRS implementation by Mann (2002) and Müller (2003) with contributions from Dell (2012) and Baykulov (2008) and written in C++ supporting Message Passing Interface (MPI) provided by Wave Inversion Technology (WIT) consortium.

Visualization and simple processing was done using the Seismic Un*x (Colorado School of Mine), Inkscape and PSTricks.

Appendix C.

Eidesstattliche Versicherung

Hiermit erkläre ich an Eides statt, dass ich die vorliegende Dissertationsschrift selbst verfasst und keine anderen als die angegebenen Quellen und Hilfsmittel benutzt habe.

Hamburg, den

Unterschrift

Acknowledgements

- I have no words to express my gratefulness to Professor Dr. Dirk Gajewski for accepting me as PhD student, for his supervision of this work and for giving me a lot of freedom in choosing my research topics. He gave me the opportunity to achieve this work and allowed me to participate in many geophysical conferences around the globe.
- I am grateful to PD Dr. Claudia Vanelle, our women leader in the group, for the co-supervision of my thesis and her encouragement during my studies. Special thank for her proofreading of most of my papers.
- I would like to say thank you to Dr. Sergius Dell for nice helpful discussions, wonderful ideas of seismic imaging.
- I would also like to say thank you to Jan Walda for helpful discussions and always being supportive to me.
- I am also grateful to Dr. Benjamin Schwarz for cheerful discussions and advices.
- I thank Yujiang Xie, Ivan Abakumov, Parsa Bakhtiari Rad and the applied seismic working group for interesting discussions, good advices and support. Special thanks to Marie Voss for proofreading my thesis.
- Many thanks to Martina Glöckner for working together with her and discussing about baby issues.
- Thanks to Manizheh Vefagh Nematollahy for the help regarding administration issues when I first arrived in Hamburg.
- I would like to say thank you to Dr. Ekkehart Tessmer, Professor Dr. Matthias Hort, Dr. Christian Hübscher and Dr. Ali Dehghani for always being helpful.
- Thanks to Prof. Dr. Boris Kashtan from Russian Academy of Sciences, Saint Petersburg, Russia for nice discussions.

- My special thanks also goes to Paola Dal Corso who always helped me with administration issues.
- I gratefully acknowledge the China Scholarship Council (CSC) and the Wave Inversion Technology (WIT) consortium for funding of my position and the conference attends.
- I thank SMAART JV and TGS for providing the 2D data. Thanks to SEG research committee for the 3D data.
- Last but not the least, I would like to thank my parents for supporting me throughout my Ph.D. I would like to thank my husband for his love and encouragement during my studies. I would also like to thank our upcoming baby, for always being there with me.